MULTI-TEMPORAL REMOTE-SENSING-BASED MAPPING AND CHARACTERIZATION OF LANDSCAPE EVOLUTION OF A MEANDERING RIVER FLOODPLAIN

A Thesis

by

MINGDE YOU

Submitted to the Office of Graduate and Professional Studies of
Texas A&M University
in partial fulfillment of the requirements for the degree of

MASTER OF SCIENCE

Chair of Committee,	Anthony M. Filippi
Co-Chair of Committee,	İnci Güneralp
Committee Member,	Huiyan Sang
Head of Department,	David M. Cairns

August 2016

Major Subject: Geography

ABSTRACT

Large meandering river floodplains are critical components of the Earth ecosystems for their high biodiversity and productivity. However, it is challenging to study these regions because of their complex land-covers and dynamic surface processes. This study applies soft classification and change-detection analysis to five Landsat 5 Thematic Mapper (TM) satellite images to examine long-term surface-cover composition and configuration change of the Rio Beni floodplain in Bolivia from 1987 to 2006.

One hard/crisp classification algorithm (i.e., ISODATA) and two soft classification algorithms (i.e., Bayes classification and fuzzy classification) were applied to the study-area satellite images to examine the performances of classifying and mapping meandering river-floodplain environments between hard and soft classification approaches. In all five scenes, three algorithms achieved ~90% classification accuracy via hard classification outputs. However, the two soft algorithms were of more utility in this study because their results were less affected by “salt-and-pepper” noise and provided extra land-cover probability/membership layers.

A novel change-detection algorithm was proposed in this study, namely Modified Change Vector Analysis (MCVA). The MCVA operated in fuzzy-membership space, considered change uncertainty during the thresholding stage, and utilized change-vector directions to modify the determination of change/no-change status for each pixel. A fuzzy Markov Random Field (FMRF) model was applied to further refine the change

maps by incorporating spatial change uncertainty. A second thresholding stage was also applied to separate a type of change referred to as “transitional change,” which preserved fuzzy membership information and provided a concise map output. Compared with three traditional change-detection algorithms, the MCVA achieved higher change-detection accuracy and provided more detailed change dynamics regarding the land-surface change.

Dynamics of major floodplain cover types (i.e., oxbow lakes, river, sand, forest, non-forest vegetation, and dry and wet soil) were investigated via multi-temporal analysis. Over the observing period of 1987 to 2006, 74.4% of pixels remained the same land-cover, 20% experienced clear land-cover change and 5.6% experienced transitional land-cover change. The riparian area experienced more dramatic change than other parts of the Rio Beni floodplain during this period. Additional analysis of landscape metrics provided information regarding the spatial patterns of the land-cover, but future work would be needed to further examine its utility in understanding floodplain dynamics.

This study provides information on remote-sensing-based mapping and quantitative characterization methods for meandering river floodplains. The spatiotemporal patterns of landscape on Rio Beni floodplain can be used in sustainable management and protection of floodplain ecosystems.

DEDICATION

I dedicate this thesis to my loving parents.

ACKNOWLEDGEMENTS

I would like to thank my committee chair, Dr. Anthony Filippi, my committee co-chair, Dr. İnci Güneralp, and my committee member, Dr. Huiyan Sang, for their guidance and support throughout the course of this research and the pursuit of my master's degree.

I would also like to thank Dr. Burak Güneralp for his help and support to my research. Thanks also go to my friends and colleagues, and the department faculty and staff for making my time at Texas A&M University a great experience.

Finally, thanks to my mother and father for their endless love, support and encouragement.

TABLE OF CONTENTS

Page

LIST OF FIGURES

Page

LIST OF TABLES

Page

1. INTRODUCTION

1.1 Introduction

Meandering river floodplains are complex systems with dynamic landscape changes. Such dynamics of landforms are controlled and driven by multiple earth surface processes. Floodplains are critical maintaining regional and global ecological integrity, as they perform a variety of ecosystem functions, such as providing habitats for aquatic/riparian plants and animals (Amoros and Bornette 2002), being an indispensable part of nutrient and biogeochemical cycles (Schramm Jr et al. 2009), and uniquely influencing arrangement of landforms (Hughes 1997). The vast tropical floodplain in South America, not only limited to Amazonia, is one of the most dynamic and ecologically-productive regions on Earth (Pereira, Congalton, and Zarin 2002). Previous research has paid attention to long-term change of land-use and land-cover (Jung et al. 2010; Mertes et al. 1995; Pereira, Congalton, and Zarin 2002), but further efforts are still required to study the temporal and spatial dynamics of meandering river floodplains (Hudson, Heitmuller, and Leitch 2012). A better understanding of spatiotemporal landscape patterns in tropical floodplains, as well as the influences from the underlying processes, is necessary to predict future landscape dynamics and implement effective resource management strategies (Pereira, Congalton, and Zarin 2002).

Remote-sensing data and techniques have been widely used to study floodplain landscape change (Jung et al. 2010; Pereira, Congalton, and Zarin 2002). Among previous studies, traditional pixel-based crisp classification methods are popular to map

and monitor the change of fluvial land-covers. However, this old scheme may omit crucial information in the areas where land-cover borders are not clear (e.g., transforming buffer zones in riparian areas), which is not suitable for a binary or crisp representation (Schmitt, Bizzi, and Castelletti 2014; Legleiter and Goodchild 2005). Recently, new mapping methods, including fuzzy classification, have been introduced to the field of geoscience to address this general issue (Benz et al. 2004; Colditz, Schmidt, and Dech 2008; Dronova, Gong, and Wang 2011; Townsend and Walsh 2001). Many researchers have demonstrated good results of introducing soft classification and analysis schemes to explore gradual transition change information of floodplain environments, which aimed to characterize floodplain landscapes change without huge loss of information (Dronova, Gong, and Wang 2011; Legleiter and Goodchild 2005; Townsend and Walsh 2001). However, hard/crisp change-detection approaches remain very popular among change-detection studies and applications, given its simple procedure and clarity in evaluation (Suess et al. 2015, Zhang and Stuart 2001). Therefore, in order to retain and utilize the advantages of both soft and hard change-detection approaches, this research provides a novel change-detection algorithm based on a hard change vector analysis (CVA). Two specific thresholding stages are applied to produce a "transitional change" type that not only preserves fuzzy membership information but also enables a concise change map.

Also, landscape metrics analysis is also an effective approach to quantitatively characterize land-cover change (Apan, Raine, and Paterson 2002; Herzog et al. 2001; Schuft et al. 1999). These statistical indicators can synthesize multiple variables to

extract spatial configurations of landscapes, which are useful complementary information for the numerical statistics of land-cover distribution produced by image classification and change-detection (McGarigal et al. 2005). As McGarigal, Cushman, and Ene (2012) indicated that landscape metrics analysis is still limited by a lack of proper interpretation framework, this research aims to advance the work of selecting and interpreting proper landscape metrics to describe spatial configuration of riparian vegetation and other critical land-covers on floodplains.

Overall, by combining an effective classification method, a novel change-detection approach, and a landscape metrics-based analysis, this research aims to develop a framework to improve the abilities to characterize the spatial patterns and long-term landscape evolution of a large dynamic meandering river floodplain.

1.2 Objectives

1) Comparison of the performances of multiple pixel-based, hard and soft classification algorithms. This objective aims to explore which classification paradigm is more accurate and informative in mapping floodplain land covers.
2) Development of a novel change-detection algorithm by incorporating fuzzy land-cover information. This objective aims to address the incompatibility between traditional crisp classification and transitional areas on floodplains.
3) Multi-temporal analyses of image-derived variables/characteristics are conducted to facilitate understandings of long-term floodplain evolution. In particular, the

effectiveness of using landscape metrics to characterize land-cover on floodplains and to explain the underlying processes is examined.

1.3 Organization of the Thesis

The thesis is composed of six sections. The content of each section is summarized below:

- Section 1 is an introduction to the subject and objectives of this research.
- Section 2 is the literature review which provides a coherent and comprehensive summary of remote-sensing image classification, change-detection algorithms, and landscape metrics analysis.
- Section 3 introduces materials and methods used in this research.
- Section 4 presents the results of this research.
- Section 5 discusses the findings of this research, including the efficacy of the methods used, and the characterization of the Rio Beni floodplain landscape change based on the synthetic analysis of the observed results.
- Section 6 is the conclusion of this research which summarizes this research and discusses future research work.

2. LITERATURE REVIEW

2.1 Image Classification

Regarding multi-year floodplain evolution, it is challenging but critical for understanding the nature of landscape dynamics; meandering-river floodplains can be difficult to characterize due to their complexity and dynamics (Legleiter and Goodchild 2005; Poole, Frissell, and Ralph 1997; Roper et al. 2002; Schmitt, Bizzi, and Castelletti 2014). Geographic information science (GIS) and remote-sensing technology provide utilitarian means of observing Earth surface processes across varying scales, and such methods have been effectively employed to monitor long-term evolution of floodplain landscapes (Freeman, Stanley, and Turner 2003; Jung et al. 2010; Mertes et al. 1995; Michalková 2009; Camporeale et al. 2005; Hamilton et al. 2007; Pavri and Aber 2004; Pereira, Congalton, and Zarin 2002). These studies have shown that digital images collected by various remote-sensing sensors and platforms assure sufficient data sources that cover large spatial extent and long period, and the GIS tools provide powerful functions and abilities that enable researchers to extract information and analyze their problems of interest.

Image classification is a classic processing step to turn raw image resources into basic data that reflect the land-cover types within study areas, which is commonly the first step of conducting studies related to land-cover change (Jensen 2005). Most researchers have adopted traditional hard pixel-based data-processing and analysis procedure because of its efficiency and effectiveness (Lu and Weng 2007). However,

there has been an emerging discussion that argues this traditional discrete mapping strategy is not able to fully describe the real-world landscape (Bardossy and Samaniego 2002; Fangju 1990; Zhang and Stuart 2001). Traditional mapping of land-cover is crisp, which is not compatible with the fact that land-cover is best represented via a continuous field, especially in a fluvial environment (Legleiter and Goodchild 2005; Schmitt, Bizzi, and Castelletti 2014). Such discrepancy may cause information loss in areas where land-cover boundaries are not clear (Fangju 1990), such as episodic interconnected zones on floodplains or transitional ecotones (Burrough 1989).

Alternatively, soft (or fuzzy) classification and analysis have been introduced to geographers since late 1980s (Kent and Mardia 1988; Wang 1989). In general, soft classifications assign possibilities/memberships of every class to pixels in the image (Jensen 2005). Fangju (1990) examined the loss of information in traditional classification method, and how fuzzy classification could be used to reduce the loss. Foody and Boyd (1999) identified partial changes in an ecological transect in West Africa where a forest-savanna transition occurred based on fuzzy classification. Fuzzy membership values of four classes were presented to illustrate the general trends and gradual transitions in land-cover along the transect. Townsend and Walsh (2001) applied fuzzy set theory to the accuracy assessment of remote-sensing classification on plant composition in the vegetated floodplain. It showed that a continuous scale of membership could simulate the natural variability and transitional nature of the study area. Benz et al. (2004) studied the synergetic use of object-based and statistical signal processing methods (e.g., fuzzy classification) to explore richer information that enables

more detailed representation of floodplain and wetland. Colditz, Schmidt, and Dech (2008) indicated that soft classification is also effective with coarse spatial resolution time-series images. These works have demonstrated the promising potentials of introducing soft classification and analysis schemes to explore the unique information to characterize floodplain environments.

As discussed above, both hard and soft classifications have their advantages, but there are only a few studies that compared their performances (Marpu, Wijaya, and Gloaguen 2008; Pepe et al. 2010). For example, Shanmugam, Ahn, and Sanjeevi (2006) compared the soft classification based on linear spectral mixture modeling (LSMM) with traditional ISODATA and MLC algorithms on their results of mapping and monitoring coastal wetland ecosystems. Results demonstrated the LSMM had higher reliability compared to the two traditional approaches, and LSMM was suitable to identify small wetland habitats with sub-pixel inclusions and to represent continuous gradations between different habitat types. Bastin (1997) compared three different soft classifiers for pure coarse pixel signatures. The author claimed that as soft classifiers performed very differently and had different strengths, their suitability for specific research purposes and applications need to be experimentally determined. All these studies were conducted based on a specific geographic background (e.g., coastal wetland, Alpine landscape), and they indicated there is a need to select suitable schemes and classifiers according to the purpose of study and type of study area. So far, no detailed comparison of hard and soft classifications has been made specifically for a meandering river floodplain environment. Thus, a classification comparison is required to examine which

approach can extract more accurate information to better map and provide valuable data to study floodplain landscape evolution.

2.2 Change-Detection Methods

Land-use/land-cover change is an important field in environmental change research (Ramankutty and Foley 1999). Precise mapping of land-use/land-cover changes becomes necessary foundation for further understanding of the mechanism of Earth surface dynamics and the impact of change on environments and ecosystems (Singh 1989). Remote-sensing change-detection is the process of identifying areas that experienced surface change and classifying different types of land-cover changes using remote-sensing imagery of the same geographic area acquired at different times (Jensen 2005). In the past few decades, change-detection of remote-sensing has become a popular research field, and numerous change-detection techniques have been developed and implemented on different projects and applications (Hussain et al. 2013; Lu et al. 2004; Radke et al. 2005; Singh 1989; Tewkesbury et al. 2015). Overall, six broad categories of these change-detection methods have been identified and summarized by Tewkesbury et al. (2015): (1) layer arithmetic that based on numerical comparison of image radiance or derivative features; (2) post-classification change (PCC) that based on the comparison of multiple classification maps; (3) direct classification that based on classification of a stack of multi-temporal data; (4) transformation that based on a mathematical transformation to highlight variance between images; (5) change vector analysis (CVA) that based on the computation of difference vectors; and (6) hybrid

change-detection that uses multiple comparison methods within a workflow. Among these six categories, PCC and CVA are two very popular categories with many successful examples and applications (Tewkesbury et al. 2015). However, PCC is limited by the quality of input classification maps and error accumulation (Lu et al. 2004), whereas CVA is more useful and operational for investigating land-cover change because it effectively avoids the cumulated errors and provides "from-to" change types (Chen et al. 2003; Warner 2005; Ye, Chen, and Yu 2016). Therefore, in this research, the change-detection algorithm is developed based on CVA concept.

2.2.1 Overlapping Issue in CVA Thresholding

The CVA technique requires to compute a multi-dimensional change vector for each pair of pixels of two images acquired at different times to represent the corresponding change magnitude and direction during this period (Jensen 2005). This results in a difference image of change magnitude and usually a thresholding step is followed to determine pixels as changed or unchanged (Bovolo and Bruzzone 2011; Bruzzone and Prieto 2000; Chen et al. 2003; Singh and Talwar 2015). Simply, if the change magnitude of a pixel is lower than a specific threshold value, the pixel is grouped as an unchanged pixel; otherwise, it is a changed pixel. Although many thresholding techniques have been developed and intensively studied, a critical drawback still exists: there is an overlapping zone in the change magnitude space between the changed and unchanged pixel groups where a single static threshold value fails to perform the discrimination (Bazi, Melgani, and Al-Sharari 2010; Bovolo, Bruzzone, and Marconcini

2008). Therefore, the resulting change map produced by a single global threshold can be severely affected by the errors generated from the overlapping zone. Also, Bovolo and Bruzzone (2007) noted that most applications related to CVA only use change magnitude to identify changed pixels, which usually results in incomplete exploitation of information. Also, Xian, Homer, and Fry (2009) indicated that if a single threshold is used to segregate areas of change or no-change for all land cover "from-to" change types, then changed areas can be either over-extracted or under-extracted.

For some other prior studies related to CVA, soft computing methods have been used to separate pixels into change/no-change categories (Baisantry, Negi, and Manocha 2012; Ghosh, Mishra, and Ghosh 2011; Velloso and Souza 2002). For example, Baisantry, Negi, and Manocha (2012) applied principal component analysis (PCA) to difference image and set a threshold by incorporating fuzzy change information from an inverse triangular function. Several papers from Ghosh and Mishra (Ghosh, Mishra, and Ghosh 2011; Mishra, Ghosh, and Ghosh 2012a, 2012b) used unsupervised fuzzy clustering algorithms and considered contextual information to cluster pixels into change/no-change groups without determining a static global threshold. Velloso and Souza (2002) adopted a 2-D histogram with CVA change magnitude and average magnitude of neighboring pixels. They determined the change threshold by searching the maximum fuzzy entropy. Although these studies may not suffer from the overlapping issue as either the threshold determination incorporated some fuzzy information or there was not a threshold determination at all, no evidence or further study has been put forward to prove their effectiveness to resolve the overlapping issue.

The present research focuses on addressing the overlapping issue based on a global thresholding method. Given the above discussion, a new thresholding approach to overcome the drawback of the overlapping issue in a conventional CVA approach will make a marked contribution to the literature via its efficacy in achieving higher change-detection accuracy.

2.2.2 Conundrum Between Fuzzy Membership Information and Practicability

Same as the traditional hard image classification scheme, traditional change-detection approaches (e.g., CVA) produce discrete land-cover change maps. However, again, in reality, landscape evolution is a continuous process that is not likely to form significant discrete boundaries between different land-covers, especially in areas with dramatic change and controlled by multiple natural processes (Guevara and Laborde 2008; Hollenhorst, Host, and Johnson 2006). There is thus still a profound discrepancy between the landscape representations provided by traditional change-detection approaches and the actual situation (i.e., the actual spatial and spatiotemporal variability), which can lead to information loss and the potential for misinterpretation (Fangju 1990), no matter how good the change-detection accuracy is.

In the late 1990s, the fuzzy concept also started to be used in various research related to change-detection in remote sensing. Foody and Boyd (1999) identified partial changes in an ecological transect in West Africa where a forest-savanna transition occurred based on fuzzy classification. Fuzzy membership values of four classes were presented to illustrate the general trends and gradual transitions in land-cover along the

transect. Fisher et al. (2006) presented a fuzzy change matrix method to map subtle variations of land-cover changes in ecotones. Such a matrix consisted of fuzzy membership-value maps and “from-to” change maps of different land-cover types and change in those types. They also indicated that this method could provide more accurate gain and loss of a land-cover type. Dronova, Gong, and Wang (2011) studied the major wetland cover types at Poyang Lake based on object-based analysis and fuzzy change-detection. They presented the spatial distribution and value of the change in fuzzy membership of four major land-cover types and discussed the uncertainty and fuzziness regarding land-cover change. Suess et al. (2015) demonstrated the use of class probabilities to map gradual transitions in shrub vegetation. Their approach provided both discrete output maps and sub-pixel cover fraction-estimation maps to improve qualitative and quantitative descriptions of gradual transitions. Zhu, Woodcock, and Olofsson (2012) proposed a Continuous Monitoring of Forest Disturbance Algorithm (CMFDA) uses all available Landsat images in the monitoring period to detect where and when forest disturbance happens due to human interference. CMFDA applies a multi-date differencing algorithm to determine a disturbance pixel by the number of times that showing change happens. Pixels showing change for one or two times is flagged as “probable change.” If a third consecutive change is found, the pixel is assigned to “change” class. This “probable change” class contains some degree of fuzzy information, but this algorithm requires at least several consecutive Landsat images as input, which limits/hinders its utility.

However, despite the results and development in fuzzy change-detection so far, hard/crisp change-detection approaches remain very frequently used, given its simple procedure and clarity in evaluation for many applications (Suess et al. 2015, Zhang and Stuart 2001). Indeed, the lack of practicability and interpretability seems to be a common issue in much research related to fuzzy change-detection. These studies have focused on exploring the fuzzy membership information, but have not allocated much attention to hardening the output maps for enhanced/ease of interpretation. For example, in Fisher et al. (2006), there were only four major land-cover types considered, but the fuzzy change matrix consisted of 16 maps, which made it difficult to interpret. Also, although Dronova et al. (2011) reclassified the fuzzy membership-change maps to generalize the results, there were still 12 maps for four land-cover types. These studies maximally retained the fuzzy membership information by presenting soft maps at the expense of some clarity by not producing hard/crisp results. To address this issue, some researchers have implemented basic hardening methods to produce hard change maps, i.e., assigning the class with maximum membership value to each pixel is a common procedure (Foody and Boyd 1999, Legleiter and Goodchild 2005). This is a simple method that provides traditional crisp change maps, but the fuzzy membership information is largely lost during the process.

As this research is focused on a meandering river floodplain environment, precise and accurate representation of floodplain transition areas is important to characterize fluvial landscape evolution. Information of such precision and accuracy is not available from traditional crisp methods because some changes in these areas are too

subtle and gradual to be detected—particularly over relatively short time periods—by traditional pixel-based approaches. However, a pure fuzzy change-detection approach is also not appropriate as it will result in high volume of output data and hinder an effective interpretation and analysis. Therefore, in order to retain and utilize the advantages from both soft and hard outputs, this research aims to provide a new change-detection algorithm that based on CVA concept but includes two thresholding stages. The first thresholding steps aims to improve change-detection accuracy by addressing the drawback from the overlapping issue in CVA; the second thresholding step aims to not only include the land-cover change fuzziness (i.e., transitional change) but also gives consideration to concise, discrete outputs (i.e., hardening the fuzzy change results with a more considerable threshold criterion).

2.3 Landscape Metrics

In study and analysis of landscape change and evolution, a traditional approach is to explore information from a variety of statistical data that quantify the nature of landscape change (Ferreira, Aguiar, and Nogueira 2005; Gurnell 1997; Gurnell et al. 1998; Looy, Meire, and Wasson 2008). Particularly in the background of image classifications of remote sensing, it becomes common in counting and analyzing the number of pixels changed and their types of “from-to” change based on the resulting maps of image classification and change-detection (Jensen 2005; Lu et al. 2004; Tewkesbury et al. 2015). This approach can quantitatively demonstrate and generalize the composition of land-cover types, their abundance, and the phenomenon of change

from one land-cover to another (Jensen 2005). However, it considers all pixels independently and ignores the spatial patterns, structures, and configurations of landscape patches – homogenous areas differing from surroundings land-covers (Forman and Godron 1981; Gustafson 1998). Results from floodplain landscape geomorphological and ecological studies suggest that incorporating spatial relationships and structures is necessary to reflect and characterize critical underlying processes (Gurnell et al. 1998; Turner 1989). Also, Tormos et al. (2012) indicated that future work needs to determine better spatial indicators to represent the status of riparian areas. Thus, an effective and quantitative measurement of the structure of floodplain landscapes is necessary in order to thoroughly investigate floodplain landscape evolution (Turner 1990; Turner et al. 2003).

Landscape metrics are algorithms and indices that quantitatively describe spatial configurations as well as spatial relationships among patches, classes of patches, or entire landscape (McGarigal et al. 2005; McGarigal 2014). A wide range of landscape metrics has been developed to quantify categorical patterns, which covers aspects including spatial characteristics, landscape arrangement, positions or orientation of patches (McGarigal, Cushman, and Ene 2012). Many studies have investigated the effectiveness of landscape metrics as a tool to characterize the structures of riparian/floodplain vegetation and other landscape components (Apan, Raine, and Paterson 2002; Fernandes, Aguiar, and Ferreira 2011; Freeman, Stanley, and Turner 2003; Herzog et al. 2001; Schuft et al. 1999). For example, Apan, Raine, and Paterson (2002) conducted a case study to map and analyze changes in the riparian landscape

structure based on a combination of both traditional statistical approach and landscape metrics. Results indicated that this combined approach was capable of describing the structural change of the riparian landscape and could be beneficial to develop supporting policies and management strategies for stream segment rehabilitation and preservation. Fernandes, Aguiar, and Ferreira (2011) used landscape metrics to describe spatial configuration and inter-connectivity of riparian vegetation. They demonstrated that a certain combination of landscape metrics was suitable to detect alterations in spatial patterns of riparian vegetation due to land use pressure. They also indicated that an optimal selection of landscape metrics should be based on the specific study area and the purpose of the study.

Although aforementioned studies have provided comprehensive discussion that landscape metrics are capable of characterizing riparian landscape structures within an ecological perspective, only a few studies have discussed the relationships between landscape metrics and their change in a geomorphological context. Shoshany and Kelman (2006) applied five landscape metrics to characterize the complementary soil and vegetation patterns. The mutual variations in soil and vegetation represented by those metrics revealed differentiations between different pattern evolution stages (e.g., perforation, dissection, fragmentation), which might be an indication of underlying hydro-geomorphological process. Hamylton and Spencer (2011) developed an explanatory model to investigate factors influencing the linearity of alternating carbonate sand and seagrass patches on a reef flat based on a combination of landscape ecology metrics and spatial statistical procedures. Both studies indicated that different measures

and metrics of shape and pattern were expected to produce different information contents with regard to the geomorphological processes shaping the landscape. However, further work is needed on further developing a proper data interpretation framework in order to fully understand the information behind each landscape metric (McGarigal, Cushman, and Ene 2012).

As discussed above, previous literature has proved the promising potentials in combining landscape metrics and conventional statistical approach to investigate landscape change. However, questions remain in the selection of suitable landscape metrics for specific applications, which should reflect some assumptions about the observed landscape and what processes might be responsible for that landscape pattern (McGarigal, Cushman, and Ene 2012). Also, a proper interpretation of the landscape metrics is required to better understand the relationships between the structural landscape phenomena and underlying responsible geomorphic processes.

3. MATERIALS AND METHODS

3.1 Study Area

The study area lies on the mid-stream portion of Rio Beni (the Beni River) floodplain in northern Bolivia (Figure 1). The extent of the study area is between 12°31′34″ - 13°49′19″ south latitude and 66°54′04″ - 67°32′05″ west longitude. This is a banding shape area with about 2060 km^2 and the borders are about 3.6 km away from the main river channel of Rio Beni. The study area is located in the center-right portion of the Landsat 5 Thematic Mapper scene on Path 1 and Row 69. This position in a Landsat scene only has little geometric distortion, which provides a nice foundation for accurate land-cover classification and analysis.

The study area is entirely within the Bolivian part of Amazonia and it has a typical tropical climate with mean annual precipitation of 1894 mm and mean temperature of 25.1 °C. Despite its year-round warm and humid climate, the study area is characterized by a pronounced seasonal variability. Precipitation is most likely around February, occurring in 48% of days. Precipitation is least likely around September, occurring in 16% of days. High water level occurs during the warm season (December - April), January - March containing half of the time-integrated discharge of the river (Gautier et al. 2007). Lowest discharges occur during June to August due to low precipitation. Over the entire year, the most common forms of precipitation are light rain, thunderstorms, and moderate rain.

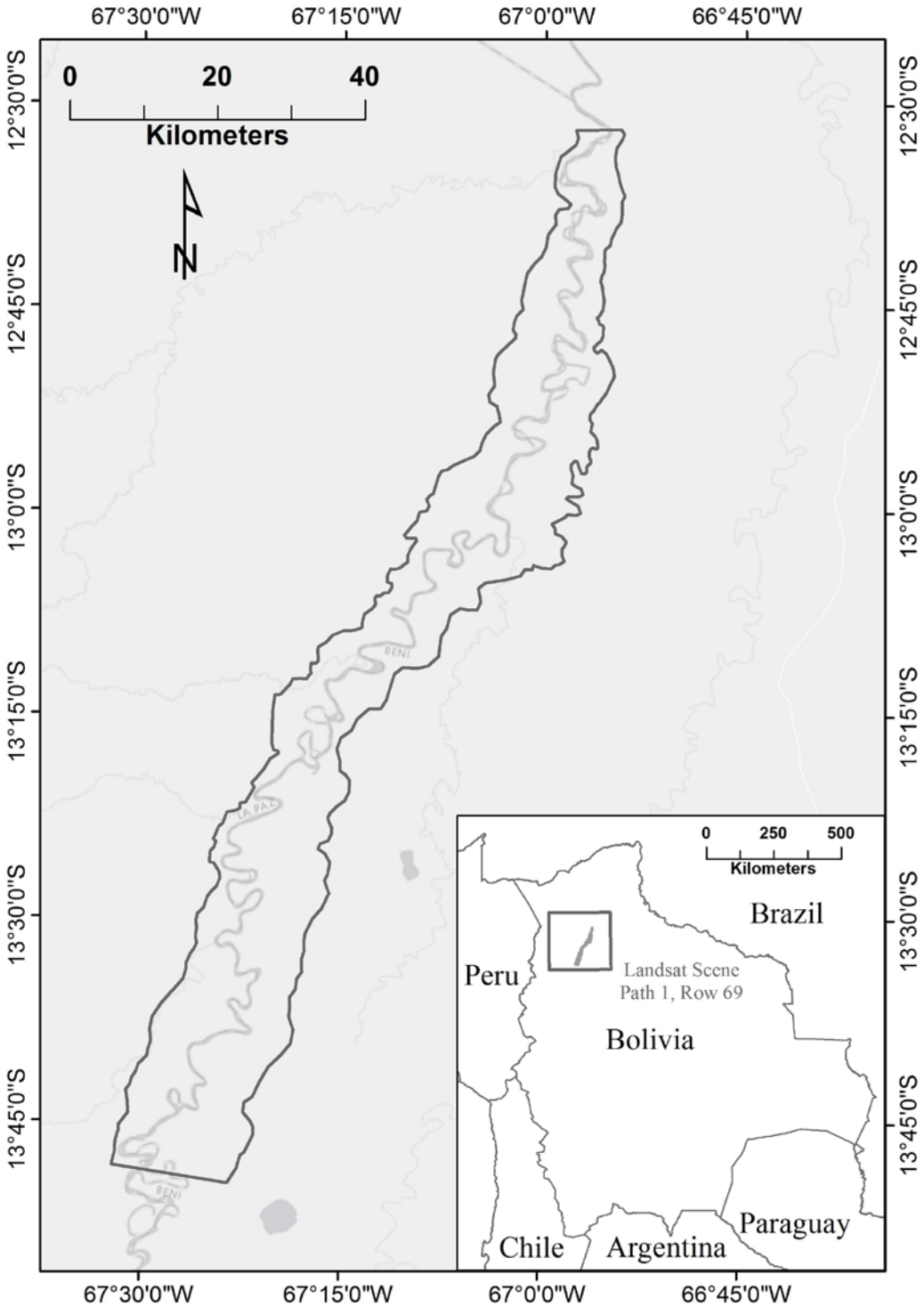

Figure 1. Location map of the study area within Landsat 5 Thematic Mapper (Landsat 5 TM) scene (Path 1, Row 69).

This section of Rio Beni main channel has an approximate length of 320.7 km throughout the observing years from 1987 - 2006. It is a very active meandering river (Figure 2), with the sinuosity index varies between 1.5 and 2 in the upper part of the floodplain and from 3.5 - 4 downstream (Gautier et al. 2010). This area is full of oxbow lakes and abandoned channel scars that indicate the dramatic change of meandering river and surrounding landscapes. The gauge downstream of the study area is located at Rurrenabaque with a mean annual discharge of 2200 $m^3 s^{-1}$ (Aalto et al. 2003). Due to variation in precipitation, discharge is also irregular annually. Major floods usually happen during February - March with maximum discharge from 12000 - 20000 $m^3 s^{-1}$; whereas the lowest discharge can be as low as about 1500 $m^3 s^{-1}$.

The land-cover types at the study area are primarily oxbow lakes, mature tropical forest, non-forest vegetation (e.g., smaller trees and shrubs), sand-bars along the river, and bare soil surfaces (dry and wet conditions). Riparian vegetation consists of a community of *Tessaria integrifolia*, including young *Salix humboldtiana*, and *Gynerium sagittatum*. Besides riparian areas, non-forest vegetation is also observed significantly on abandoned channel scars and around oxbow lakes. Dense vegetation, such as forest area, is dominated by *Cecropia membranacea* (Gautier et al. 2010). It distributes abundantly in areas with less active river migrating processes along/away from the main river channel. Sand-bars that formed by sediment deposited around meanders can be easily observed along this section of Rio Beni. Overall, the study area is essentially pristine, without artificial levees, dams, dredging, roads, significant deforestation,

cultivation to affect the geochronology or other complications detracting from the study of natural floodplain and fluvial processes (Aalto and Nittrouer 2012).

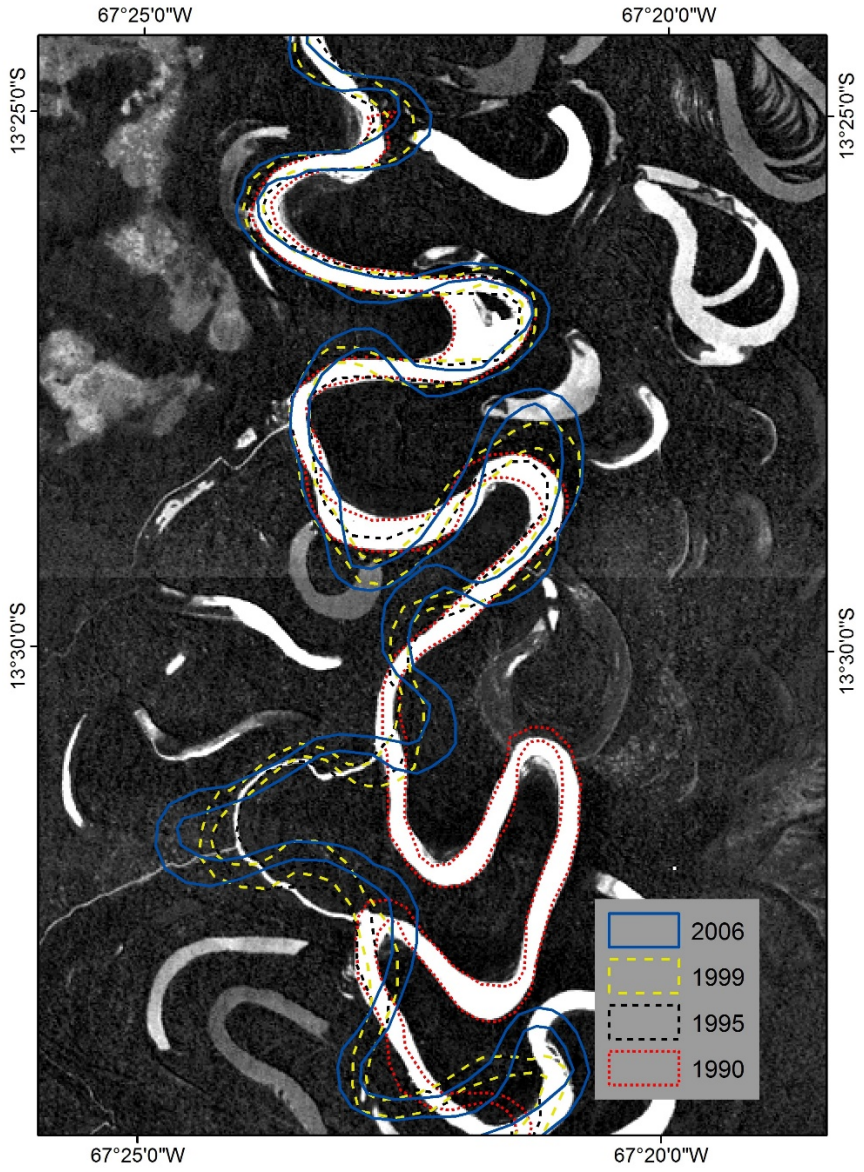

Figure 2. 1987–2006 migration of the meandering bends in middle section of study area (background image: Landsat 5 TM in 1987).

3.2 Data

In order to conduct the study of long-term landscape evolution on a floodplain at this scale, Landsat 5 TM images were selected as primary input data based on its long term-image archive, multiple spectral bands, and suitable spatial resolution. Landsat 5 was launched in March 1984 and served more than 18 years before it was decommissioned in January 2013. It carried the Multispectral Scanner System (MSS) sensor and the Thematic Mapper (TM) sensor with a 16-day repeat cycle, referenced to the Worldwide Reference System-2. TM is a more sophisticated, whisk broom multi-spectral scanner that was designed to achieve higher image resolution, sharper spectral separation, improved geometric fidelity and greater radiometric accuracy and resolution than the MSS sensor. TM takes seven spectral band images simultaneously across its ground track. Band spectrum range is 0.45 - 12.5 μm. A TM scene entails a ground-projected instantaneous field-of-view (GIFOV) of 30 m × 30 m in bands 1-5 and 7, whereas band 6 has a GIFOV of 120 m × 120 m. In this research, only bands 1-5 and 7 were used. Table 1 below lists the specifications of each band used.

Table 1. Spectral bands for Landsat 5 Thematic Mapper (excluding band 6).

Band Number	Spectral Range (μm)	Resolution (m)
1	0.45-0.52	30
2	0.52-0.60	30
3	0.63-0.69	30
4	0.76-0.90	30
5	1.55-1.75	30
7	2.08-2.35	30

Five Landsat 5 TM images of the study area were selected for analysis from the years 1987, 1990, 1995, 1999, and 2006 during July to September, respectively (Table 2). The selection is based on two factors: cloud and landform situations. The study area is often cloudy with median cloud cover ranging from 52% (partly cloudy) to 91% (mostly cloudy) (WeatherSpark 2016). Such environmental characteristics cause problems in collecting effective Landsat TM data as TM sensors cannot penetrate cloud and scan radiations from ground land-covers. The clearer part of the year begins in July and end in October, and the five selected scenes are completely cloud-free. Also, the study area is in dry season during these months due to low precipitation. Low water level ensures the revelation of most landforms without disturbance of flood events, which provide more information about the landscape evolution. All files were downloaded from USGS EarthExplorer (http://earthexplorer.usgs.gov/).

Table 2. Landsat 5 TM images analyzed in this research.

Image ID	Description	Format
LT50010641987214XXX02	Landsat 5 TM image for Aug-02-1987	GeoTIFF
LT50010641990270CUB01	Landsat 5 TM image for Sep-27-1990	GeoTIFF
LT50010641995188CUB00	Landsat 5 TM image for Jul-07-1995	GeoTIFF
LT50010641999215XXX03	Landsat 5 TM image for Aug-03-1999	GeoTIFF
LT50010692006186COA00	Landsat 5 TM image for Jul-05-2006	GeoTIFF

The original Landsat 5 TM scene covers an area of 185 km east-west by 172 km north-south with 7456 samples and 7032 lines (Figure 3). As its extent is much larger than the study area, the images were spatially subset via the ENvironment for Visualizing Images (ENVI) software (version 4.8) to eliminate peripheral areas outside floodplain boundaries. Figure 4 shows the processed images.

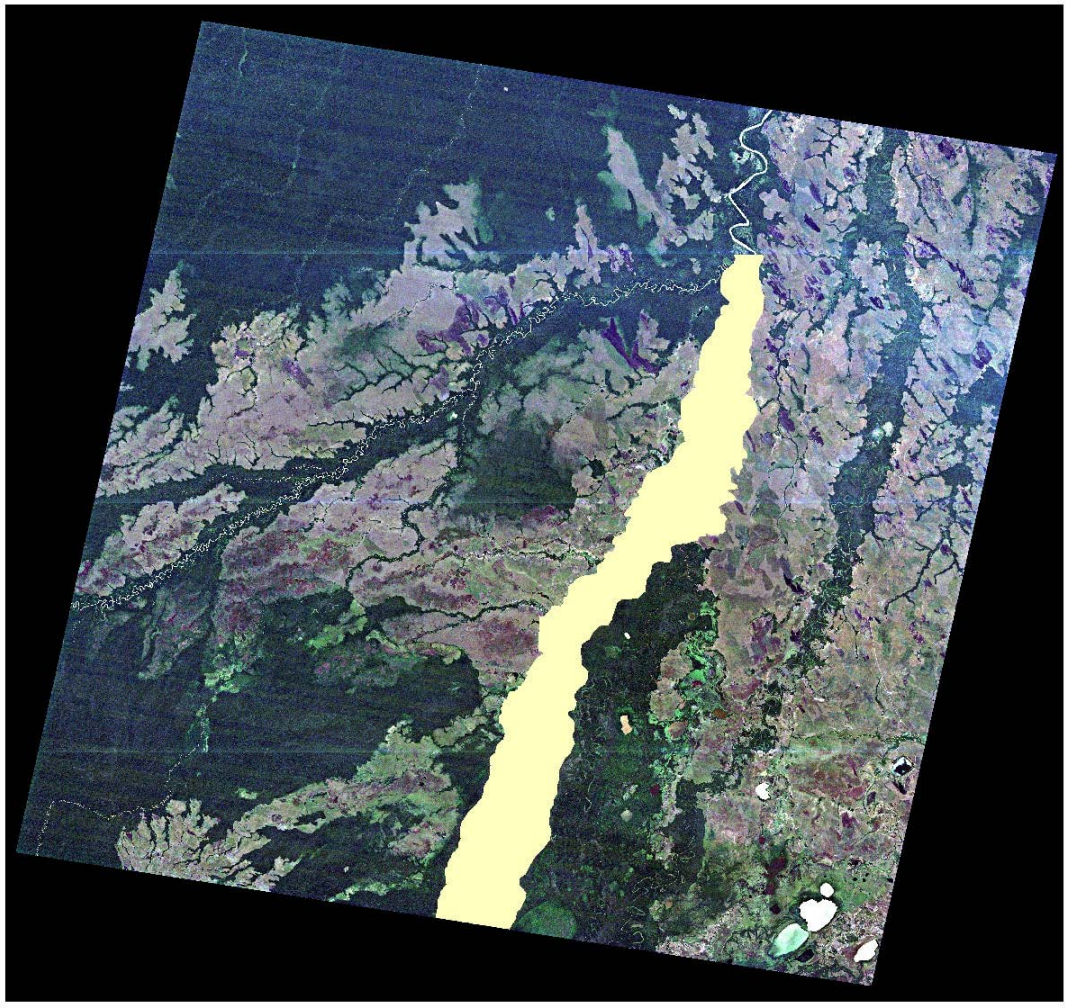

Figure 3. The Landsat 5 TM scene (Row: 1, Path: 69) and the extent of study area in yellow.

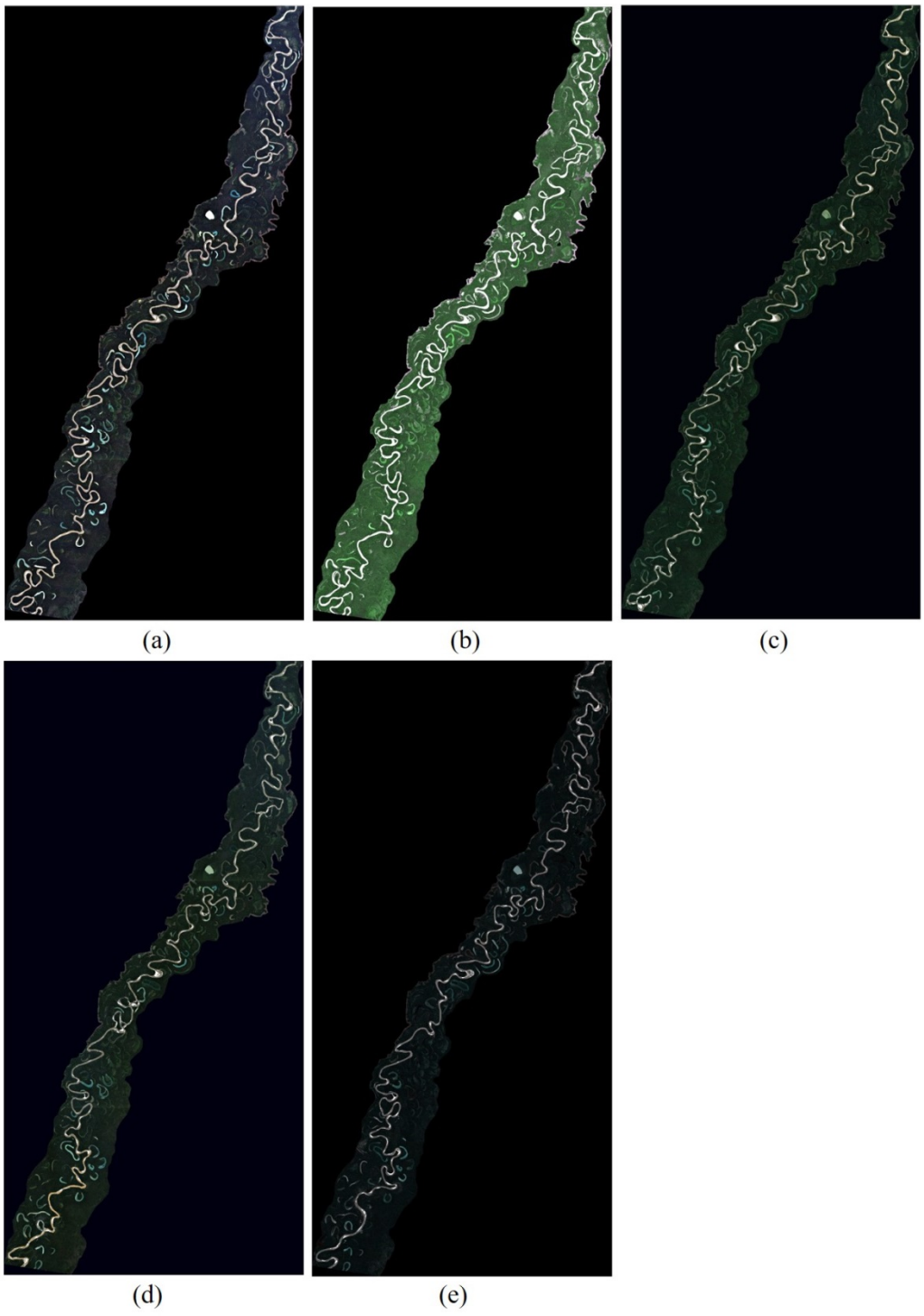

Figure 4. Landsat 5 TM image of the study area after spatial subsetting, displayed with bands 3, 2, 1 as R,G,B. (a) Aug-02-1987; (b) Sep-27-1990; (c) Jul-07-1995; (d) Aug-03-1999; and (e) Jul-05-2006.

3.3 Image Pre-Possessing

Historically, two processing systems have generated the Landsat standard data products for USGS – Level 1 Product Generation System (LPGS) and National Land Archive Production System (NLAPS). Most Landsat 5 TM scenes/images, including the five images in this research, were processed through LPGS before being made publically accessible. There are three correction levels within LPGS: Standard Terrain Correction (Level 1T, or L1T), Systematic Terrain Correction (Level 1GT, or L1GT), and Systematic Correction (Level 1G, or L1G). L1T provides systematic radiometric and geometric accuracy by using ground control points and a digital elevation model (DEM) to account for topographic displacement; this correction level provides the best correction in those three levels, and the five Landsat 5 TM scenes used in this research were Level 1T data products.

In addition to the systematic corrections, further atmospheric correction was also necessary to achieve significant spectral signatures from ground land-covers. Atmospheric correction is an important image preprocessing step for some analyses of multi-data remote sensor data (Song et al. 2001). Removal or minimization of atmospheric effects facilitates the maximization of exploitation of information content in remotely-sensed images of the Earth surface. Among various atmospheric correction algorithms and methods, the Fast Line-of-sight Atmospheric Analysis of Spectral Hypercube (FLAASH®) radiative transfer model was performed to atmospherically-correct the Landsat 5 TM images. FLAASH is a first-principles atmospheric correction module to remove atmospheric effects in most multispectral and hyperspectral imagery

(with wavelengths ranging from visible to shortwave infrared regions) by converting image spectral radiance to surface spectral reflectance. FLAASH is based on MODTRAN4 radiation transport model that has been developed collaboratively by Spectral Sciences, Inc. and the U.S.A. Air Force Research Laboratory (AFRL), with assistance from the Spectral Information Technical Applications Center (SITAC) and Research Systems, Inc. (RSI) (Perkins et al. 2005).

FLAASH was performed within the model in ENVI version 4.8. Several image parameters are required by FLAASH module in order to successfully correct the Landsat 5 TM images. These parameters include sensor type, pixel size, ground elevation, scene center latitude/longitude, sensor altitude, visibility, flight date and flight time, atmospheric model, aerosol model, water vapor retrieval, spectral polishing, and wavelength calibration. Many of these systematic parameters (e.g. scene center, flight time) could be found in metadata file or were filled in automatically based on sensor type. The most decisive user-defined parameters were the atmospheric model, aerosol model, and aerosol retrieval. The atmospheric model could be selected among six standard MODTRAN model atmospheres: Sub-Arctic Winter (SAW), Mid-Latitude Winter (MLW), U.S. Standard (US), Sub-Arctic Summer (SAS), Mid-Latitude Summer (MLS), and Tropical (T). Based on the seasonal-latitude surface temperature model table provided by ENVI, the Tropical atmospheric was selected for this research (Table 3). The aerosol model used here was the standard MODTRAN rural model. For aerosol retrieval, FLAASH module includes a procedure to retrieve the aerosol amount and estimate the average visibility of a given image based on a dark pixel reflectance ratio

method (Kaufman et al. 1997). In this research, the 2- band K-T method was employed, where for Landsat 5 TM images, bands 7 and 3 were utilized as aerosol bands.

Table 3. Seasonal-latitude surface temperature model table (Source: ENVI Docs Center, http://www.exelisvis.com/docs/FLAASH.html).

Latitude (°N)	Jan	March	May	July	Sept	Nov
80	SAW	SAW	SAW	MLW	MLW	SAW
70	SAW	SAW	MLW	MLW	MLW	SAW
60	MLW	MLW	MLW	SAS	SAS	MLW
50	MLW	MLW	SAS	SAS	SAS	SAS
40	SAS	SAS	SAS	MLS	MLS	SAS
30	MLS	MLS	MLS	T	T	MLS
20	T	T	T	T	T	T
10	T	T	T	T	T	T
0	T	T	T	T	T	T
-10	T	T	T	T	T	T
-20	T	T	T	MLS	MLS	T
-30	MLS	MLS	MLS	MLS	MLS	MLS
-40	SAS	SAS	SAS	SAS	SAS	SAS
-50	SAS	SAS	SAS	MLW	MLW	SAS
-60	MLW	MLW	MLW	MLW	MLW	MLW
-70	MLW	MLW	MLW	MLW	MLW	MLW
-80	MLW	MLW	MLW	MLW	MLW	MLW

3.4 Image Classification

To explore the utility of soft classification algorithms in mapping floodplain environments and compare the classification performance with traditional hard classification, one hard classification and two soft classification algorithms algorithm were applied to classify the Landsat 5 TM images. The hard classifier is the Iterative Self-Organizing Data Analysis Technique (ISODATA), and two soft classifiers are Bayesian classifier and Fuzzy classifier.

3.4.1 Iterative Self-Organizing Data Analysis Technique (ISODATA)

Iterative Self-Organizing Data Analysis Technique is an unsupervised classification algorithm that has been widely used in classifying multispectral satellite images (Jensen 2005). ISODATA is an iteration classifier that calculates cluster means in the multispectral feature space and group remaining pixels to the specific cluster with the minimum distance. The algorithm recalculates cluster means and reclassifies pixels with respect to the new means in each iteration. ISODATA includes procedures to merge, split, or delete class. If distances between clusters in the feature space is less than the user-defined value, two clusters merge into one; if the inter-variance of one cluster is larger than the user-defined threshold, it splits into two different clusters. The iteration process continues until certain requirements are reached, including maximum number of iterations, change ratio of pixels in each cluster, minimum pixel number in each cluster, etc. ISODATA is a modification of the k-means classifier. Thomas et al. (2011) indicated that classifying Landsat images using ISODATA is an effective way to analyze

long-term floodplain changes. Therefore, ISODATA in ENVI version 4.8 was used to crisply classify the Landsat 5 TM image and served as the baseline classifier in this research. Specifically, the maximum number of spectral clusters and the maximum number of iterations were set to 50 and 100, respectively. The output clusters were merged and labeled manually into seven land-cover classes: oxbow lake, river, sand-bar, dry soil, wet soil, forest, and non-forest vegetation (Table 4). These seven land-cover classes were also used by other two soft classification algorithms.

Table 4. Land-cover classes and descriptions.

Land-Cover Class	Description
Forest	Tropical forest
Non-forest Vegetation	Shrub, grass, small tree, etc.
Oxbow Lake	U-shaped water body not constantly connected to river
River	Main river channel
Sand	Sand, shoal
Dry Soil	Bare soil with low moisture
Wet Soil	Bare soil with high moisture

3.4.2 Bayes Classifier

Bayesian classifier is a supervised classifier that computes the posterior probability of each class according to Bayes' Theorem:

$$p(h|e)=\frac{p(e|h)*p(h)}{\sum_i p(e|h_i)*p(h_i)} \quad (1)$$

where p(h|e) is the probability of hypothesis being true given the evidence (posterior probability); p(e|h) is the probability of finding that evidence given the hypothesis being true (multivariate conditional probability, assessed based on training data); and p(h) is prior probability (Eastman 2009). p(h) is based on previous knowledge about the distribution conditions of each class, which would help the classifier perform better. As no previous knowledge was known regarding the prior probabilities with which each class can occur, which was often the case in practice, an equal prior probability for each class was applied. Bayes classifier in IDRISI generated probability layers for each class that show the probability of each pixel belongs to a particular class.

3.4.3 Fuzzy Classifier

The fuzzy classifier is a supervised classifier based on fuzzy set theory to indicate the degree of membership of a pixel to any class (Eastman 2009; Zadeh 1965). Fuzzy membership is calculated based on standardized Euclidean distance from the mean spectral signature of each class, via a sigmoidal membership function. This assumes that the mean of a spectral signature is the ideal representation of the class with the fuzzy membership value of 1. As Euclidean distance increases, fuzzy membership decreases according to the sigmoidal membership function until it reaches a specified z-score distance where fuzzy membership becomes 0. A z-score distance of 1.96 forces 5% of the pixels to have a fuzzy membership of 0, whereas a distance of 2.58 forces 1% of pixels to have a value of 0. Hence, fuzzier results are accrued with larger specified z-score distances. Since the aim of this research is to detect/discover potentially subtle but

important spatial land-cover graduation in the transition zones between classes (e.g., between the main river channel and the oxbow lakes), a z-score distance of 2.58 was used. The other parameter setting is whether membership values should be normalized. Normalization assumes that the classes employed are exhaustive (as is the case with the Bayes classifier), and thus, that membership values for all classes for a given pixel sum to 1. Therefore, fuzzy classifier generated normalized membership output layers for each class that show the membership of each class for any pixel in the image.

3.4.4 Training Sample Selection for Supervised Classifications

For supervised classification algorithms, training sample data are needed to train the classifiers before actual classification can be performed. In this research, training samples were delineated based on manual interpretation of Landsat 5 TM bands, spectral curves, tasseled-cap images, and Google Earth© images for each land-cover class described above. Table 5 lists the statistics of training samples. The distinction between forest and non-forest was in accordance with the United Nations Food and Agriculture Organization (FAO) definition of forest (i.e., non-agricultural ecosystems with a minimum of 10% crown cover of trees) (Food and Agriculture Organization of the United Nations, 2010), to the extent possible with a training sample selection process based on manual image interpretation. Also, the distinction between dry soil and wet soil was determined with synthesized considerations of visual interpretation, spectral curve, and tasseled-cap wetness index.

Table 5. Statistics of training samples.

Land-Cover Class	Number of Training Pixels
Oxbow Lake	610
Dry Soil	1804
Forest	7947
Non-forest Vegetation	7096
River	924
Sand	648
Wet Soil	113

3.4.5 Image Classification Accuracy Assessment

For all three classification algorithms, only hard classification accuracy assessments were performed due to no fuzzy in situ ground reference data was available (Filippi and Jensen 2006). Accuracy assessment was based on index-assisted visual interpretation. Specifically, Landsat 5 TM bands, spectral curves, tasseled-cap images, and high spatial resolution Google Earth© images (if images with relatively small temporal offsets with respect to the Landsat images of interest were available) were used as reference data. Prior to the assessment, soft classification results were hardened, whereby for each pixel, the class with maximum probability or fuzzy-membership (for Bayes and fuzzy classifications, respectively) was selected for class assignment. Note that as it was difficult to separate multiple water classes when generating reference data, two water classes (i.e., oxbow lake and river water) were treated as the same water class for accuracy-assessment purposes.

A minimum sample size of 50 samples per land-cover class has been recommended for conducting accuracy assessments of remote-sensing image

classifications (Congalton 1991; Foody 2010). Thus, a set of test sample locations for accuracy assessment was generated via stratified random sampling method, with 100 sample points per class (total of 600 locations per image).

Classification confusion matrices of each image were calculated to quantitatively report the producer's, user's accuracies, overall accuracy, and the Kappa coefficient. Producer's accuracy corresponds to the omission error. It refers to the accuracy that pixels in a certain land-cover class in the reference data are labeled correctly. Producer's accuracy is calculated by dividing the counts in the major diagonal for a specific class by the total counts of samples in that column. On the other hand, user's accuracy corresponds to the commission error. It refers to the accuracy that pixels labeled as a certain land-cover class on the classified image are actually what they are in reality. User's accuracy is calculated by dividing the counts in the major diagonal for a specific class by the total counts of samples in that row. Overall accuracy is calculated by dividing the total counts in the major diagonal by the total number of samples. The Kappa coefficient measures of the agreement between the classification map and the reference data by taking both diagonal and non-diagonal cells into account.

3.5 Multi-Temporal Change-Detection

Tewkesbury et al. (2015) conducted a review of the development of change-detection techniques and grouped them into six categories. Among all change-detection techniques, post-classification change (PCC) and change vector analysis (CVA) are two very popular categories with many successful examples and applications. However, both methods suffer from different defects: PCC is limited by the quality of input classification maps and error accumulation (Lu et al. 2004); whereas CVA has a strict requirement of radiometric consistency and problems of discriminating different change types when the number of bands involved is large (Chen et al. 2003). Tewkesbury et al. (2015) mentioned in their review that hybrid change-detection, which includes more than one comparison methods or stages, has showed a promising trend in recent research. Among many hybrid methods, Chen et al. (2011) proposed a method named change vector analysis in probability space (CVAPS), combing PCC and CVA to accommodate the disadvantages from both sides.

The CVA technique, including CVAPS, requires to compute a multi-dimensional change vector for each pair of pixels of two images acquired at different times to represent the corresponding change magnitude and direction during this period. This step results in a difference image, and usually a thresholding step is followed to determine pixels as changed or unchanged (Bovolo and Bruzzone 2011; Bruzzone and Prieto 2000; Chen et al. 2003; Singh and Talwar 2015). Due to the overlapping issue discussed in Section 2, the change map produced by a single threshold can be severely affected by the errors resulted from the overlapping zone. The overlapping zone contains pixels with

high uncertainty about their change status, but the traditional thresholding approaches ignore such uncertainty and result in misdetection and false alarm errors.

Based on the concept of CVAPS, a modified change vector analysis (MCVA) was developed to operate in the space of land-cover class fuzzy membership (fuzzy membership layers generated by the fuzzy classification). By utilizing fuzzy member ship information, MCVA aims to address the overlapping issue and provide concise, discrete change maps with preservation of some degree of fuzziness during the landscape change process. There are three major steps in MCVA: 1) a modified dynamic thresholding stage to address overlapping issue; 2) fuzzy Markov Random Field (FMRF) to further refine the unchanged/changed and reduce “salt-and-pepper” errors; 3) a second threshold stage to separate the changed class into two parts, namely “change” and “transitional change”, which aims to include the land-cover change fuzziness. Figure 5 illustrates the work flow of MCVA.

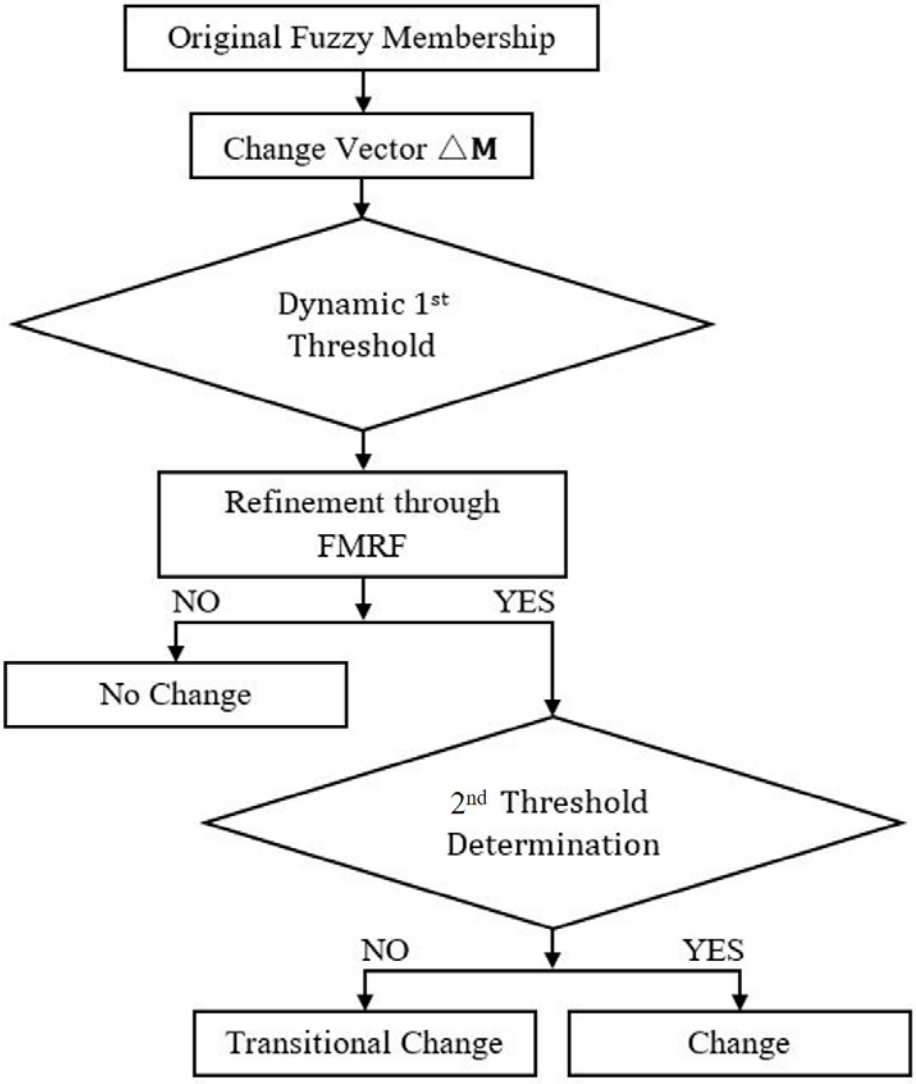

Figure 5. Flowchart of MCVA algorithm.

3.5.1 Modified Change Vector Analysis Algorithm (MCVA)

In CVAPS, each pixel has the corresponding pixel vector $\mathbf{P^{(1)}} = (p_1, \ldots, p_n)$ represents the posterior probabilities of that pixel belongs to class 1 to class n in date 1 and $\mathbf{P^{(2)}}$ in date 2. In this research, as it is operated on the fuzzy membership space, **M** will be used in the following context to represents membership vector for each pixel.

Then the change vector $\Delta\mathbf{M}$ of each pixel was computed as $\mathbf{M}^{(1)} - \mathbf{M}^{(2)}$, and the change magnitude was denoted as $\|\Delta\mathbf{M}\|$. This resulted in a change magnitude map, which was the basic operational space for a CVA algorithm.

3.5.1.1 Dynamic 1st Threshold

For a conventional approach, only a single thresholding step is applied to determine whether a pixel is changed or unchanged. Due to the overlapping issue derived from such simple approach, this step of MCVA developed a dynamic threshold approach as following:

First, a traditional single threshold was searched in a supervised manner. Assuming the threshold was searched within the change magnitude ranged between [min, max], a search increment i=(max-min)/r was set, where r is an integer to control the search precision and computational time (Song and Bo 2011). The threshold T_0 was the value that provided the best training accuracy of changed/unchanged status for the training sample set. Training samples were visually labelled the change/no-change status. Then the mean change magnitude of the changed and unchanged training samples were calculated as T_c and T_n, which were representative characteristics of changed and unchanged status. Instead of simply dividing pixels by T_0, the change uncertainty of each pixel was estimated by the fuzzy *c*-means (FCM) algorithm (Bezdek 1981). Prior studies in different fields, including remote-sensing and engineering, have indicated that fuzzy set and membership value can be used as a way of expressing uncertainty (Bone, Dragicevic, and Roberts 2005; Raina and Thomas 2012). For the change magnitude of

any particular pixel, the further away from T_0 and closer to T_c or T_n, the more certain that pixel could be identified as changed or unchanged pixel. Here, T_0 was considered as the cluster center of uncertainty, and T_c/T_n as the cluster center of certainty (to changed/unchanged), and the uncertainty of each pixel's change status was estimated by the following functions:

$$u_c = \frac{1}{1+\left(\frac{d^2(\|\Delta\mathbf{M}\|, T_0)}{d^2(\|\Delta\mathbf{M}\|, T_c)}\right)^{[1/(w-1)]}} \quad (2)$$

$$u_n = \frac{1}{1+\left(\frac{d^2(\|\Delta\mathbf{M}\|, T_0)}{d^2(\|\Delta\mathbf{M}\|, T_n)}\right)^{[1/(w-1)]}} \quad (3)$$

where u_c and u_n is the uncertainty of change and no-change, respectively; $\|\Delta\mathbf{M}\|$ is the change magnitude of a pixel; *w* is a weighting exponent; and $d^2(\|\Delta\mathbf{M}\|, T)$ is the squared Euclidean distance between change magnitude $\|\Delta\mathbf{M}\|$ and the cluster center (T_0, T_c, or T_n). If a pixel's $\|\Delta\mathbf{M}\|$ was larger than T_c, it was certain to be changed pixel, and the same happened to a pixel with $\|\Delta\mathbf{M}\|$ lower than T_n (but it would be an unchanged pixel). For pixels with $\|\Delta\mathbf{M}\|$ between T_c, and T_n, the FCM membership would estimate how certain could the T_0 be used to separate changed/unchanged pixels.

For pixels with a high uncertainty (i.e., pixels in the overlapping zone), the change magnitude threshold is very likely to fail as a reliable discriminating criterion. Bovolo and Bruzzone (2007) pointed out that most applications related to CVA only

used change magnitude to identify changed pixels, which usually resulted in incomplete exploitation of information. Also, Xian, Homer, and Fry (2009) indicated that if a single threshold was used to segregate areas of change or no-change for all land cover "from-to" change types, then changed areas could be either over-extracted or under-extracted. To fill this gap, the novel dynamic threshold approach was used to aid the separation of changed and unchanged pixels based on different "from-to" change types. Within the framework of CVAPS, land-cover membership can be used for the determination of "from-to" change type. Each pixel has a representative "from-to" type; the difference is whether the pixel is considered to be changed or unchanged by the threshold T_0 with different uncertainty u_c or u_n. This means each "from-to" type has its sub-groups of potentially changed and unchanged pixels. Then the weighted mean change magnitude of every sub-group of changed and unchanged can be calculated as following:

$$S_c = \frac{\sum_{n=1}^{N_c} u_{cn} * \Delta \mathbf{P}}{\sum_{n=1}^{N_c} u_{cn}} \tag{4}$$

$$S_n = \frac{\sum_{n=1}^{N_n} u_{nn} * \Delta \mathbf{P}}{\sum_{n=1}^{N_n} u_{nn}} \tag{5}$$

where for each "from-to" change type, S_c and S_n are the weighted mean magnitude of potentially changed and unchanged pixels for each "from-to" change type, respectively; N_c and N_n are number of potentially changed and unchanged pixels,

respectively; u_{cn} and u_{nn} are the uncertainty for changed or unchanged of a pixel depending on the potential status. With S_c and S_n for each change type, the FCM algorithm was applied again to estimate the membership of a pixels' change status within its particular "from-to" type. The changed and unchanged membership, m_c and m_n, now represent a more detailed change status estimation as it restricts the generosity of the global threshold T_0 by only considering pixels with the same change type behavior. In order to balance the information from both global uncertainty and "from-to" uncertainty, the following determination was adopted:

$$U_{fc} = \frac{u_c + \alpha m_c}{1+\alpha} \tag{6}$$

$$U_{fn} = \frac{u_n + \alpha m_n}{1+\alpha} \tag{7}$$

the changed/unchanged status was determined by argmax (U_{fc},U_{fn}). Here α is a scaling factor to balance between the global and "from-to" components.

Note that as this is a supervised method, the quality of the change-detection is largely based on the selection and quality of training samples. During the training step in a supervised classification or change-detection, the fundamental criterion is to provide representative statistics for each land-cover class or type of land-cover change, which facilitates accurate results from the classifier. Usually, this means selecting training

samples that are or are very close to pure members of the relevant class or change type. In both fields of supervised classification and change-detection, most research regarding training samples has aimed to improve the selection of pure samples (Arai 1992; Büttner, Hajós, and Korándi 1989; Cazes, Feitosa, and Mota 2004; Li and Xu 2010). Foody and Arora (1996) conducted tests on maximum likelihood and neural network classifiers with pure and mixed sample sets. Their results indicated that pure samples generally achieved better accuracy and therefore preferable in classification; but if mixed samples were abundant in the training sample set, they should be accommodated. Although Foody and Mathur (2006) contended that the conventional design of acquiring pure-pixel samples might not be a universal solution and that mixed pixels may constitute an alternative training sample-selection strategy for SVM classifier based on its unique characteristics, the use of mixed-pixel training samples have been so far mostly restricted to SVM-related studies (Mountrakis, Im, and Ogole 2011; Okujeni et al. 2013; Van Der Linden et al. 2007). For other classifiers and situations, selecting pure pixels is still the goal during the training process (Kavzoglu 2009). In addition, although there are some methods for selecting mixed pixels as training samples in a single-image classification, it is very difficult to accurately/confidently identify pixels that represent mixed or transitional land-cover change between pairs of remotely-sensed images. Therefore, the typical procedure in supervised change-detection is to select pixels/sites with clear land-cover change as training samples (Lu et al. 2004; Tewkesbury et al. 2015).

3.5.1.2 Fuzzy Markov Random Field (FMRF)

Besides the dynamic 1st thresholding method, a modified fuzzy Markov Random Field (FMRF) was also adopted to further improve the change accuracy. MRF model has been used in many applications of change-detections and has been proved to be a valid method to reduce the classification errors and "salt-and-pepper" effect by incorporating spatial information (Bruzzone and Prieto 2000; Liu et al. 2008). As the change in transition area is subtle, it would generate errors by only considering each pixel individually. By incorporating MRF into MCVA, it is possible to reduce errors from the "salt-and-pepper" effect. Note that a disadvantage of MRF is that the change map refined by MRF is usually over-smooth (Tso and Olsen 2005; Wang and Wang 2004). The reason for this phenomenon might be the hard spatial function of the MRF energy function, which simply considers the number of neighbors with the same label but ignores the certainty of the label. Therefore in this FMRF, fuzzy spatial function that considers the certainty of change labels was adopted in order to solve the over-smooth problem and further improve the change-detection accuracy.

In a conventional MRF model, the energy function of change type $C_l(i,j)$ for a pixel (i, j) is expressed as:

$$U\left(C_l(i,j)\right)=\frac{1}{Z}e^{-(U_{value}[C_l(i,j)]+U_{context}[C_l(i,j)])} \quad (8)$$

where Z is a normalizing factor, U_{value} and $U_{context}$ is the Gibbs energy function of change probability value and contextual information based on neighboring pixels. The energy function of pixel value is a log function of probability of change type C_l:

$$U_{value}[C_l(i,j)] = -\ln(p[C_l(i,j)]) \quad (9)$$

where $p[C_l(i,j)]$ is the certainty in change type C_l. The contextual energy is given as:

$$U_{context}[C_l(i,j)]=U_{context}\left[\frac{C_l(i,j)}{C_l(g,h),\ (g,h)\in N(i,j)}\right]=\sum_{(g,h)\in N(i,j)}\beta\delta_k(C_l(i,j),C_l(g,h)) \quad (10)$$

where δ_k is the Kronecker delta function, β is a controlling constant of the contextual influential weight, and

$$\delta_k\big(C_l(i,j),C_l(g,h)\big)=\begin{cases}-1, \text{ if } C_l(i,j)=C_l(g,h)\\ 0, \text{ if } C_l(i,j)\neq C_l(g,h)\end{cases} \quad (11)$$

Also, N is noted as the neighbors of pixel (i,j). Usually, a second-order neighborhood system is used. This function might lead to the over-smooth phenomenon as the separation is hard (-1 and 0). Here, a modification was adopted to switch the standard contextual energy component from hard format to the following fuzzy format:

$$\delta_k\left(C_l(i,j),C_l(g,h)\right)=\begin{cases}-U_{fc}, \text{ if } C_l(i,j)=C_l(g,h)\\ -U_{fn}, \text{ if } C_l(i,j)\neq C_l(g,h)\end{cases} \quad (12)$$

where U_{fc} and U_{fn} are the change/no-change uncertainties discussed above. This means neighboring pixels with higher certainty will play more important roles in the energy function. By incorporating the uncertainty of the change label, the MRF should be able to consider more detailed change information and deal with the over-smooth problem.

With the fuzzy contextual energy function, the iterated conditional modes (ICM) algorithm (Besag 1986) was used to converge to a local minimum of the energy function equation (8) and produced the refined changed/unchanged map.

3.5.1.3 2nd Threshold of Transitional Change

The first two steps in MCVA aim to improve the changed/unchanged detection accuracy, but the output is still a traditional discrete map. The third step, namely the 2nd threshold of transitional change, is developed to produce a novel output with a focus on change fuzziness in order to explore a more delicate landscape change scenario. To retain and utilize the advantages from both soft and hard outputs, the 2nd threshold stage here was developed to separate changed pixels into two forms – change and transitional change. Specifically, change status refers to the common "from-to" change, which is a form of nearly pure change from one land-cover class to another; whereas transitional change status refers to a less pure, fuzzier change status. The extra transitional change type represents the fuzziness during landscape change process, which provides another critical information for floodplain landscape characterization. After the dynamic 1st

threshold determination and FMRF, changed pixels were selected and unchanged pixels were masked out. Then, these changed pixels were compared with training samples to determine whether they exhibited change or transitional change status. The pure training samples represent clear and significant land-cover change, as discussed above, were used again to separate changed pixels. However, at this stage, the threshold was not determined by overall change magnitude, but rather by the following pixel fuzziness indices:

1) Pixel uncertainty index (Eastman 2009);

$$\text{Pixel Uncertainty Index} = 1 - \frac{\max - \frac{\text{sum}}{n}}{1 - \frac{1}{n}} \tag{13}$$

where max is the maximum class membership value for that pixel, sum is the summation of class membership values for that pixel, and *n* is the number of classes. This is an indicator of how certain a pixel can be classified as a particular land-cover type, and a clear land-cover change should entail a low pixel uncertainty index after the change.

2) Shannon's entropy (Ibrahim, Arora, and Ghosh 2005; Shannon 1948);

$$\text{Shannon's Entropy} = -\sum_{i=1}^{n} u_i \log_2(u_i) \tag{14}$$

where u_i is the fuzzy membership of class i, and n is number of classes. This is an indicator of membership diversity. Change status should show lower entropy than transitional change status as membership tends toward concentrating in one class.

3) Ratio of change magnitude from the dominant “from-to” change type (if there is complete land-cover change, the change magnitude should mostly come from the dominant “from-to” change type) to the total change magnitude:

$$\text{Dominant Change Ratio} = \frac{\text{Change Magnitude of Dominant "From-To" Change}}{\text{Total Change Magnitude}} \quad (15)$$

These three indices/parameters cover different aspects of the characteristics of fuzziness in land-cover change, which were used to indicate the degree of completeness of land-cover change. The average values of these parameters derived from pure training samples were the representative statistics of the absolute change type. If changed pixels showed equivalent or higher certainty in its change type than the training samples, they were classified as “change”; otherwise, change pixels were classified as “transitional change”. The “from-to” change maps with three change status – unchanged, transitionally changed, and changed – were produced for each pair of images in the entire time series.

3.5.2 Change-Detection Accuracy Assessment

Change-detection accuracy assessments were performed to evaluate the performance of MCVA. Accuracy assessment was based on index-assisted visual interpretation. Specifically, the Landsat 5 TM bands, spectral curves, tasseled-cap images, and high-spatial resolution Google Earth© images (when quasi-spatio-temporally coincident) were used as reference data. Classification confusion matrices for each image were calculated to quantitatively report the producer's and user's accuracies, the overall accuracy, and the Kappa coefficient.

First, in order to assess the errors derived from the overlapping issue, all pixels were put into twenty (20) bins based on their change magnitude, with ten (10) bins on each side of the threshold T_0 (Figure 6). The bins on each side were equally-spaced. Then 50 samples, as suggested in various remote-sensing studies (Congalton 1991; Foody 2010), were drawn from each bin and used to assess the change-detection accuracies of each bin. Also, the combined accuracy with a total of 1000 samples was calculated.

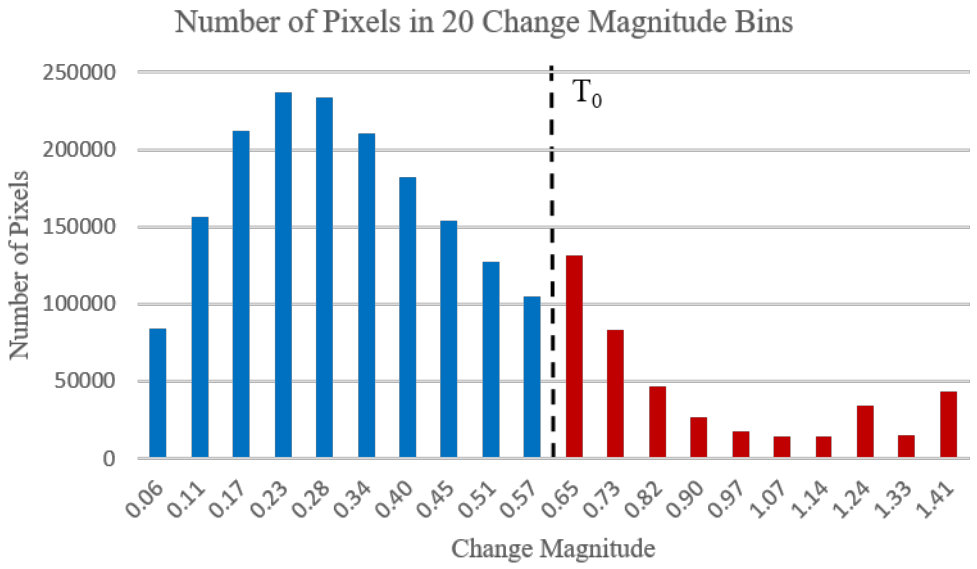

Figure 6. Example of binning processing based on pixels' change magnitude (blue bars represent unchanged pixel bins, and red bars represent changed pixel bins).

In addition, accuracy assessments were also conducted on standard post-classification comparison (PCC) and standard change vector analysis (CVA) which are the two basic techniques related to CVAPS. This comparison would allow a comprehensive evaluation of the improvement of MCVA. Change-detection error matrices of each algorithm were calculated. Besides conventional overall accuracy and Kappa coefficient, two extra indices namely quantity disagreement and allocation disagreement were also derived from the error matrices for evaluation. The quantity disagreement and allocation disagreement were proposed by Pontius Jr and Millones (2011) to replace Kappa coefficient, as this conventional index has been criticized for being redundant with the overall accuracy and not providing any information on the spatial distribution of errors (Foody 2005). The quantity disagreement is defined as the

amount of difference between classified imagery and reference imagery that is due to the less than perfect match in proportions of all categories. Quantity disagreement of a specific category is calculated by dividing the absolute value of the difference between the total counts of samples in that column and the total counts of samples in that row by two. On the other hand, allocation disagreement is defined as the amount of difference between classified imagery and reference imagery that is due to less than perfect match in spatial allocations of all categories. Quantity disagreement of a specific category is calculated by taking two times of the minimum value between the subtraction of sample counts in the major diagonal and the total counts in that column and the subtraction of the sample counts in the major diagonal and the total counts in that row. A full description of quantity disagreement and allocation disagreement can be found in Pontius Jr and Millones (2011).

3.6 Landscape Metrics

In temporal analysis of land-cover/landscape change, a traditional approach is to explore information from a set of statistical data showing the area of change in each land-cover class. Especially in the background of image classifications of remote sensing, this becomes counting and analyzing the number of pixels changed, the types of "from-to" change, etc. Such statistical approach is able to quantitatively demonstrate and generalize the composition of land-cover types, their abundance, and the phenomenon of change from one land-cover to another. However, it considers all pixels independently and ignores the spatial patterns, structures, and configurations of landscape patches –

homogenous areas differing from surroundings land-covers. The spatial structures of these patches reflect the influence of geomorphological and ecological processes on floodplain evolution. Thus, an effective and quantitative measurement of the structure of floodplain landscapes is needed to provide this critical yet missing information (Turner 1990; Turner et al. 2003). Landscape metrics have been utilized to characterize the structure of riparian/floodplain vegetation and other landscape components (Apan, Raine, and Paterson 2002; Fernandes, Aguiar, and Ferreira 2011; Freeman, Stanley, and Turner 2003). Landscape metrics are algorithms and indices that quantitatively describe spatial configurations as well as spatial relationships among patches, classes of patches, or entire landscape. A wide range of landscape metrics has been developed to quantify categorical patterns, which covers aspects including spatial characteristics, landscape arrangement, positions or orientation of patches (McGarigal, Cushman, and Ene 2012).

In this research, thirteen landscape metrics were calculated to provide information regarding spatial configuration, connectivity, and distribution/interspersion of patches associated with the classes of interest. Table 6 lists the selected landscape metrics and their contributions to characterize the spatial configurations of floodplain landscape. The selection was based on the work of Fernandes, Aguiar, and Ferreira (2011) and additional experiments. Landscape metrics were calculated in class level using FRAGSTATS version 4.2 (McGarigal, Cushman, and Ene 2012). Input data of the landscape metrics calculation were the hardened fuzzy classified images of the five Landsat 5 TM images used in this research.

Table 6. Categories, descriptions, and contributions of landscape metrics.

Category	Landscape Metrics	Acronym	Description	Contributions
Area	Number of Patches	NP	Number of patches.	Basic indicators of land-cover distributions and spatial patterns
	Mean Patch Area	MPA	Mean patch area.	
	Patch Area Coefficient of Variation	PACV	Variation in patch area.	
Shape	Mean Shape Index	MSI	Measurement of complexity of patch shape.	Advanced indicators related to patch morphologies, which provide information to quantitatively explore and distinguish geomorphological patterns and processes.
	Shape Index Coefficient of Variation	SICV		
	Mean Fractal Index	MFI	Measurement of irregularity of patch shape.	
	Fractal Index Coefficient of Variation	FICV		
	Mean Related Circumscribing Circle	MRCC	Measurement of patch elongation.	
	Related Circumscribing Circle Coefficient of Variation	RCCCV		
	Mean Contiguity Index	MCI	Measurement of patch spatial connectedness.	
	Contiguity Index and Coefficient of Variation	CICV		
Aggregation	Interspersion Juxtaposition Index	IJI	Measurement of proximity	Spatial distributions and connectivity of patches
	Patch Cohesion Index	PCI	Measurement of connectivity	

3.7 Buffer Zones

Four spatial buffer zones were created to evaluate the proximal and distal land-cover and landscape based on distance to main river channel (Table 7). As average river width is ~440 m, buffer distances of four buffer zones were decided as 0 – 1320 m (3 times river width), 1320 – 2200 m (5 times river width), 2200 – 3080 m (seven (7) times the river width), and 3080 – 3960 m (nine (9) times the river width), respectively. Results from previous steps (i.e., classifications, change-detection, and landscape metrics) were analyzed within each buffer zone and the entire floodplain to provide a comprehensive investigation of floodplain landscape evolution.

Table 7. Four buffer zones based on distance to main river channel.

Buffer Number	Distance to River (m)	Accumulated Distance
1	0 - 1320	3 times river width
2	1320 - 2200	5 times river width
3	2200 - 3080	7 times river width
4	3080 - 3960	9 times river width

4. RESULTS

4.1 Image Classification

Classified maps were generated via the ISODATA, Bayes, and Fuzzy classifiers. The classification performances and comparisons of these classification algorithms are shown and described in this subsection.

4.1.1 ISODATA Results

Maps of land-cover were constructed by classifying the Landsat 5 TM images using the ISODATA algorithm (Figure 7). The maximum number of clusters set for the ISODATA algorithm was 50, and the initial outputs were then manually merged and labeled into seven land-cover classes. For all five classified images, the main channel of Rio Beni showed high-level activities in channel migration and meander cut-offs. More oxbow lakes were created due to this active geomorphological and hydrological process, although a small amount of oxbow lakes re-connected to the main river channel. Sand was mostly located along river meanders, change and evolve with the river. Two vegetation types occupied a huge number of the area throughout the entire study area. Forest cover was more often to be observed away from the main river channel compared to non-forest vegetation, and the distribution of forests is more concentrated and stable. Non-forest vegetation was more fragmented compared to forest. It occupied areas along main river channel where active processes happen, and it also colonized the newly-formed abandoned channels and some old oxbow lakes. Two types of bare soil scattered

throughout the area, the only few clusters were spotted in the peripheral regions near floodplain boundary.

In all five dates, the dominant land-cover class was forest with percentages of total area range from 43 – 59 % (Table 8). Non-forest vegetation also occupied area percentage from 26 – 40 %. Overall, two vegetation classes occupied approximately 80% of the total study area. Two types of bare soil together only contributed 6 – 7 % of the total floodplain are. Sand contributed only about 2% of the total area, which was the least abundant land-cover type. Similarly, the oxbow lakes represented a slight amount of floodplain land-covers, but the proportions increased from 2 % to 3.3 % with an increasing trend.

Table 8. Area and percentage of each land-cover that encompasses the study area based on ISODATA classification images.

Land-Cover Class	1987		1990		1995		1999		2006	
	Area (km^2)	% of Total Area	Area (km^2)	% of Total Area	Area (km^2)	% of Total Area	Area (km^2)	% of Total Area	Area (km^2)	% of Total Area
Forest	979.2	48.3	1183.7	58.4	1200.8	59.2	879.0	43.3	989.4	48.8
Non-forest Vegetation	687.6	33.9	541.4	26.7	467.5	23.0	813.7	40.1	638.5	31.5
Oxbow Lake	54.7	2.7	52.9	2.6	41.0	2.0	61.9	3.1	66.7	3.3
River	143.6	7.1	130.7	6.4	120.5	5.9	118.5	5.8	123.9	6.1
Sand	42.2	2.1	37.4	1.8	54.7	2.7	51.2	2.5	38.2	1.9
Dry Soil	109.9	5.4	68.7	3.4	126.3	6.2	88.6	4.4	157.1	7.7
Wet Soil	11.1	0.5	13.7	0.7	17.5	0.9	15.5	0.8	14.5	0.7

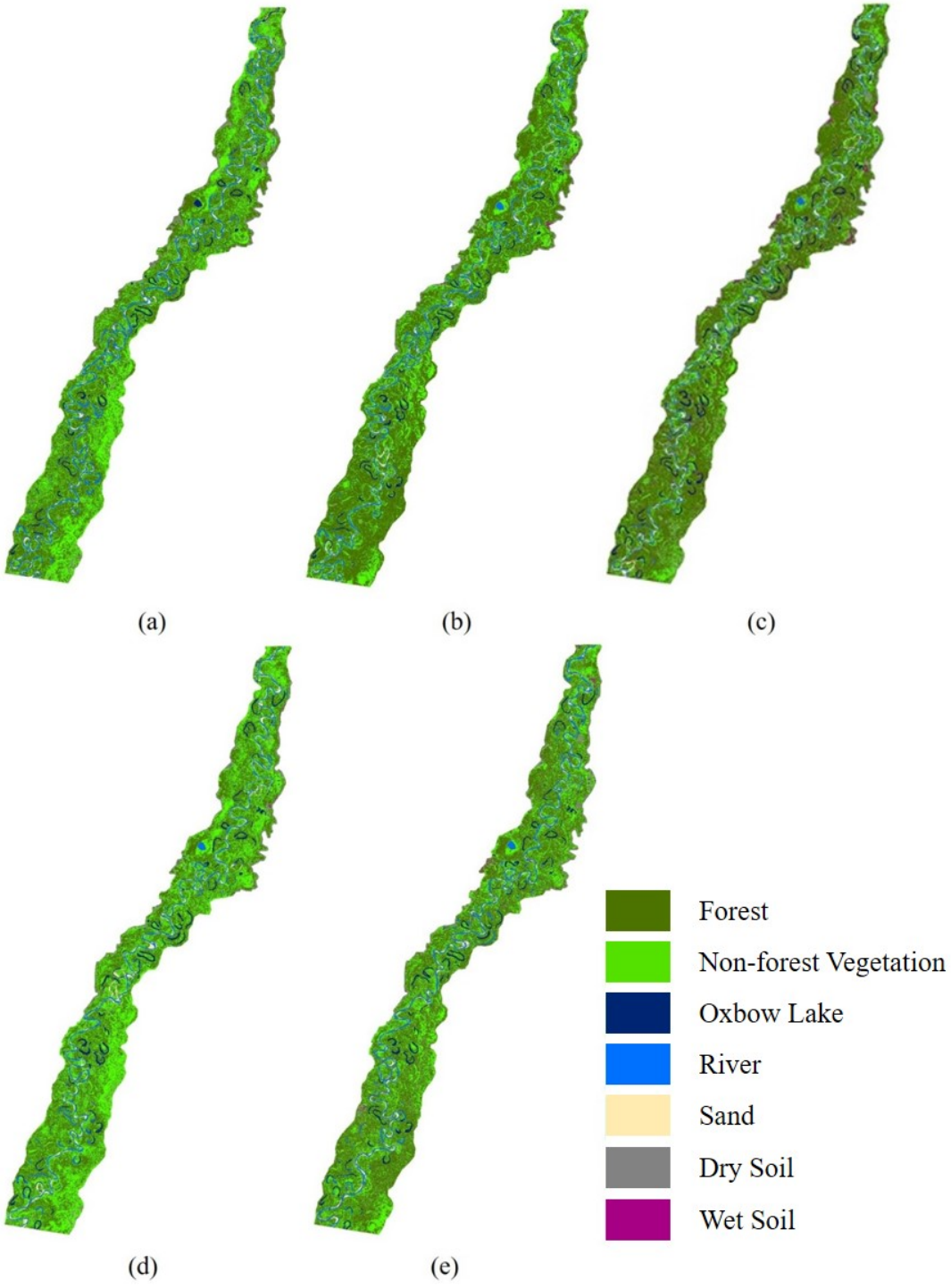

Figure 7. Classified images of each date based on the ISODATA: (a) Aug-02-1987; (b) Sep-27-1990; (c) Jul-07-1995; (d) Aug-03-1999; and (e) Jul-05-2006.

4.1.2 Bayes Classification Results

In the field of pattern recognition, Bayes classifier has often been considered as an optimal classifier for many cases and applications if proper conditions are met. Bayes classifier estimates the posterior probability of pixels belong to a particular land-cover class through Bayes theorem based on the training samples and prior probability described in the previous section. For each image, Bayes classifier produced posterior probability layer for each land-cover class, which were a total of 7 posterior probability layers per image (Figure 8). A hardened classified map can be produced from Bayes classifier output layers by assigning the land-cover class with the highest posterior probability to each pixel (Figure 9). In this way, the hardened outputs were results generated from a Maximum Likelihood Classification (MLC).

The additional land-cover posterior probability layers from Bayes classifications obviously provide extra information compared to traditional hard classification methods like ISODATA. With the extra posterior probability layers, the land-cover change can now not only be investigated in the significant shift from one land-cover to another, but also in the subtle change within a single land-cover class and between two land-cover classes. The utility of this useful information would be discussed more thoroughly in the next subsection in the combination of a novel change-detection algorithm and classification scheme.

Despite being a soft classifier, a simple hardening process transformed posterior probability layers from the Bayes classifier to traditional classified maps (Figure 9). From visual interpretation compared to ISODATA classified maps, resulting maps

generated by Bayes classifier were smoother with less “salt-and-pepper” effect. However, the overall layout of landscape appearances was similar between Bayes classifier and ISODATA. Table 9 lists the detailed statistics of land-cover class distribution based on the hardened Bayes classification images. Compared to statistics based on ISODATA, forest was still the most dominant land-cover, with even higher percentages range from 52 % to 61 %. Non-forest vegetation had a significant drop that its land-cover percentages were from 18 % to 27 %, although it was still the second dominant land-cover class. Two bare soil types had more area coverage in this classification approach. Oxbow lake, river, and sand class remained similar area coverage.

Table 9. Area and percentage of each land-cover that encompasses the study area based on hardened Bayes classification images.

Land-Cover Class	1987		1990		1995		1999		2006	
	Area (km^2)	% of Total Area	Area (km^2)	% of Total Area	Area (km^2)	% of Total Area	Area (km^2)	% of Total Area	Area (km^2)	% of Total Area
Forest	1241.5	61.3	1226.9	60.5	1051.9	51.9	1148.1	56.6	1200.0	59.2
Non-forest Vegetation	375.8	18.5	485.4	24.0	519.2	25.6	549.5	27.1	447.1	22.0
Oxbow Lake	53.6	2.6	56.4	2.8	58.4	2.9	61.9	3.1	65.1	3.2
River	109.9	5.4	110.9	5.5	106.5	5.2	98.9	4.9	103.4	5.1
Sand	82.7	4.1	57.2	2.8	51.4	2.5	80.6	4.0	71.9	3.5
Dry Soil	81.0	4.0	60.3	3.0	163.0	8.0	66.4	3.3	92.7	4.6
Wet Soil	81.8	4.0	31.2	1.5	78.0	3.8	23.0	1.1	48.2	2.4

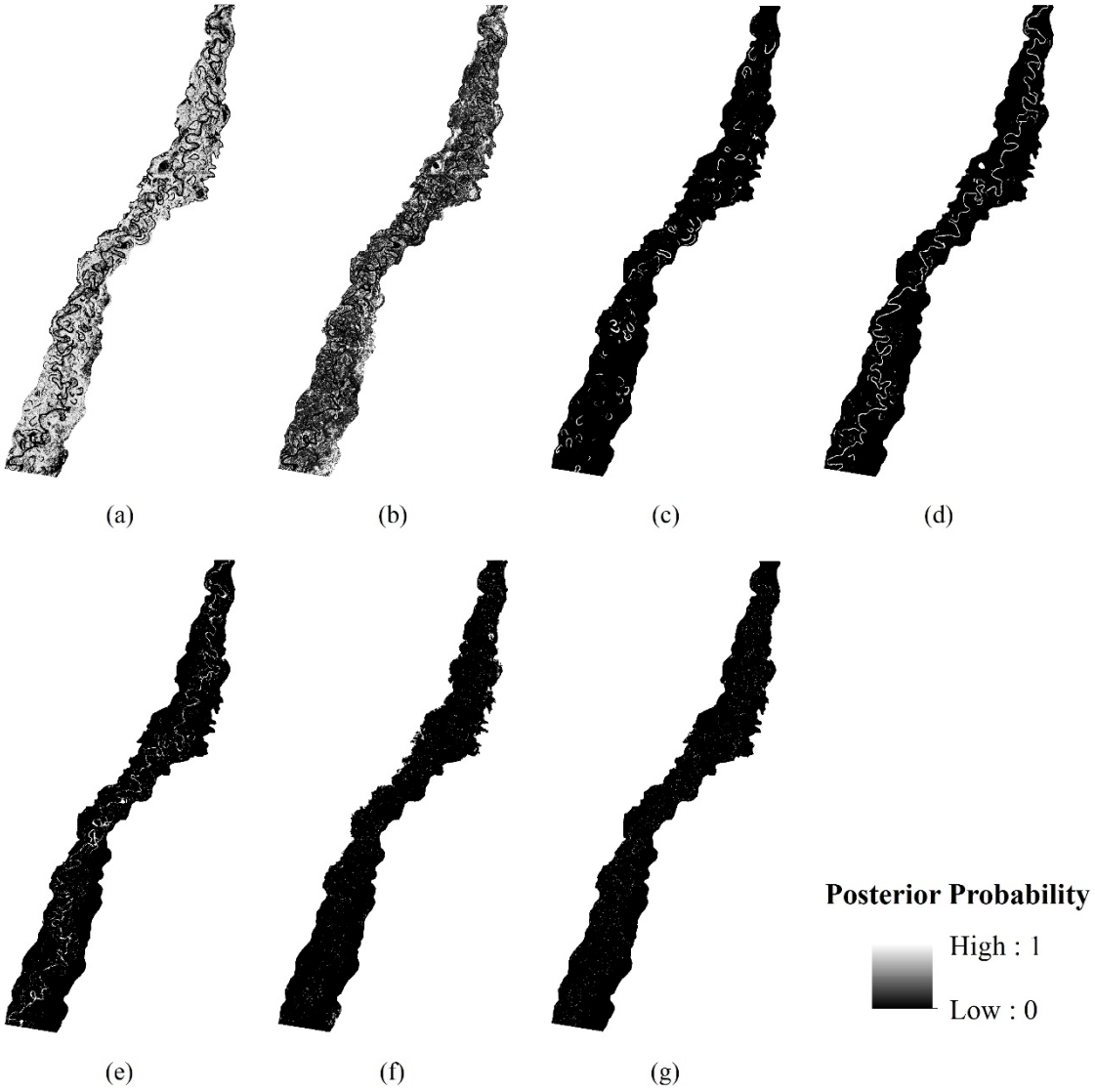

Figure 8. A set of land-cover posterior probability layers from Bayes classifier: (a) forest; (b) non-forest vegetation; (c) oxbow lake; (d) river; (e) sand; (f) dry soil; and (g) wet soil.

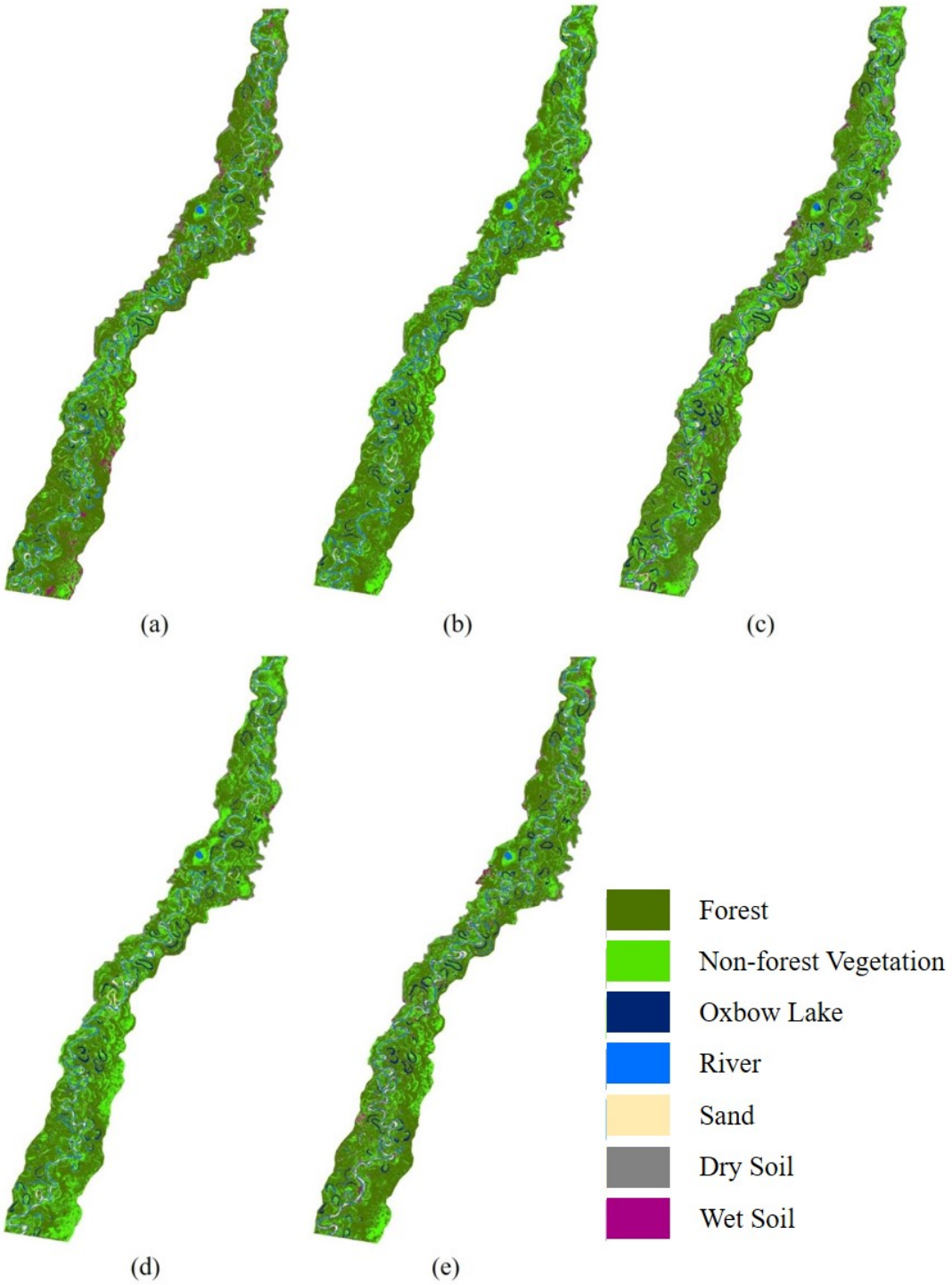

Figure 9. Hardened classified images of each date based on the Bayes classifier: (a) Aug-02-1987; (b) Sep-27-1990; (c) Jul-07-1995; (d) Aug-03-1999; and (e) Jul-05-2006.

4.1.3 Fuzzy Classification Results

The fuzzy classifier is based on fuzzy set theory to indicate the degree of membership of a pixel belongs to a particular land-cover class. Fuzzy membership is calculated based on standardized Euclidean distance from the mean spectral signature of each class, via a sigmoidal membership function. Similar to Bayes classifier, fuzzy classifier produced fuzzy membership layer for each land-cover class, which were a total of seven (7) land-cover membership layers per image (Figure 10). Hardened classified maps can be produced from fuzzy classifier output layers by assigning the land-cover class with the highest fuzzy membership to each pixel (Figure 11).

Compared to Bayes posterior probability layers for land-cover classes, the fuzzy membership layers generated by fuzzy classifier were “fuzzier”. This was that the Bayes posterior probability had a larger number of pixels with a value near the tails (0 and 1) of the data distribution, whereas values in fuzzy membership layers were less extreme. This difference should come from the different mechanisms of the two classifiers.

A simple hardening process was also conducted to transform fuzzy membership layers from the fuzzy classifier to traditional classified maps (Figure 11). From visual interpretation compared to ISODATA and hardened Bayes classified maps, the hardened fuzzy classified maps also looked smoother than ISODATA but had more isolated classified pixels than Bayes classified maps. Table 10 lists the detailed statistics of land-cover class distribution based on the hardened fuzzy classification images. The statistics shown were closer to those in ISODATA. Forest still occupied the most area of the floodplain, with percentages of the total area range from 45 % to 56 %. Non-forest

vegetation had percentages of the total area range from 24 to 38 %, and it was still the second dominant land-cover class. Two types of bare soil totally contributed about 8 %, and sand contributed only about 2% of the total area. The oxbow lakes still represented a small amount of floodplain land-covers, but the proportions increased from 2.3 % to 3.0 % stably.

Table 10. Area and percentage of each land-cover that encompasses the study area based on hardened fuzzy classification images.

Land-Cover Class	1987		1990		1995		1999		2006	
	Area (km^2)	% of Total Area	Area (km^2)	% of Total Area	Area (km^2)	% of Total Area	Area (km^2)	% of Total Area	Area (km^2)	% of Total Area
Forest	1139.9	56.3	910.1	44.9	1009.8	49.8	915.1	45.1	1018.2	50.2
Non-forest Vegetation	502.2	24.8	767.2	37.9	541.4	26.7	738.5	36.4	635.7	31.3
Oxbow Lake	47.5	2.3	48.8	2.4	56.6	2.8	60.8	3.0	59.9	3.0
River	111.2	5.5	108.6	5.4	96.2	4.7	98.7	4.9	102.5	5.1
Sand	47.5	2.3	37.6	1.9	38.5	1.9	82.0	4.0	56.2	2.8
Dry Soil	83.0	4.1	63.5	3.1	198.1	9.8	78.8	3.9	59.3	2.9
Wet Soil	95.0	4.7	92.6	4.6	87.9	4.3	54.3	2.7	96.5	4.8

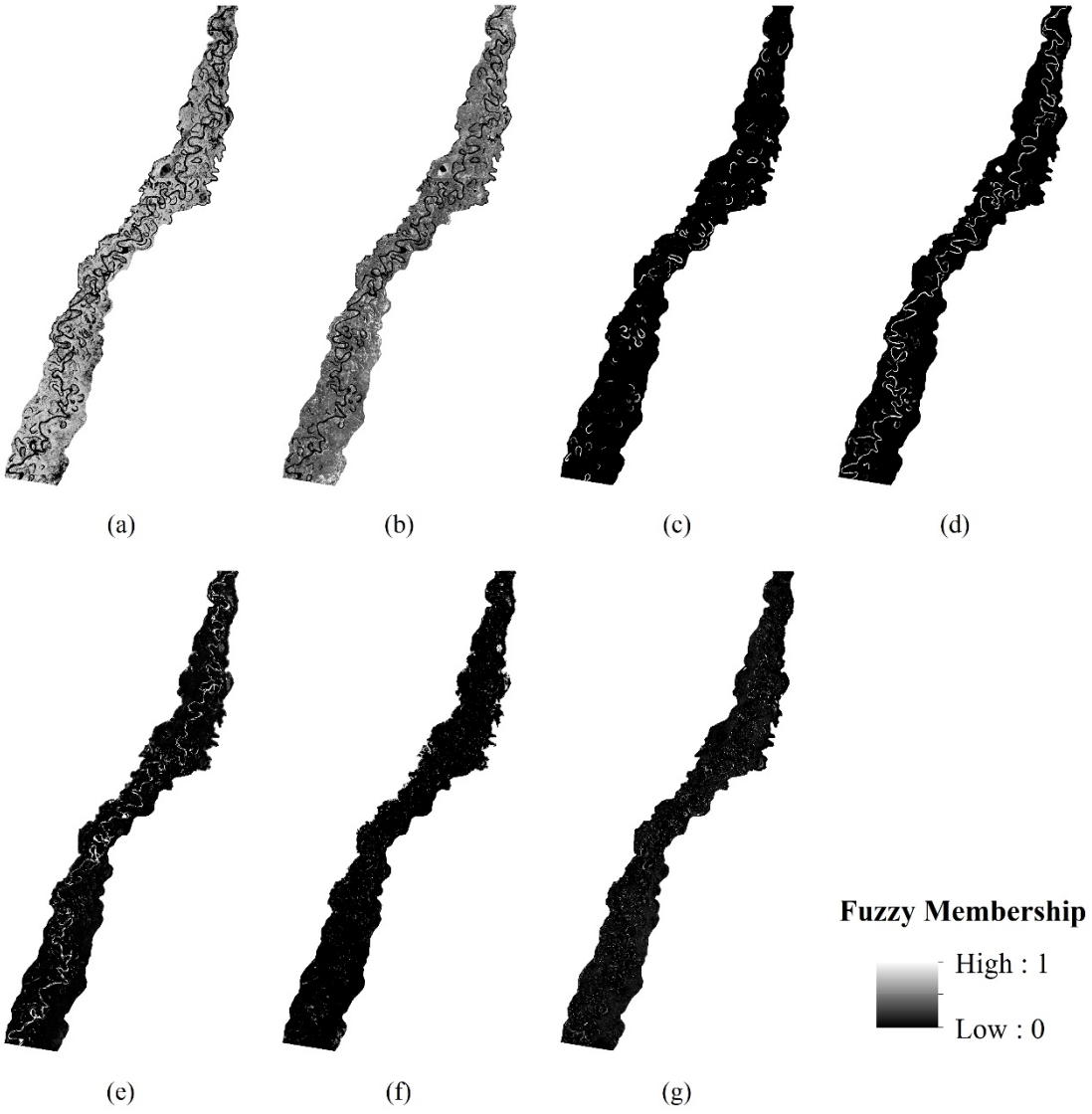

Figure 10. A set of land-cover fuzzy membership layers from fuzzy classifier: (a) forest; (b) non-forest vegetation; (c) oxbow lake; (d) river; (e) sand; (f) dry soil; and (g) wet soil.

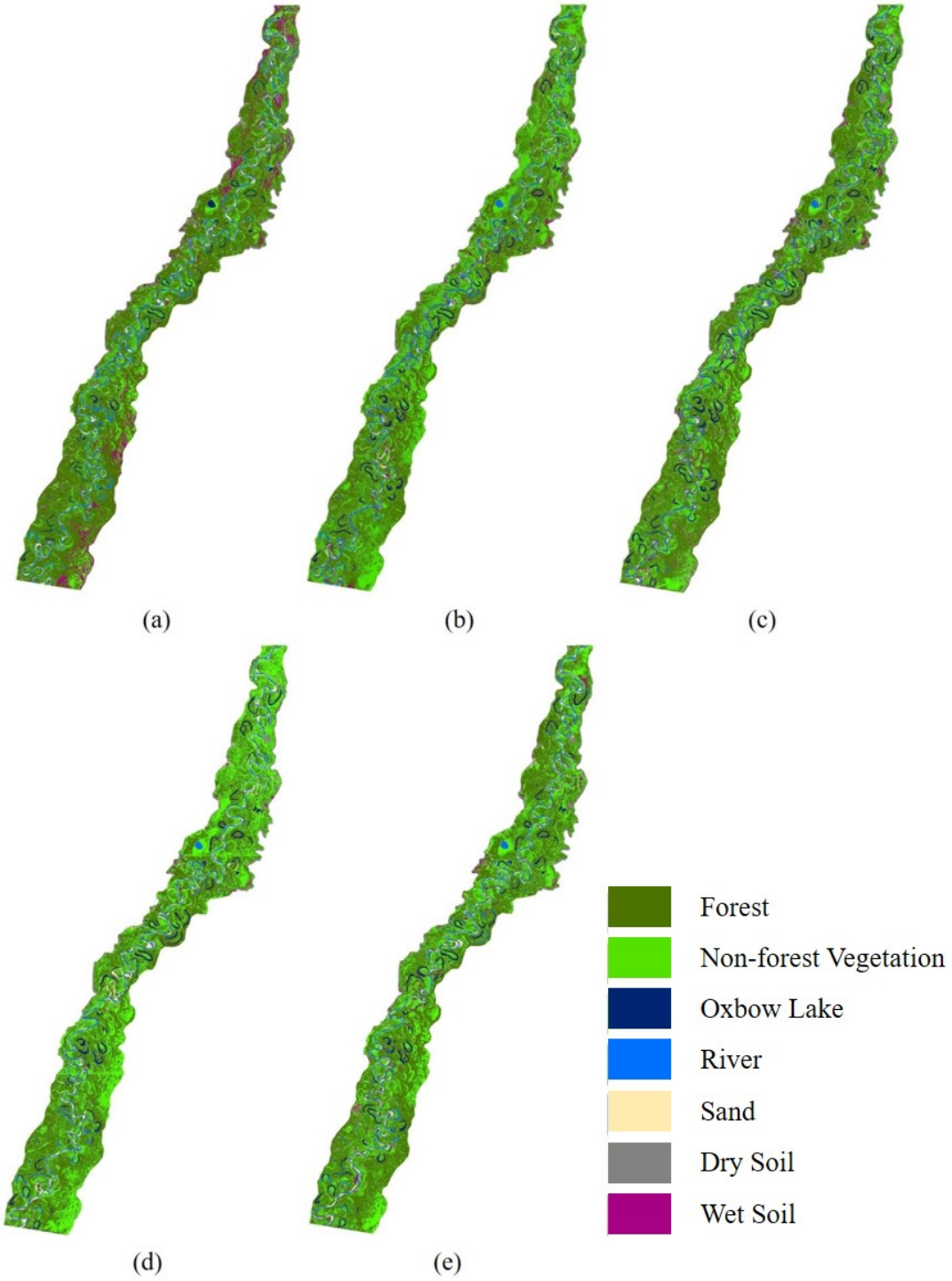

Figure 11. Hardened classified images of each date based on the fuzzy classifier: (a) Aug-02-1987; (b) Sep-27-1990; (c) Jul-07-1995; (d) Aug-03-1999; and (e) Jul-05-2006.

4.1.4 Classification Accuracy Assessment

Classification performance of the three tested classification algorithms was evaluated via standard accuracy assessment of remote sensing classified images. This step is necessary to assess the capacity of these three methods to characterize the landscape correctly on Rio Beni floodplain. 100 stratified random sample pixels per land-cover class (600 samples per image) were used to construct an error matrix for each image generated in the classification procedure. As shown below, Tables 11 – 15 are the error matrices of three tested classification algorithms from the accuracy assessment of the land-cover classification for the five Landsat 5 TM images.

Table 11 (a) – (c) lists the error matrices for Landsat 5 TM image date Aug-02-1987, which summarize the user's accuracy, producer's accuracy, overall accuracy, and Kappa coefficient from the ISODATA, Bayes, and fuzzy classifications, respectively. ISODATA achieved an overall accuracy of 91.33% with Kappa coefficient of 0. 8960, whereas the overall accuracies of Bayes and fuzzy classifications were 89.17% and 90.17%, respectively, with Kappa coefficients of 0. 8700 and 0.8820, respectively. Regarding user's accuracy, ISODATA also performed the best with most classes achieved accuracies of 100%, but forest and non-forest vegetation only had producer's accuracies at about 80%. Regarding user's accuracy, ISODATA and Bayes classifications had similar results, and fuzzy classification had the worst accuracies that most user's and producer's accuracies were below 90%. In all three different classifications, water class (oxbow lake and river) achieved 100% user's accuracy, which is not a surprise as this land-cover class can be easily identified in a TM image

due to the distinguishable spectral characteristics. However, only ISODATA was able to achieve a 100% user's accuracy for water class, whereas other two algorithms only provided 86% and 82%. This error of commission came from the confusion between water class and sand class. As sand-bars were located along the main river channel and some oxbow lakes, sometimes it is difficult to classify them correctly due to a mixture of both classes in a pixel. From both user's accuracy and producer's accuracy, confusions between dry soil and wet soil could be observed due to similar spectral signatures. Forest and non-forest vegetation were another pair of land-cover classes that were easily misclassified to each other.

Table 12 (a) – (c) lists the error matrices for Landsat 5 TM image date Sep-27-1990, which summarize the user's accuracy, producer's accuracy, overall accuracy, and Kappa coefficient from the ISODATA, Bayes, and fuzzy classifications, respectively. Bayes classification achieved the best overall accuracy of 93.17% with Kappa coefficient of 0. 9180, whereas the overall accuracies of ISODATA and fuzzy classifications were 91.33% and 90.17%, respectively. With the overall best performance, Bayes classifications had user's accuracies and producer's accuracies of at least 95% for most land-cover classes. The only significant misclassification was from non-forest vegetation class which was confused with two soil classes and the forest class. ISODATA had accuracies that were similar to the Bayes classification, with only a slight decrease. It also performed badly when classifying non-forest vegetation. Fuzzy classicization was the worst classifier for this image. The misclassifications between two soil land-cover classes and two vegetation classes were significant. User's accuracies

and producer's accuracies for these classes range from 83% - 87%, where many of them were below 85%.

Table 13 (a) – (c) lists the error matrices for Landsat 5 TM image date Jul-07-1995, which summarize the user's accuracy, producer's accuracy, overall accuracy, and Kappa coefficient from the ISODATA, Bayes, and fuzzy classifications, respectively. ISODATA had an overall accuracy of 90.33% with Kappa coefficient of 0.8840, Bayes classifier had an overall accuracy of 90.50% with Kappa coefficient of 0.8860, and fuzzy classifier had an overall accuracy of 91.00% with Kappa coefficient of 0.8920. For this Landsat 5 TM scene, the results of three tested classification algorithms did not have a significant difference. Water and sand classes entailed the highest classification accuracies, as both commission and omission errors were less than 5%. Dry soil and wet soil land-cover classes had high commission errors, ranging from 10% - 20%, whereas their omission errors remained low. On the contrary, forest and non-forest vegetation had lower user's accuracies (less than 80%). Compared with other land-cover classes in this image, these two vegetation classes were severely misclassified, with confusion with each other and the two soil classes.

Table 14 (a) – (c) lists the error matrices for Landsat 5 TM image date Aug-03-1999, which summarize the user's accuracy, producer's accuracy, overall accuracy, and Kappa coefficient from the ISODATA, Bayes, and fuzzy classifications, respectively. ISODATA had an overall accuracy of 89.83% with Kappa coefficient of 0.8780, Bayes classifier had an overall accuracy of 91.83% with Kappa coefficient of 0.9020, and fuzzy classifier had an overall accuracy of 89.83% with Kappa coefficient of 0.8780. In this

scene, Bayes classifier provided the best overall classification accuracy. Especially, water, sand, dry soil, and forest were land-cover classes with the most agreement between the classified images and the reference data. Their user's and producer's accuracies were all above 90%. ISODATA and fuzzy classifier performed the same regarding overall accuracy. Compared to Bayes classification, these two classifiers did not perform well in non-forest vegetation and wet soil class as they produced higher commission errors.

Table 15 (a) – (c) lists the error matrices for Landsat 5 TM image date Aug-03-1999, which summarize the user's accuracy, producer's accuracy, overall accuracy, and Kappa coefficient from the ISODATA, Bayes, and fuzzy classifications, respectively. ISODATA had an overall accuracy of 88.67% with Kappa coefficient of 0.8640, Bayes classifier had an overall accuracy of 90.00% with Kappa coefficient of 0.8800, and fuzzy classifier had an overall accuracy of 88.67% with Kappa coefficient of 0.8640. Again in this scene, Bayes classifier provided the best overall classification accuracy. Regarding both user's accuracy and producer's accuracy, results from Bayes classification had at least 85% correctness, whereas several accuracies in ISODATA and fuzzy classifications were lower than 75%. These two classifiers performed especially badly in classifying dry soil, forest, and non-forest vegetation.

Table 11. Error matrices for image date Aug-02-1987 based on three different classification algorithms: (a) ISODATA; (b) Bayes Classifier; and (c) Fuzzy Classifier.

		Reference Data							
	(a)	Forest	Non-forest Vegetation	Water	Sand	Dry Soil	Wet Soil	Row Total	User's Accuracy (%)
Classified Imagery	Forest	90	10	0	0	0	0	100	100.00
	Non-forest Vegetation	10	89	0	0	0	1	100	92.00
	Water	0	0	100	0	0	0	100	94.00
	Sand	1	3	0	92	0	4	100	83.00
	Dry Soil	2	1	0	0	94	3	100	90.00
	Wet Soil	10	7	0	0	0	83	100	89.00
Column Total		113	110	100	92	94	91	600	
Producer's Accuracy (%)		79.65	80.91	100	100	100	91.21		
Overall Accuracy (%)		**91.33**		**Kappa Coefficient**		**0. 8960**			

		Reference Data							
	(b)	Forest	Non-forest Vegetation	Water	Sand	Dry Soil	Wet Soil	Row Total	User's Accuracy (%)
Classified Imagery	Forest	94	6	0	0	0	0	100	94.00
	Non-forest Vegetation	9	88	0	0	0	3	100	88.00
	Water	0	0	100	0	0	0	100	100.00
	Sand	0	0	21	78	0	1	100	78.00
	Dry Soil	1	6	0	0	86	7	100	86.00
	Wet Soil	1	0	0	0	10	89	100	89.00
Column Total		105	100	121	78	96	100	600	
Producer's Accuracy (%)		89.52	88.00	82.64	100	89.58	89.00		
Overall Accuracy (%)		**89.17**		**Kappa Coefficient**		**0.8700**			

		Reference Data							
	(c)	Forest	Non-forest Vegetation	Water	Sand	Dry Soil	Wet Soil	Row Total	User's Accuracy (%)
Classified Imagery	Forest	90	10	0	0	0	0	100	90.00
	Non-forest Vegetation	9	86	4	0	0	1	100	86.00
	Water	0	0	100	0	0	0	100	100.00
	Sand	0	1	8	90	1	0	100	90.00
	Dry Soil	0	0	3	0	92	5	100	92.00
	Wet Soil	0	5	1	0	11	83	100	83.00
Column Total		99	102	116	90	104	89	600	
Producer's Accuracy (%)		90.91	84.31	86.21	100.0	88.46	93.26		
Overall Accuracy (%)		**90.17**		**Kappa Coefficient**		**0. 8820**			

Table 12. Error matrices for image date Sep-27-1990 based on three different classification algorithms: (a) ISODATA; (b) Bayes Classifier; and (c) Fuzzy Classifier.

		Reference Data							
	(a)	Forest	Non-forest Vegetation	Water	Sand	Dry Soil	Wet Soil	Row Total	User's Accuracy (%)
Classified Imagery	Forest	90	10	0	0	0	0	100	90.00
	Non-forest Vegetation	9	86	0	0	4	1	100	86.00
	Water	0	1	96	0	0	3	100	96.00
	Sand	1	1	4	94	0	0	100	94.00
	Dry Soil	0	0	0	0	95	5	100	95.00
	Wet Soil	0	4	0	0	3	93	100	93.00
	Column Total	100	102	100	94	102	102	600	
	Producer's Accuracy (%)	90.00	84.31	96.00	100.0	93.14	91.18		
Overall Accuracy (%)		**92.33**			**Kappa Coefficient**		**0.9080**		

		Reference Data							
	(b)	Forest	Non-forest Vegetation	Water	Sand	Dry Soil	Wet Soil	Row Total	User's Accuracy (%)
Classified Imagery	Forest	94	6	0	0	0	0	100	94.00
	Non-forest Vegetation	4	84	0	0	6	6	100	84.00
	Water	0	0	100	0	0	0	100	100.00
	Sand	0	0	5	95	0	0	100	95.00
	Dry Soil	0	3	0	2	94	1	100	94.00
	Wet Soil	1	4	1	1	1	92	100	92.00
	Column Total	99	97	106	98	101	99	600	
	Producer's Accuracy (%)	94.95	86.60	94.34	96.94	93.07	92.93		
Overall Accuracy (%)		**93.17**			**Kappa Coefficient**		**0.9180**		

		Reference Data							
	(c)	Forest	Non-forest Vegetation	Water	Sand	Dry Soil	Wet Soil	Row Total	User's Accuracy (%)
Classified Imagery	Forest	93	7	0	0	0	0	100	93.00
	Non-forest Vegetation	7	86	1	0	3	3	100	86.00
	Water	0	0	100	0	0	0	100	100.00
	Sand	3	0	1	93	0	3	100	93.00
	Dry Soil	0	1	2	4	87	6	100	87.00
	Wet Soil	6	4	2	0	5	83	100	83.00
	Column Total	109	98	106	97	95	95	600	
	Producer's Accuracy (%)	85.32	87.76	94.34	95.88	91.58	87.37		
Overall Accuracy (%)		**90.33**			**Kappa Coefficient**		**0.8840**		

Table 13. Error matrices for image date Jul-07-1995 based on three different classification algorithms: (a) ISODATA; (b) Bayes Classifier; and (c) Fuzzy Classifier.

		Reference Data							
	(a)	Forest	Non-forest Vegetation	Water	Sand	Dry Soil	Wet Soil	Row Total	User's Accuracy (%)
Classified Imagery	Forest	92	8	0	0	0	0	100	92.00
	Non-forest Vegetation	10	86	0	0	4	0	100	86.00
	Water	0	0	100	0	0	0	100	100.00
	Sand	0	0	3	96	1	0	100	96.00
	Dry Soil	6	8	0	0	86	0	100	86.00
	Wet Soil	13	1	0	0	4	82	100	82.00
Column Total		121	103	103	96	95	82	600	
Producer's Accuracy (%)		76.03	83.50	97.09	100.0	90.53	100		

Overall Accuracy (%) 90.33 **Kappa Coefficient 0.8840**

		Reference Data							
	(b)	Forest	Non-forest Vegetation	Water	Sand	Dry Soil	Wet Soil	Row Total	User's Accuracy (%)
Classified Imagery	Forest	93	7	0	0	0	0	100	93.00
	Non-forest Vegetation	15	85	0	0	0	0	100	85.00
	Water	0	0	100	0	0	0	100	100.00
	Sand	0	0	4	95	1	0	100	95.00
	Dry Soil	2	6	0	0	90	2	100	90.00
	Wet Soil	7	8	0	1	4	80	100	80.00
Column Total		117	106	104	96	95	82	600	
Producer's Accuracy (%)		79.49	80.19	96.15	98.96	94.74	97.56		

Overall Accuracy (%) 90.50 **Kappa Coefficient 0.8860**

		Reference Data							
	(c)	Forest	Non-forest Vegetation	Water	Sand	Dry Soil	Wet Soil	Row Total	User's Accuracy (%)
Classified Imagery	Forest	94	6	0	0	0	0	100	94.00
	Non-forest Vegetation	12	87	0	0	1	0	100	87.00
	Water	0	0	100	0	0	0	100	100.00
	Sand	0	0	0	100	0	0	100	100.00
	Dry Soil	5	6	2	4	83	0	100	83.00
	Wet Soil	9	3	2	0	4	82	100	82.00
Column Total		120	102	104	104	88	82	600	
Producer's Accuracy (%)		78.33	85.29	96.15	96.15	94.32	100.0		

Overall Accuracy (%) 91.00 **Kappa Coefficient 0.8920**

Table 14. Error matrices for image date Aug-03-1999 based on three different classification algorithms: (a) ISODATA; (b) Bayes Classifier; and (c) Fuzzy Classifier.

		Reference Data							
	(a)	Forest	Non-forest Vegetation	Water	Sand	Dry Soil	Wet Soil	Row Total	User's Accuracy (%)
Classified Imagery	Forest	89	11	0	0	0	0	100	89.00
	Non-forest Vegetation	10	87	0	0	2	1	100	87.00
	Water	0	0	100	0	0	0	100	100.00
	Sand	0	2	7	91	0	0	100	91.00
	Dry Soil	0	1	0	1	91	7	100	91.00
	Wet Soil	6	11	0	0	2	81	100	81.00
Column Total		105	112	107	92	95	89	600	
Producer's Accuracy (%)		84.76	77.68	93.46	98.91	95.79	91.01		

Overall Accuracy (%) 89.83 **Kappa Coefficient 0.8780**

		Reference Data							
	(b)	Forest	Non-forest Vegetation	Water	Sand	Dry Soil	Wet Soil	Row Total	User's Accuracy (%)
Classified Imagery	Forest	93	7	0	0	0	0	100	93.00
	Non-forest Vegetation	5	85	0	0	2	8	100	85.00
	Water	0	0	100	0	0	0	100	100.00
	Sand	0	2	5	90	0	3	100	90.00
	Dry Soil	0	2	0	0	96	2	100	96.00
	Wet Soil	2	3	0	0	8	87	100	87.00
Column Total		100	99	105	90	106	100	600	
Producer's Accuracy (%)		93.00	85.86	95.24	100.0	90.57	87.00		

Overall Accuracy (%) 89.83 **Kappa Coefficient 0.8780**

		Reference Data							
	(c)	Forest	Non-forest Vegetation	Water	Sand	Dry Soil	Wet Soil	Row Total	User's Accuracy (%)
Classified Imagery	Forest	93	7	0	0	0	0	100	93.00
	Non-forest Vegetation	8	88	0	0	1	3	100	88.00
	Water	0	0	100	0	0	0	100	100.00
	Sand	0	5	10	82	2	1	100	82.00
	Dry Soil	0	1	0	0	90	9	100	90.00
	Wet Soil	3	3	3	0	5	86	100	86.00
Column Total		104	104	113	82	98	99	600	
Producer's Accuracy (%)		89.42	84.62	88.5	100.0	91.84	86.87		

Overall Accuracy (%) 91.83 **Kappa Coefficient 0.9020**

Table 15. Error matrices for image date Jul-05-2006 based on three different classification algorithms: (a) ISODATA; (b) Bayes Classifier; and (c) Fuzzy Classifier.

		Reference Data							
	(a)	Forest	Non-forest Vegetation	Water	Sand	Dry Soil	Wet Soil	Row Total	User's Accuracy (%)
Classified Imagery	Forest	91	9	0	0	0	0	100	91.00
	Non-forest Vegetation	13	83	0	0	1	3	100	83.00
	Water	0	0	100	0	0	0	100	100.00
	Sand	0	0	1	99	0	0	100	99.00
	Dry Soil	13	5	0	0	75	7	100	75.00
	Wet Soil	5	8	0	0	3	84	100	84.00
Column Total		122	105	101	99	79	94	600	
Producer's Accuracy (%)		74.59	79.05	99.01	100.0	94.94	89.36		

Overall Accuracy (%) 88.67 **Kappa Coefficient 0.8640**

		Reference Data							
	(b)	Forest	Non-forest Vegetation	Water	Sand	Dry Soil	Wet Soil	Row Total	User's Accuracy (%)
Classified Imagery	Forest	94	6	0	0	0	0	100	94.00
	Non-forest Vegetation	11	87	0	0	0	2	100	87.00
	Water	0	0	100	0	0	0	100	100.00
	Sand	0	0	9	91	0	0	100	91.00
	Dry Soil	0	0	0	0	84	16	100	84.00
	Wet Soil	0	2	1	0	13	84	100	84.00
Column Total		105	95	110	91	97	102	600	
Producer's Accuracy (%)		89.52	91.58	90.91	100.0	86.6	82.35		

Overall Accuracy (%) 88.67 **Kappa Coefficient 0.8640**

		Reference Data							
	(c)	Forest	Non-forest Vegetation	Water	Sand	Dry Soil	Wet Soil	Row Total	User's Accuracy (%)
Classified Imagery	Forest	93	7	0	0	0	0	100	93.00
	Non-forest Vegetation	14	83	1	0	0	2	100	83.00
	Water	0	0	100	0	0	0	100	100.00
	Sand	0	5	0	92	2	1	100	92.00
	Dry Soil	0	2	0	0	78	20	100	78.00
	Wet Soil	1	3	4	0	6	86	100	86.00
Column Total		108	100	105	92	86	109	600	
Producer's Accuracy (%)		86.11	83.00	95.24	100.0	90.70	78.90		

Overall Accuracy (%) 90.00 **Kappa Coefficient 0.8800**

In summary, Bayes and fuzzy classifiers achieved the best overall classification accuracy in two Landsat 5 TM images, respectively, and ISODATA yield the highest overall accuracy for one image date. Table 16 lists the average overall accuracy and Kappa coefficient in five images for these three classifiers. Three classifications had very similar average overall accuracies and Kappa coefficients. Significance test was also performed by calculating the Z-statistic to indicate whether there is a significant difference among these three tested classification algorithms. If the absolute value of Z-statistic is greater than 1.96, the difference between different results is significant at the 95% confidence level (Congalton and Green 2009). Table 17 (a)-(d) lists results of pairwise comparison in five image classifications. The results show no statistically significant differences for all pairwise comparisons of the classified images for the algorithms considered, for all five images. This indicates that the hardened classification accuracies of these three methods entail little difference for this research. However, as the two soft classifications are able to provide probability or membership information, a soft classification approach is of higher utility for this research.

Table 16. Average overall accuracy and Kappa coefficient of the three tested classification algorithms.

Classifier	Average Overall Accuracy (%)	Average Kappa Coefficient
ISODATA	90.97	0.8917
Bayes	90.45	0.8853
Fuzzy	90.17	0.8800

Table 17. Test for significant differences between error matrices for the classification algorithms for image date: (a) Aug-02-1987; (b) Sep-27-1990; (c) Jul-07-1995; (d) Aug-03-1999; and (e) Jul-05-2006.

(a)

Pairwise Comparison	Z-Statistic	Result
ISODATA and Bayes	1.0399	NS
ISODATA and Fuzzy	0.5721	NS
Bayes and Fuzzy	0.4679	NS

(b)

Pairwise Comparison	Z-Statistic	Result
ISODATA and Bayes	0.4546	NS
ISODATA and Fuzzy	1.0088	NS
Bayes and Fuzzy	1.4618	NS

(c)

Pairwise Comparison	Z-Statistic	Result
ISODATA and Bayes	0.0805	NS
ISODATA and Fuzzy	0.3259	NS
Bayes and Fuzzy	0.2453	NS

(d)

Pairwise Comparison	Z-Statistic	Result
ISODATA and Bayes	0.9848	NS
ISODATA and Fuzzy	0.0000	NS
Bayes and Fuzzy	0.9849	NS

(e)

Pairwise Comparison	Z-Statistic	Result
ISODATA and Bayes	0.6155	NS
ISODATA and Fuzzy	0.0000	NS
Bayes and Fuzzy	0.6151	NS

NS = non-significant result at the 95% confidence level.

Regarding each land-cover class, the classification accuracies showed different situations. Water class was the class with the most agreement between the classified image data and reference data. Its producer's accuracies were very high in all three classifications, whereas the user's accuracies were not very high in the two soft classifications. On the other hand, the sand class had high user's accuracies in all three methods, but Bayes classifier was not able to provide good producer's accuracy. For the soft classifications, water and sand were misclassified to each other significantly. Two bare soil classes had fairly good accuracies around 90%. However, these two land-cover

classes could be misclassified as each other due to similar spectral signatures. For the same reason, forest and non-forest were also relatively easy to be confused and difficult to separate in some situations. Therefore the producer's accuracies and user's accuracies of forest and non-forest were not very high, but still considered acceptable in this research.

4.2 Land-Cover Change-Detection

4.2.1 Change-Detection Accuracy Assessment

Change-detection performance of the MCVA algorithm was evaluated via accuracy assessment. As MCVA was developed based on the concept that an overlapping zone exists in the traditional single-thresholding approach, where a large portion of the total change-detection error originates, an initial assessment was conducted to evaluate the errors from the potential overlapping zone. The entire change magnitude space was divided into 20 bins, with 10 bins on each side of the threshold T_0. The bins on each side were equally-spaced within the corresponding change magnitude range. Then, 50 samples were drawn from each bin to ensure the sample set covers the entire change-magnitude space equally, which was a key step in assessing the influence of the overlapping zone. Manual interpretation/visual assessment was performed to assess the accuracy of change detection within each bin.

Table 18 and Figure 12 show the test results of change-detection accuracy in the period from 1987 to 1990. They confirm that the change accuracy declined as the change magnitude became closer to the threshold T_0, whereas pixels with change magnitude

away from the threshold had very high change accuracies (11 peripheral bins showed accuracies over 90%, and 7 of them achieved 100% accuracy). In particular, bins 9, 10, and 11 showed very low accuracies because these change-magnitude ranges constitute the major portion of the potential overlapping zone, as they were closest to the threshold on either side of the threshold. With this sampling strategy, the overall accuracy was calculated as the summation of the weighted accuracy of each bin (weighted on the number of pixels), and thus, the overall accuracy is 79.75%.

Table 18. Change-detection (1987-1990) accuracy in each bin with thresholding approach.

Bin	1	2	3	4	5	6	7	8	9	10
Change Magnitude	[0, 0.06)	[0.06, 0.11)	[0.11, 0.17)	[0.17, 0.23)	[0.23, 0.28)	[0.28, 0.34)	[0.34, 0.4)	[0.4, 0.51)	[0.51, 0.57)	[0.51, 0.57)
Accuracy (%)	100	100	100	94	90	78	70	74	**58**	**32**

Bin	11	12	13	14	15	16	17	18	19	20
Change Magnitude	[0.57, 0.65)	[0.65, 0.73)	[0.73, 0.82)	[0.82, 0.9)	[0.9, 0.97)	[0.97, 1.07)	[1.07, 1.14)	[1.14, 1.24)	[1.24, 1.33)	[1.33, 1.41]
Accuracy (%)	**34**	72	78	82	92	94	100	100	100	100

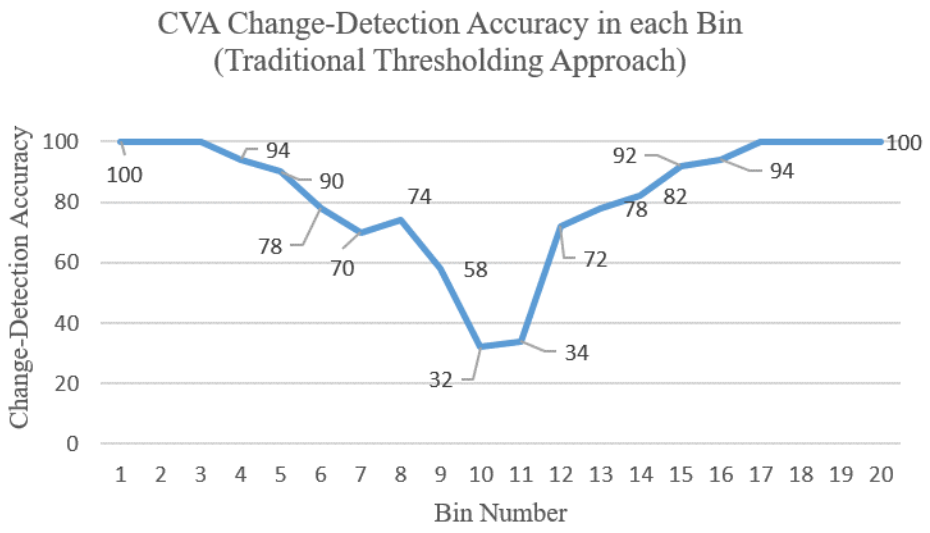

Figure 12. CVA change-detection (1987 - 1990) accuracy in each bin with traditional thresholding approach.

The MCVA algorithm proposed in this research aims to improve change-detection accuracy by improving the separation of changed/unchanged pixels in the overlapping zone while maintaining the good accuracy in either tail of the change-magnitude space. Table 19 summarizes the change-detection accuracy of the dynamic 1st thresholding stage of MCVA algorithm. With dynamic thresholding approach, only pixels in bins 8 – 12 were affected and experienced label change. These results suggest that this modification was able to target the pixels in the overlapping zone. In particular, Figure 13 was generated to illustrate the improvement in bins 8 – 12. For all five (5) bins, the proposed method was able to achieve improvement in change-detection accuracy. Especially for bins 9-11, which were severely affected by the overlapping issue, the proposed method successfully improved the change-detection accuracy by 15%, 37%, and 38%, respectively. Under the novel dynamic-thresholding technique, the

algorithm achieved an overall accuracy of 85.49% at this stage, which was a 5.74% overall improvement compared to the traditional approach. This result demonstrates that the proposed dynamic-thresholding method is able to address the overlapping issues with the traditional thresholding method to some extent and provide better change-detection accuracy.

Table 19. Change-detection (1987-1990) performance in each bin with proposed dynamic 1st thresholding stage.

Bin	1	2	3	4	5	6	7	8	9	10
Num. of Affected Pixels	0	0	0	0	0	0	0	79181	119073	97887
Accuracy (%)	100	100	100	94	90	78	70	**82**	**73**	**69**
Accuracy Improvement (%)	0	0	0	0	0	0	0	**8**	**15**	**37**

Bin	11	12	13	14	15	16	17	18	19	20
Num. of Affected Pixels	9719	1849	0	0	0	0	0	0	0	0
Accuracy (%)	**72**	**74**	078	082	092	094	100	100	100	100
Accuracy Improvement (%)	**38**	**2**	0	0	0	0	0	0	0	0

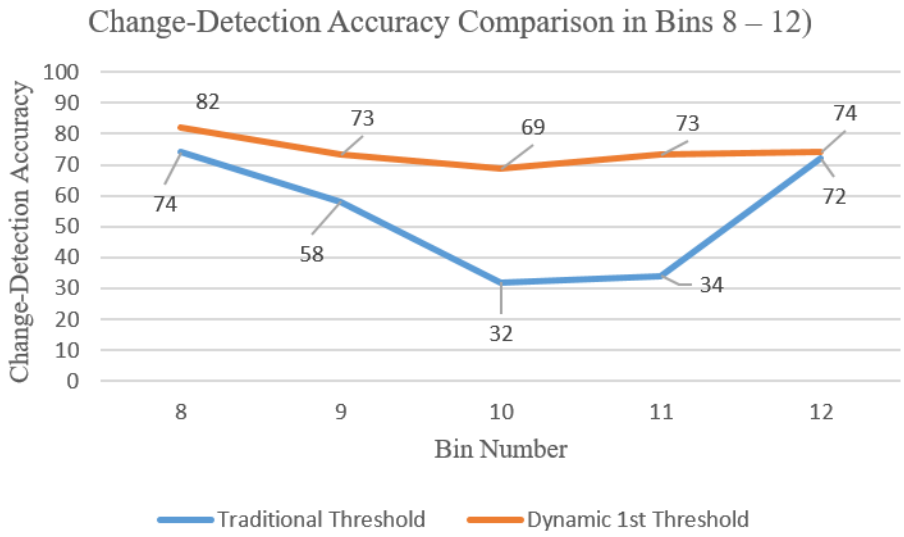

Figure 13. Change-detection (1987-1990) accuracy comparison in bins 8-12.

In addition, to assess the effect of using fuzzy-labeling information on the MCVA algorithm, both FMRF and conventional MRF were applied to the results after the proposed dynamic 1st thresholding stage of MCVA. This procedure would therefore only show the difference in the using fuzzy and hard change label. Table 20 reports the quantitative change-detection accuracy assessment for each MRF model. The overall accuracies of fuzzy MRF and conventional MRF were 90.90% and 89%, respectively. The Kappa coefficients for fuzzy MRF and conventional MRF were 0.818 and 0.78, respectively. Both models were able to improve the original change-detection result produced by the dynamic 1st thresholding approach, but the fuzzy MRF achieved better change-detection accuracy.

Table 20. Accuracy assessment for fuzzy MRF and conventional MRF results (from operating on the results generated by proposed dynamic 1st thresholding stage).

Method	Overall Accuracy (%)	Kappa Coefficient
Fuzzy MRF	90.90	0.818
Conventional MRF	89.00	0.780

As the quantitative improvement in change-detection accuracy garnered by incorporating fuzzy-membership information (i.e., change uncertainty) might not be very significant, a further illustration is presented in Figure 14. From the visual analysis, both results were able to capture major changes between the two dates. The result from conventional MRF was smoother than the result from FMRF, as fewer isolated changed pixels were found. However, over-smooth problem was detected in the conventional MRF result, as some subtle changes, such as changes in channel scars and riparian areas, were overly-smoothed, and thus, many details were lost. This was because the conventional MRF process did not consider the uncertainty from change labels of neighboring pixels. However, FMRF considered the change uncertainty in the spatial function and preserved more change details and structures.

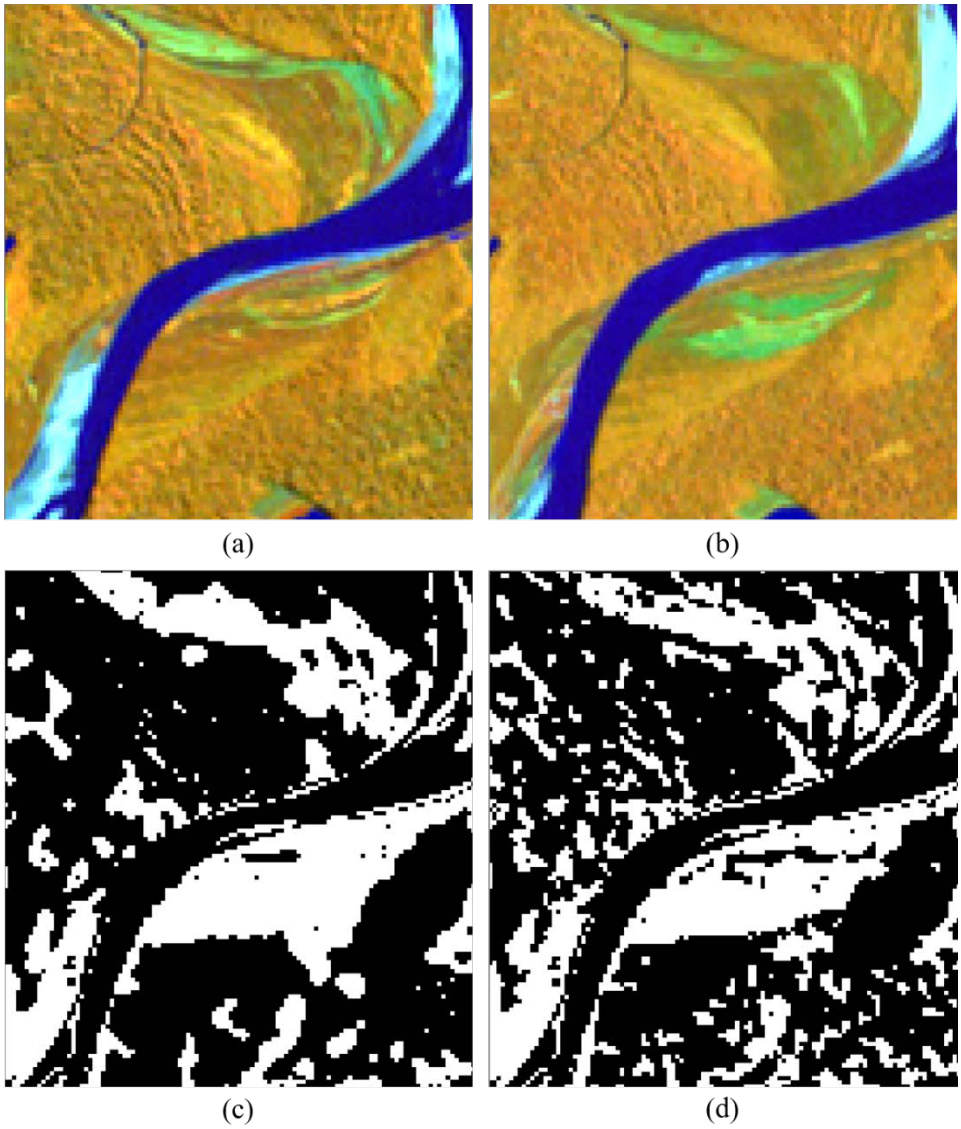

Figure 14. Spatial subset of the study area: (a) Landsat 5 TM image in 1987; (b) Landsat 5 TM image in 1990, displayed with bands 4, 5, 1 as R,G,B; (c) changed (white) / unchanged (black) image after conventional MRF; and (d) changed/unchanged image after FMRF.

In order to comprehensively evaluate MCVA, experiments were also conducted on standard post-classification comparison (PCC) and standard change vector analysis (CVA), and CVAPS. This set of baseline change-detection algorithms for comparison was selected given that MCVA was developed based on CVAPS, and CVAPS was developed based on a combination of PCC and conventional CVA. The evaluation quantities for this comparison are overall change-detection accuracy and Kappa coefficient derived from standard error matrices. Table 21 (a)-(d) lists the change-detection error matrices from PCC, CVA, CVAPS, and MCVA, respectively. This table reports the producer's accuracy, user's accuracy, overall accuracy, and Kappa coefficient.

Table 21. Change-detection (1987-1990) error matrices for four different algorithms: (a) PCC; (b) CVA; (c) CVAPS; and (d) MCVA.

(a)

		Reference Data			
		No Change	Change	Row Total	User's Accuracy (%)
Classified Imagery	No Change	**392**	108	500	78.40
	Change	135	**365**	500	73.00
	Column Total	527	473	1000	
	Producer's Accuracy (%)	74.38	77.17		
	Overall Accuracy (%)	**75.70**		**Kappa Coefficient**	**0.514**

(b)

		Reference Data			
		No Change	Change	Row Total	User's Accuracy (%)
Classified Imagery	No Change	**399**	101	500	79.80
	Change	124	**376**	500	75.20
	Column Total	523	477	1000	
	Producer's Accuracy (%)	76.29	78.83		
	Overall Accuracy (%)	**77.50**		**Kappa Coefficient**	**0.550**

Table 21. Continued.

(c)

		Reference Data			
		No Change	Change	Row Total	User's Accuracy (%)
Classified Imagery	No Change	**398**	102	500	79.60
	Change	84	**416**	500	83.20
	Column Total	482	518	1000	
	Producer's Accuracy (%)	82.57	80.31		
	Overall Accuracy (%)	**81.40**		**Kappa Coefficient**	**0.628**

(d)

		Reference Data			
		No Change	Change	Row Total	User's Accuracy (%)
Classified Imagery	No Change	**449**	51	500	89.80
	Change	40	**460**	500	92.00
	Column Total	489	511	1000	
	Producer's Accuracy (%)	91.82	90.02		
	Overall Accuracy (%)	**90.90**		**Kappa Coefficient**	**0.818**

The quantity disagreement and allocation disagreement were also derived from the error matrices. Figure 15 shows the two disagreements for the four tested change-detection algorithms. The two disagreements are stacked to show the total disagreement. The proposed MCVA algorithm achieved the lowest disagreements between the classified image and reference samples, whose quantity disagreement was 0.011 and allocation disagreement was 0.08. The relative ranking of quantity disagreement, allocation disagreement, and total disagreement was identical to the relative ranking of overall accuracy among the four algorithms tested. Each bar in the figure also demonstrates that the quantity disagreement only accounted a small amount of total disagreement. The differences in quantity disagreement among the four algorithms tested were smaller than the differences in allocation disagreement.

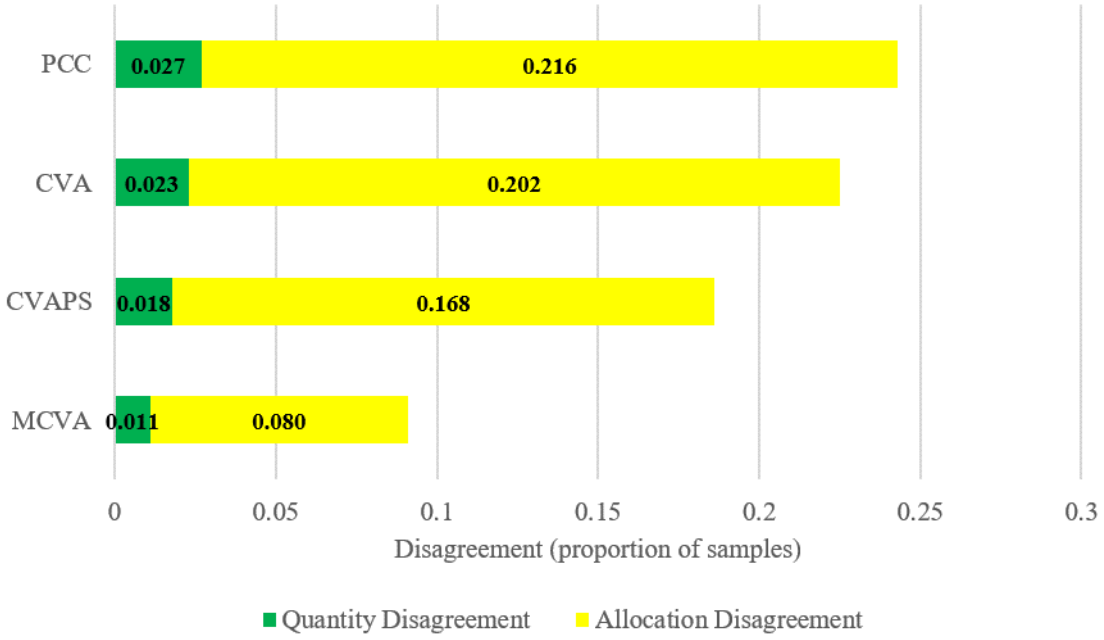

Figure 15. Quantity disagreement, allocation disagreement for four algorithms tested.

To help interpret the results, the overall change-detection accuracies, Kappa coefficients, quantity disagreements, and allocation disagreements of each algorithm are summarized in Table 21. The overall accuracies for PCC, CVA, CVAPS and MCVA were 75.7%, 77.5%, 81.4%, and 90.9%, respectively. Kappa coefficients for PCC, CVA, CVAPS and MCVA were 0.514, 0.550, 0.628, and 0.818, respectively. The quantity disagreement for PCC, CVA, CVAPS and MCVA were 0.027, 0.023, 0.018, and 0.011, respectively; while the allocation disagreement for the four algorithms were 0.216, 0.202, 0.168, and 0.080, respectively. Significance testing was also performed by calculating the Z-statistic to indicate whether there is a significant difference between the MCVA result and the other three change-detection algorithms. If the absolute value of Z-statistic is greater than 1.96, the difference between different results is significant at

the 95% confidence level (Congalton and Green 2009). Table 23 indicates that MCVA did achieve a significant improvement in change-detection accuracy compared to other three commonly-used methods.

Although PCC and CVA have long been commonly-used change-detection techniques, both algorithms have drawbacks and limitations; for example, PCC usually overestimates change and cumulates classification errors, and CVA usually requires reliable image radiometry to ensure accuracte change-detection. These intrinsic limitations are difficult to resolve; thus, they did not achieve good change-detection accuracies in this experiment compared with the other two methods. CVAPS was built based on PCC and CVA, and it showed some improvements compared to those two methods. However, the simple single thresholding procedure has been proved to be a main source of change-detection errors, which leads to a barrier for CVAPS to achieve accurate change maps. The proposed dynamic 1st thresholding modification, which uses the static threshold as a reference point and utilizes class-change information to adjust the changed/unchanged status for each pixel, achieved an improvement compared with CVAPS. With the further refinement of the FMRF, the proposed MCVA was able to achieve change-detection accuracy over 90%, and show improvement in Kappa coefficient, quantity disagreement and allocation disagreement. In summary, the results indicate the superiority of the proposed MCVA algorithm, relative to the other algorithms tested.

Table 22. Change-detection (1987-1990) performance of different algorithms tested.

Algorithm	Overall Accuracy (%)	Kappa Coefficient	Quantity Disagreement	Allocation Disagreement
PCC	75.70	0.514	0.027	0.216
CVA	77.50	0.550	0.023	0.202
CVAPS	81.40	0.628	0.018	0.168
MCVA	90.90	0.818	0.011	0.080

Table 23. Test for significant differences between error matrices (1987-1990) for the change-detection algorithms tested.

Pairwise Comparison	Z-Statistic	Result
MCVA and PCC	9.3058	S
MCVA and CVA	8.3566	S
MCVA and CVAPS	6.2093	S

S = significant result at the 95% confidence level.

4.2.2 Changes in Areal Extent and Distribution of Land-Cover Types

The land-cover change maps of four pairs of consecutive Landsat image-acquisition dates (e.g., 1987 and 1990; 1990 and 1995, etc.) and the map pair consisting of the earliest and latest dates in the time-series studied (i.e., 1987 and 2006) were generated by the MCVA algorithm. Due to their fuzzy characteristics, the fuzzy membership layers are more suitable for use in detecting subtle/minor changes regarding land-cover/landscape change; thus, the MCVA algorithm was applied to fuzzy membership datasets. The results are shown in change matrices to understand the magnitude and type of land-cover change that occurred within the floodplain during each time period assessed. Tables 24, 27, 30, 33, and 36 consist of four land-cover change matrices that show, as a percentage, the “from” class area. This means that for each row,

the value in every column corresponds to the percentage of the row land-cover changed or transitionally changed to that particular column land-cover. On the other hand, Tables 25, 28, 31, 34, and 37 consist of four land-cover change matrices that show, as a percentage, the "to" class area. This means for each column, the value in every row corresponds to the percentage of the column land-cover was changed or transitionally changed from that particular row land-cover. In all tables, "C/N" denotes change/no-change, and "trans." denotes transitional change from one land-cover class to another. For the cells denoting no land-cover shift, such as from "Forest" to "Forest", "trans." means the fuzzy class membership increased (became purer in the dominant land-cover class).

4.2.2.1 Change in Time Period: 1987-1990

Table 24 and Table 25 show the "from-to" land-cover change from 1987 to 1990, which has the percentages of the area classified "from" and "to" each pair of land-cover classes, respectively. During this period, forest lost a significant amount area of 229.9 km^2. In 1990, only 77.38% of forest was derived from existing forest in 1987. A total of 8.86% existing forest changed to non-forest vegetation (5.70% from change, 3.16% from transitional change). It also changed to wet soil with 13.07% of its original area coverage, which is quite surprising. The existing forest in 1987 consisted of the forest area in 1990 over 98%, which means not much land-cover shifted to forest during this period. Non-forest vegetation had the biggest area increase by 265 km^2. It was able to retain 97.01% of its original coverage. New non-forest vegetation was primarily derived

from forest (11.61% change, 6.43% transitional change), and two soil classes (10.15% from change, 3.15% from transitional change). The area of oxbow lakes almost remained the same during the period. It lost 6.38% of the area to main river channel due to channel reconnection, and 8.14% to wet soil due to dry-up. In return, 30% of oxbow lake coverage was derived from main river channel in 1990. The area coverage of main river channel also remained similar with a slight decrease of 2.6 km^2, and most of it was lost to oxbow lakes and sand due to channel migration and other geomorphic processes. Sand lost about 10 km^2. Among the loss, 7.77% of existing sand in 1987 changed to dry soil, 11.41% to non-forest vegetation, 14.53% to river stream, and 20.16% to wet soil. Among the newly-formed sand cover, 28.64% was from main river channel. Dry soil also contributed 8.75% to sand cover in transition. The area of dry soil decreased 19.5 km^2. Only 56.58% of existing dry soil remained in 1990, which 54.01% of it was unchanged, and 2.84% with higher class fuzzy membership (became purer as dry soil). The most pronounced land-cover shift from dry soil was to non-forest vegetation with 22.32% change and 1.74% transitional change. Dry soil also had 10.25% and 1.56% of its area changed and transitionally changed to wet soil, respectively. New dry soil emerged primarily from wet soil (10.33%) and sand (6.28%). Wet soil retained most of its original area (63.74%). Wet soil had some area lost to non-forest vegetation (19.49 % in change, 8.29% in transitional change) and dry soil. But it significantly gained new area from forest (almost 40% of wet soil area in 1990 was shifted from forest), which is the main reason of the increasing area coverage of wet soil.

Table 24. Change of land-covers between Aug 1987 and Sep 1990 shown as percent of the From Class area.

From Class	To Class													
	Forest		Non-forest Vegetation		Oxbow Lake		River		Sand		Dry Soil		Wet Soil	
	C/N	Trans.	C/N	Trans.	C/N	Trans.	C/N	Trans.	C/N	Trans.	C/N	Trans.	C/N	Trans.
Forest	77.38	0.00	5.70	3.16	0.01	0.00	0.42	0.00	0.09	0.00	0.16	0.00	4.05	9.02
Non-forest Vegetation	0.51	0.49	94.37	2.64	0.00	0.00	0.50	0.00	0.21	0.00	0.34	0.05	0.33	0.57
Oxbow Lake	0.01	0.00	0.74	0.05	80.03	1.48	6.22	0.16	1.75	0.00	1.41	0.02	7.77	0.37
River	0.02	0.00	0.83	0.01	11.50	1.09	73.94	0.07	9.55	0.00	0.80	0.00	2.20	0.01
Sand	0.45	0.04	11.20	0.21	0.62	0.00	14.53	0.00	44.67	0.35	7.55	0.22	19.87	0.29
Dry Soil	0.72	0.04	22.32	1.74	0.08	0.00	1.98	0.00	4.25	0.20	54.01	2.84	10.25	1.56
Wet Soil	2.32	1.16	19.49	8.29	0.04	0.00	1.02	0.00	0.60	0.00	3.00	0.34	62.39	1.35

Table 25. Change of land-covers between Aug 1987 and Sep 1990 shown as percent of the To Class area.

From Class	To Class													
	Forest		Non-forest Vegetation		Oxbow Lake		River		Sand		Dry Soil		Wet Soil	
	C/N	Trans.	C/N	Trans.	C/N	Trans.	C/N	Trans.	C/N	Trans.	C/N	Trans.	C/N	Trans.
Forest	98.70	0.01	11.61	6.43	0.18	0.00	4.15	0.00	2.43	0.02	2.87	0.02	15.20	33.91
Non-forest Vegetation	0.22	0.21	65.54	1.83	0.03	0.01	1.69	0.00	1.87	0.04	2.08	0.28	0.42	0.73
Oxbow Lake	0.00	0.00	0.05	0.00	64.78	1.20	2.15	0.06	1.63	0.00	0.89	0.01	1.02	0.05
River	0.00	0.00	0.19	0.00	29.98	2.84	82.25	0.08	28.64	0.00	1.62	0.01	0.93	0.00
Sand	0.03	0.00	1.02	0.02	0.65	0.00	6.45	0.00	53.46	0.42	6.11	0.18	3.35	0.05
Dry Soil	0.07	0.00	3.35	0.26	0.14	0.00	1.45	0.00	8.36	0.39	71.83	3.78	2.84	0.43
Wet Soil	0.51	0.25	6.80	2.89	0.18	0.01	1.73	0.00	2.72	0.02	9.28	1.05	40.19	0.87

Results above have provided the amount of various types of land-cover change that occurred throughout the Rio Beni floodplain. However, the spatial distribution of change is also necessary to analyze and characterize the landscape evolution. Figure 16 is a Boolean change map of the Rio Beni floodplain that identifies where land-cover change happened between 1987 and 1990. Within the floodplain boundary, 77.25% of pixels remained with the same land-cover, whereas 13.7% experienced clear land-cover change, and 9.05% experienced transitional land-cover change. Although the changed pixels are distributed throughout the entire area, clusters of areas with the clear change were near the active water bodies, especially near river meanders. Areas of transitional change are also scattered throughout the floodplain, but they appear to be more abundant in the middle portion along the river reach of the floodplain. Some clusters of transitional change were found in oxbow lakes and abandoned channels/scars, as these areas were expected to be transitionally colonized by vegetation, or experience change in water composition due to the disconnection from active main river channel during this time frame. Clusters of areas that did not experience land-cover change were found near and away from the river, as areas near straight sections of main river channel tend to be stable, as well as areas far from the river due to lack of more pronounced hydrological and geomorphologic processes.

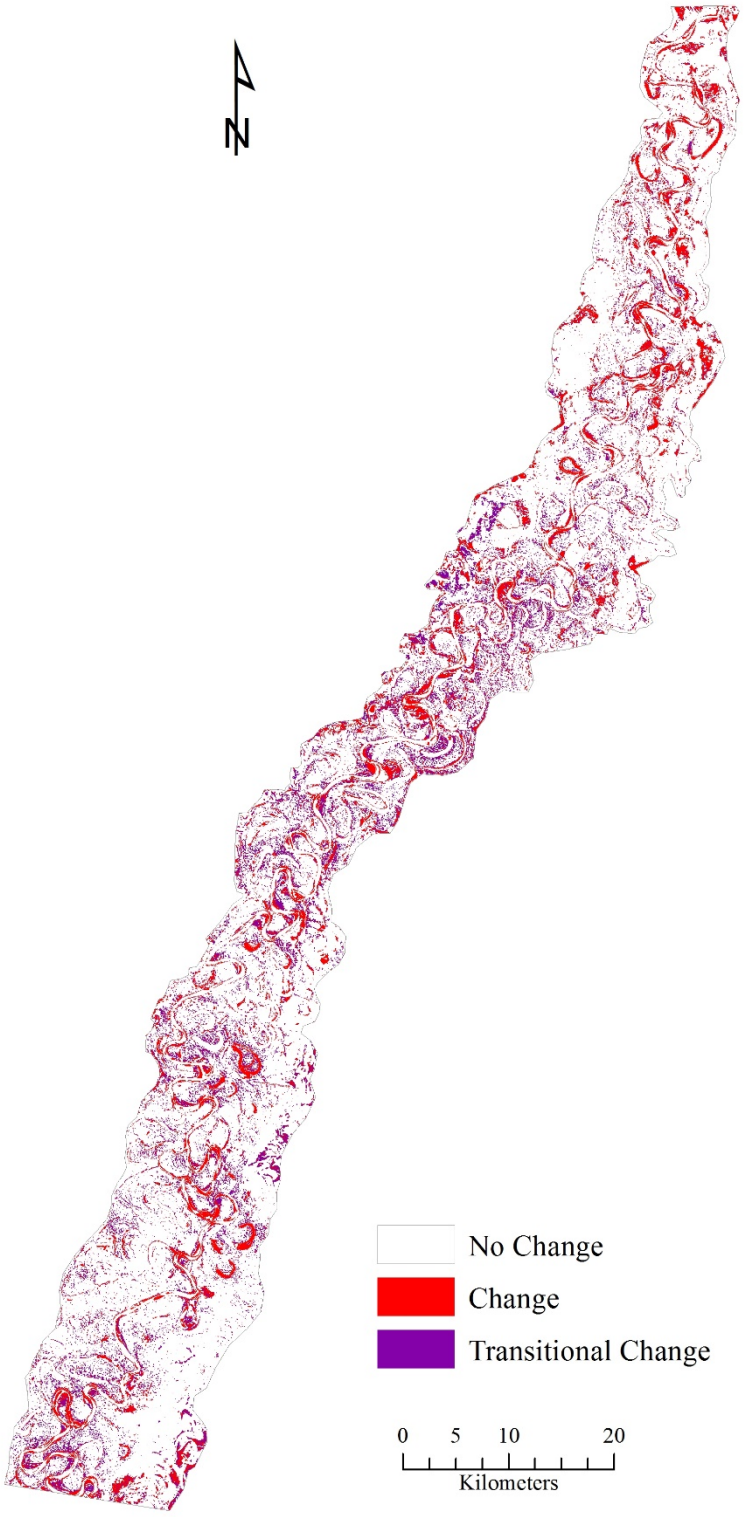

Figure 16. Map of land-cover change from 1987 to 1990.

Figure 17 contains maps that depict the land-cover class for a given pixel in 1987 before it changed (a) and the class to which the pixel changed to 1990 (b). Forest, non-forest vegetation, and wet soil were the most actively-changing land-covers.

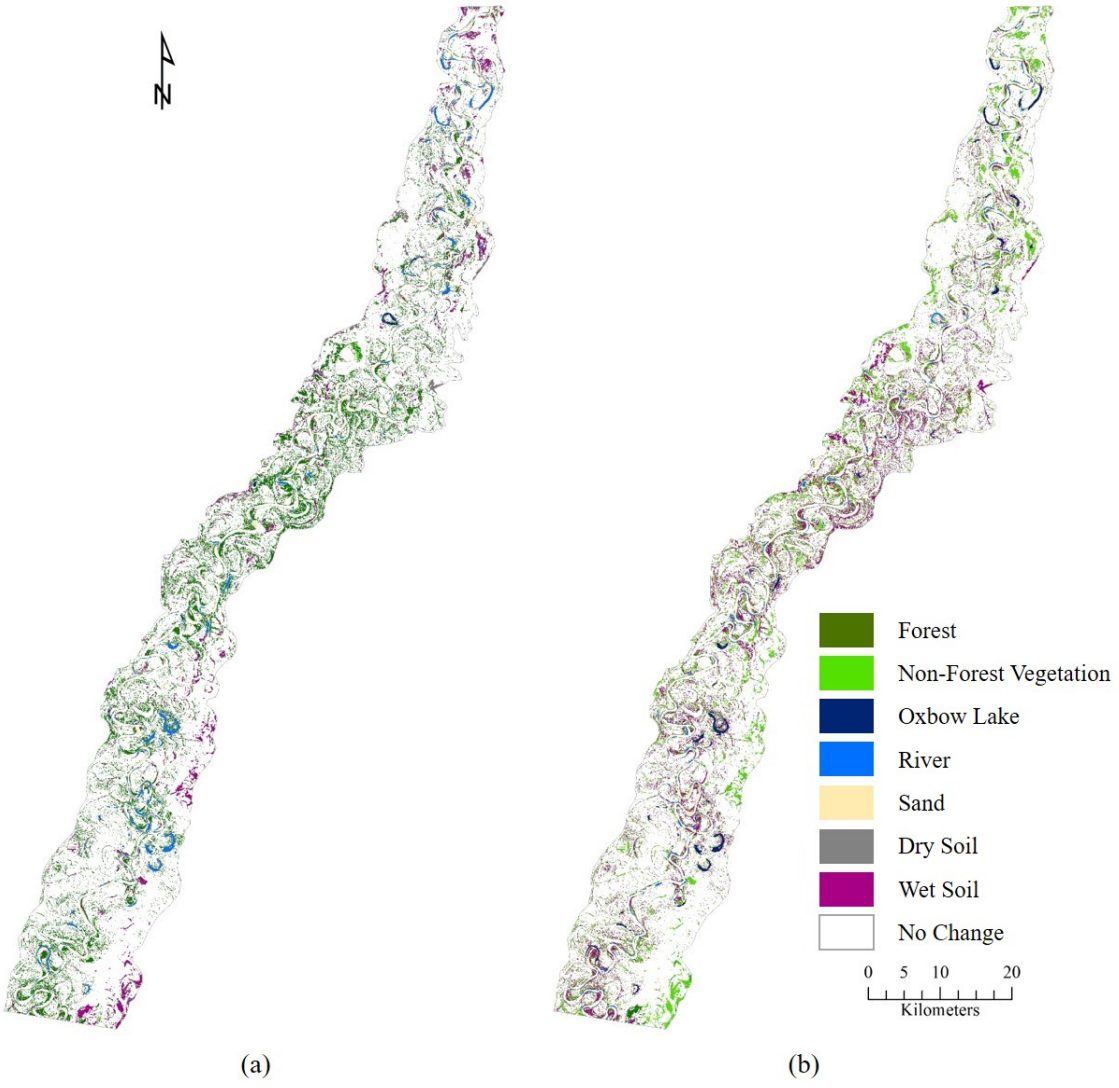

Figure 17. Land-cover changes from 1987 to 1990: (a) land-cover classes in 1987 that experienced change; (b) land-cover classes that previous classes changed to in 1990.

To better understand the spatial patterns of land-cover change, four spatial buffer zones were created to evaluate the proximal and distal land-cover and landscape based on distance away from the edge of river channel in earlier date (i.e., in 1987). Table 26 shows the percentage of land-cover change types within four spatial buffer zones from 1987 to 1990. Compared to the overall ratio of no-change pixels, which was 78.48%, buffer zone 1 was below this rate whereas other three zones had no-change ratios higher than that. Moreover, the ratio of no-change increased as the distance away from the main river channel increased, but not proportionally across zones, as the increase from zone 1 to zone 2 was much larger than that for the other zone intervals. This is expected, as areas closer to an active meandering river are typically affected to a greater degree by the geomorphologic process than regions further away. A much higher percentage of change than transitional change was also observed in zone 1, which also indicated that zone 1 experienced more dramatic landscape change.

Table 26. Percentages of land-cover change types within each buffer zone from 1987 to 1990.

Status	Zone 1	Zone 2	Zone 3	Zone 4	Average
No Change (%)	71.27	79.30	80.09	83.27	78.48
Change (%)	18.01	11.94	11.66	9.51	12.78
Transitional Change (%)	10.72	8.76	8.25	7.21	8.74

Regarding situations in the four buffer zones, not all types of “from-to” change could be found within each buffer zone. Overall, zone 1 had the largest number of change types while zone 4 had the least amount of change types. In zone 1, the most

active land-cover was forest, as the changes from forest to wet soil and non-forest vegetation were the change types with largest areas. River to sand was another change type with a high amount of area, which is understandable due to the migration of river meanders. In zone 2, forest to non-forest vegetation was again one of the most significant change types. A noticeable amount of area with land-cover shifted from the river to oxbow lakes were also found in this zone. In zone 3, some areas shifted from wet soil to non-forest vegetation. In zone 4, where the least change happened among four different zones, one significant phenomenon was that many existing forest pixels had an increasing membership and showed a transitional change within the same land-cover class. Wet soil to non-forest vegetation was another big transition.

4.2.2.2 Change in Time Period: 1990-1995

Table 27 and Table 28 show the "from-to" land-cover change from 1990 to 1995. Forest increased about 90 km^2. 90.8% of existing forest remained unchanged while 4.38% showed further growth as higher membership value was detected. 6.80 % of the forest coverage in 1999 was changed from non-forest vegetation while wet soil contributed 3.97% to the newly-gained forest cover. Non-forest vegetation decreased by 25.8 km^2 as there was no land-cover class largely shifted to non-forest vegetation during this period. The biggest loss of non-forest vegetation was from the shift to dry soil with 6.95% in change and 1.37% in transitional change. Original non-forest vegetation also converted 8.36 % to forest (6.02% in change, 2.34% in transitional change). Oxbow lake increased by 7.8 km^2 from previous date. 59.25% of original oxbow lake area remained,

whereas 32.80 % changed and 4.61% transitionally changed to main river channel. In turn, 9.72% oxbow lake area in 1995 was derived from river channel. For main river channel, 11.21% of the area in 1995 was shifted from oxbow lakes, 5.89% from non-forest vegetation, 5.33% from forest, 3.44% from sand, and 4.55% from wet soil. The area of sand only slightly increased by 0.9 km^2. However, original sand changed to dry soil by 18.15%, to forest by 10.90%, to non-forest vegetation by 6.38%, to river by 12.17%, to wet soil by 13.96%. New sand cover primarily emerged from river, which consisted of 37.91% of the sand area in 1995, and a few transitions from forest (2.98%), non-forest (3.11%), and wet soil (2.84%). Dry soil largely increased 76.1 km^2 with the largest gain from non-forest vegetation (37.40% in change, 7.37% in transitional change). Dry soil also retained 78.13% of its original coverage, with 12.68% area shifted to wet soil coverage and 3.46% to forest. Wet soil slighted decreased 4.7 km^2. The most significant shift from wet soil was to forest (23.63% in change, 3.24% in transitional change).

Table 27. Change of land-covers between Sep 1990 and Jul 1995 shown as percent of the From Class area.

From Class	To Class													
	Forest		Non-forest Vegetation		Oxbow Lake		River		Sand		Dry Soil		Wet Soil	
	C/N	Trans.	C/N.	Trans.	C/N	Trans.	C/N	Trans.	C/N	Trans.	C/N	Trans.	C/N	Trans.
Forest	90.80	4.38	1.91	0.50	0.05	0.00	0.86	0.00	0.10	0.00	0.45	0.00	0.48	0.45
Non-forest Vegetation	6.02	2.34	75.91	3.96	0.04	0.00	1.09	0.00	0.12	0.00	6.95	1.37	1.07	1.13
Oxbow Lake	0.05	0.00	0.09	0.00	58.40	0.85	32.80	4.61	0.02	0.00	1.03	0.02	2.10	0.05
River	1.26	0.00	0.35	0.00	2.76	0.21	78.60	1.21	9.21	0.00	2.87	0.01	3.50	0.02
Sand	10.88	0.03	6.35	0.03	0.22	0.00	12.17	0.00	38.21	0.00	18.08	0.08	13.95	0.00
Dry Soil	3.41	0.05	3.25	0.44	0.61	0.01	1.26	0.00	0.15	0.00	73.69	4.44	8.70	3.98
Wet Soil	23.63	3.24	3.34	1.29	2.12	0.02	4.63	0.01	0.59	0.00	5.78	1.84	49.71	3.77

Table 28. Change of land-covers between Sep 1990 and Jul 1995 shown as percent of the To Class area.

From Class	To Class													
	Forest		Non-forest Vegetation		Oxbow Lake		River		Sand		Dry Soil		Wet Soil	
	C/N	Trans.	C/N.	Trans.	C/N	Trans.	C/N	Trans.	C/N	Trans.	C/N	Trans.	C/N	Trans.
Forest	84.28	4.07	2.59	0.68	1.13	0.06	5.32	0.01	2.98	0.00	2.74	0.02	3.56	3.29
Non-forest Vegetation	4.90	1.90	90.17	4.70	0.90	0.02	5.88	0.01	3.11	0.00	37.40	7.37	6.89	7.30
Oxbow Lake	0.00	0.00	0.01	0.00	77.50	1.12	11.21	1.58	0.03	0.00	0.35	0.01	0.86	0.02
River	0.16	0.00	0.07	0.00	9.04	0.68	66.37	1.02	37.91	0.00	2.42	0.01	3.52	0.02
Sand	0.46	0.00	0.40	0.00	0.24	0.00	3.44	0.00	52.77	0.01	5.10	0.02	4.71	0.00
Dry Soil	0.24	0.00	0.34	0.05	1.13	0.02	0.60	0.00	0.36	0.00	34.98	2.11	4.94	2.26
Wet Soil	3.50	0.48	0.72	0.28	8.08	0.08	4.55	0.01	2.84	0.00	5.66	1.80	58.20	4.42

Figure 18 is a Boolean change map of the Rio Beni floodplain that identifies where land-cover change happened between 1990 and 1995. Within the floodplain boundary, 78.24% of pixels remained the same land-cover type, whereas 14.11% experienced absolute land-cover change and 7.64% experienced transitional land-cover change. The higher percentage of absolute changed than transitional change indicates a series of more dramatic change happened during this period, although the area of change decreased. Clusters of areas with absolute change mostly appeared near active river meanders. Clusters of transitional change areas could be found in channel scars away from active stream. Note that some oxbow lakes and abandoned channels demonstrated with both absolute and transitional change. This shows the advantage of modified CVA in providing more delicate change information, and such information would be discussed in later section.

Figure 19 is a set of maps that that depict the land-cover class in 1990 before it changed (a) and the class to which the pixel changed to 1995 (b). Forest and non-forest vegetation were the most active land-cover classes during this period. Forest gained area from other land-cover whereas non-forest vegetation lost many areas.

Figure 18. Map of land-cover change from 1990 to 1995.

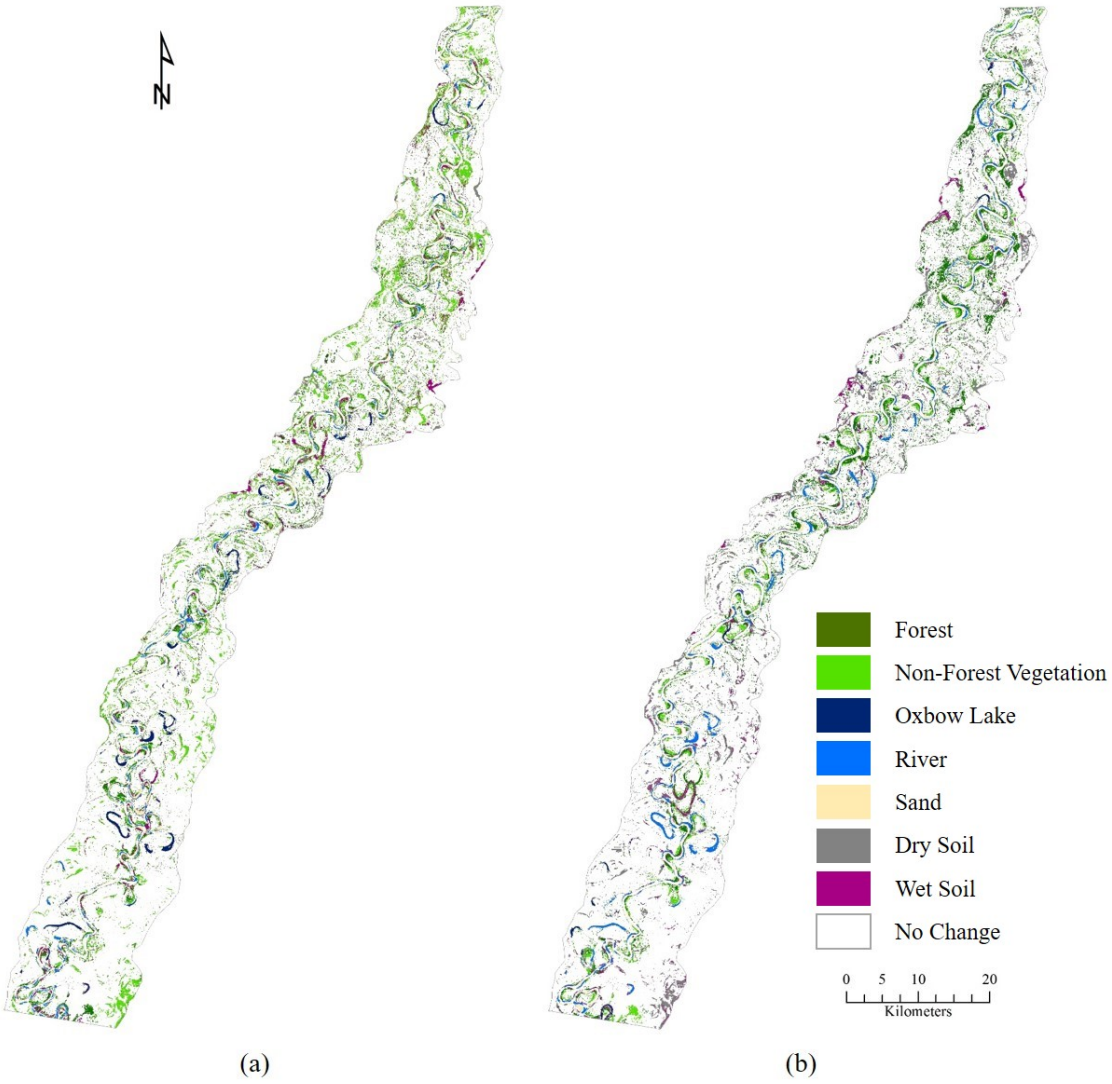

Figure 19. Land-cover changes from 1990 to 1995: (a) land-cover classes in 1990 that experienced change; (b) land-cover classes that previous classes changed to in 1995.

Table 29 shows the percentage of land-cover change types within four spatial buffer zones from 1990 to 1995. Compared to the overall 80.9% of no change, buffer zone 1 was way below it, whereas other three zones showed a higher percentage of areas with no change happened. The other three buffer zones demonstrated stable percentages

of no change ranges from 81% - 85%. They also had quite stable transitional change percentages at around 6% of the total area within the buffers. The spatial pattern was similar compared to the previous time period, that is, landscape change was more dynamic and significant near the active river channel.

Table 29. Percentages of land-cover change types within each buffer zone from 1990 to 1995.

Status	Zone 1	Zone 2	Zone 3	Zone 4	Average
No Change (%)	72.46	81.73	83.66	85.74	80.90
Change (%)	19.00	11.87	10.81	9.20	12.72
Transitional Change (%)	8.54	6.40	5.53	5.06	6.38

Regarding situations in the four buffer zones, not all types of "from-to" change could be found within each buffer zone. In zone 1, the most active land-cover was non-forest vegetation, as the shift from non-forest vegetation to forest was change types with largest areas. Non-forest vegetation itself also experienced rapid growth as the area of existing non-forest with higher membership was 2.03% of the total area. River to sand was another change type with a huge amount of area, which was 1.31 of the total area. In zone 2, forest experienced some growth as the largest shifts were from non-forest vegetation to forest and the continual growth of existing forest. In zone 3 and zone 4, non-forest vegetation shifted a large number of areas of forest and soil, in the ways of both absolute change and transitional change. The continual growth of forest was another remarkable event happened within these two zones during this time period.

4.2.2.3 Change in Time Period: 1995-1999

Table 30 and Table 31 show the "from-to" land-cover change from 1995 to 1999, which has the percentages of area classified "from" and "to" each pair of land-cover classes. Forest decreased by 94.7 km^2. Over 85% original forest was able to remain or increase the membership value. However, it also shifted to non-forest vegetation by 11.95% (6.11% in change, 5.84% in transitional change). Compared to other land-cover class, non-forest vegetation converted the most to forest, which consisted of 3.27% of the forest coverage in 1999. For non-forest vegetation, the area increased primarily came from forest (16.39%), dry soil (8.04%) and wet soil (5.02%). And as it was able to retain 91.61% existing cover in 1995, the total area of non-forest vegetation in 1999 increased more than 100 km^2. Oxbow lake was relatively stable, with 52.07 % oxbow lake area in 1999 was derived from already existing oxbow lake. 14.89% of oxbow lake area changed to main river channel. For river channel, it primarily shifted from and to oxbow lake and sand cover. As a result, river area only slightly increased 1.5 km^2. Area of sand increased significantly. In the sand classified in 1999, 27.73% coverage was shifted from river channel, 19.33% from dry soil, 6.68% from wet soil, 6.06% from non-forest vegetation, and 5.02% from forest. Dry soil decreased to 78.8 km^2 in area coverage. 31.90% original dry soil changed to non-forest vegetation, and 8.58% transitionally changed to non-forest vegetation. This was the most significant conversion. Also, dry soil also changed to sand by 6.01% in change and 6.32% in transitional change. Wet soil had a loss primarily to non-forest vegetation.

Table 30. Change of land-covers between Jul 1995 and Aug 1999 shown as percent of the From Class area.

From Class	To Class													
	Forest		Non-forest Vegetation		Oxbow Lake		River		Sand		Dry Soil		Wet Soil	
	C/N	Trans.	C/N.	Trans.	C/N	Trans.	C/N	Trans.	C/N	Trans.	C/N	Trans.	C/N	Trans.
Forest	84.36	1.55	6.11	5.84	0.03	0.00	0.71	0.00	0.46	0.01	0.17	0.02	0.62	0.13
Non-forest Vegetation	1.85	3.56	77.94	13.67	0.03	0.00	0.93	0.00	0.87	0.14	0.38	0.24	0.30	0.09
Oxbow Lake	0.09	0.01	0.79	0.03	69.05	6.58	12.60	2.29	2.23	0.02	0.66	0.01	5.46	0.19
River	0.35	0.00	1.35	0.00	17.45	1.78	55.23	0.34	20.96	0.06	1.10	0.00	1.36	0.01
Sand	7.14	0.00	10.37	0.04	0.02	0.00	3.85	0.00	72.71	0.00	1.87	0.51	3.43	0.05
Dry Soil	2.88	0.34	31.90	8.58	0.57	0.00	1.85	0.00	6.01	6.32	31.19	6.30	3.83	0.23
Wet Soil	7.47	9.98	20.88	12.15	1.71	0.04	3.71	0.01	5.18	0.39	4.93	0.57	29.75	3.22

Table 31. Change of land-covers between Jul 1995 and Aug 1999 shown as percent of the To Class area.

From Class	To Class													
	Forest		Non-forest Vegetation		Oxbow Lake		River		Sand		Dry Soil		Wet Soil	
	C/N	Trans.	C/N.	Trans.	C/N	Trans.	C/N	Trans.	C/N	Trans.	C/N	Trans.	C/N	Trans.
Forest	92.04	1.69	8.37	8.01	0.56	0.01	7.57	0.02	4.95	0.07	2.47	0.24	10.77	2.33
Non-forest Vegetation	1.12	2.15	59.26	10.40	0.26	0.01	5.47	0.01	5.23	0.82	3.12	1.91	2.93	0.90
Oxbow Lake	0.00	0.00	0.04	0.00	47.54	4.53	5.12	0.93	0.92	0.01	0.37	0.01	3.64	0.12
River	0.05	0.00	0.23	0.00	38.20	3.90	71.42	0.44	27.64	0.09	1.96	0.01	2.88	0.02
Sand	0.34	0.00	0.62	0.00	0.02	0.00	1.78	0.00	34.25	0.00	1.19	0.32	2.60	0.04
Dry Soil	0.46	0.05	6.34	1.70	1.48	0.01	2.85	0.01	9.42	9.91	66.14	13.35	9.67	0.57
Wet Soil	0.90	1.21	3.17	1.85	3.41	0.08	4.36	0.01	6.21	0.47	7.99	0.93	57.34	6.21

Figure 20 is a Boolean change map of the Rio Beni floodplain that identifies where land-cover change happened between 1995 and 1999. Within the floodplain boundary, 58.83% of pixels remained the same land-cover type, whereas 12.83% experienced clear land-cover change and 28.34% experienced transitional land-cover change. This result indicates that much change happened during this time period, where more than 40% of the total area experienced landscape change. A surprise was found in this time period was that 28.34% of the total area experienced transitional change, much more than areas with clear change. Clusters of transitional change could be easily observed near oxbow lakes, abandoned channels, and scars.

Figure 21 is a set of maps that that depict the land-cover class in 1995 before it changed (a) and the class to which the pixel changed to 1999 (b). Forest and non-forest vegetation were the most active land-cover classes. Transitional change from forest to non-forest vegetation occupied 9.59% of the total area while the transitional change from non-forest vegetation to forest also occupied 2.6% of the floodplain. Also, areas with the same class transition in forest and non-forest vegetation occupied 4.11% and 4.92%, respectively. River was also associated with two major changes: change from river to sand occupied 1.34% of total area, and transitional change from river to oxbow lake occupied 1.09% of total area.

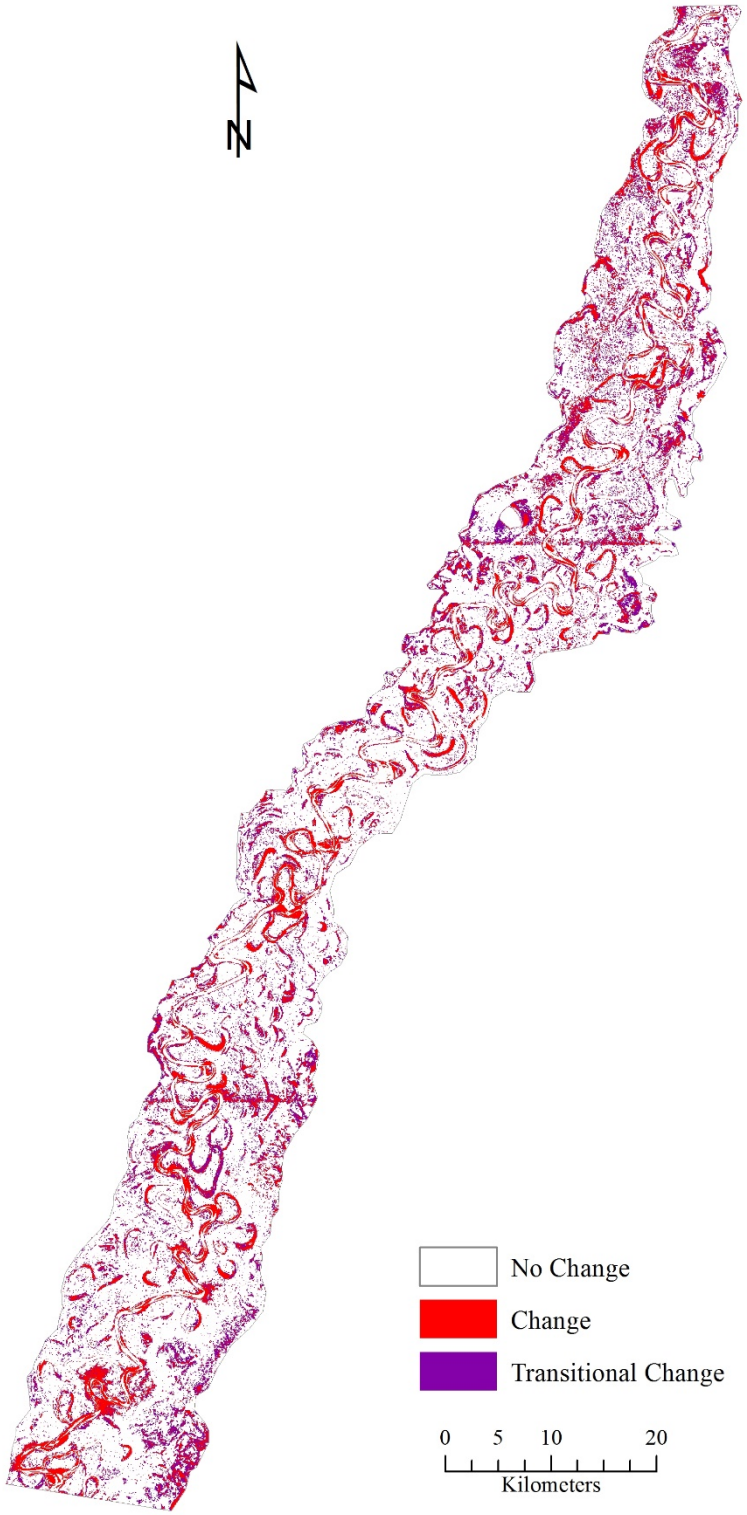

Figure 20. Map of land-cover change from 1995 to 1999.

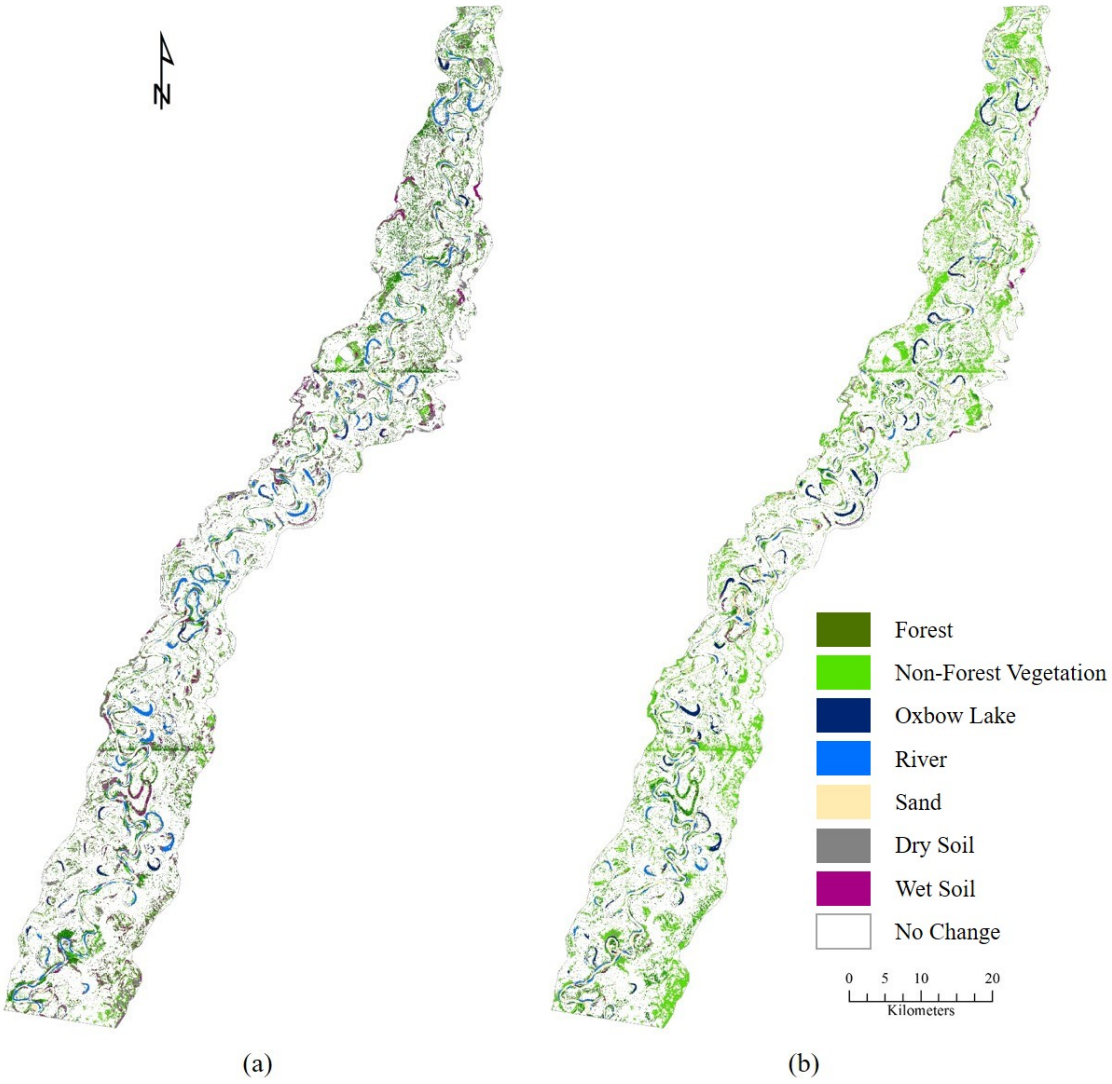

Figure 21. Land-cover changes from 1995 to 1999: (a) land-cover classes in 1995 that experienced change; (b) land-cover classes that previous classes changed to in 1999.

Table 32 shows the percentage of land-cover change types within four spatial buffer zones from 1995 to 1999. Four spatial buffer zones entailed percentages of no change at ~74%, which was quite low compared with the previous periods. However, the change of percentages in change and transitional change among four zones still revealed

a common pattern: percentages of change decreased rapidly from zone 1 to zone 2, and decreased more gradually from zone 2 to zone 4, as the distance away from the main river channel increased. This indicates that dramatic change of land-cover/landscape occurred much more near the river.

Table 32. Percentages of land-cover change types within each buffer zone from 1995 to 1999.

Status	Zone 1	Zone 2	Zone 3	Zone 4	Average
No Change	71.04	75.23	76.64	74.50	74.35
Change	19.11	12.78	11.24	10.70	13.46
Transitional Change	9.85	11.99	12.12	14.80	12.19

Regarding situations in the four buffer zones, most types of "from-to" change could be found within each buffer zone. Within all four zones, external and internal transitional changes of forest and non-forest vegetation were the most active types of change. In zone 1, change from river to sand comprised another major change type. The absolute change from river to sand occupied 3.2% of the entire zone 1. In zone 2, the transitional change from river to oxbow lakes occupied 2.4% of area in zone 2, which was the largest change type except classes associated with vegetation. In zone 3 and 4, several transitional changes associated with two vegetation classes were the major land-cover change types.

4.2.2.4 Change in Time Period: 1999-2006

Table 33 and Table 34 show the "from-to" land-cover change from 1999 to 2006, which has the percentages of the area classified "from" and "to" each pair of land-cover classes. Forest increased by 103.1 km^2. It was able to retain 94.88% of the already existing forest. For the newly-formed forest area, the shifts from non-forest vegetation and sand contributed the most. For non-forest vegetation, the area decreased about 100 km^2. Although it was able to retain much of its original area (87.8%), a large amount of loss happened during the conversion to forest and wet soil, and no apparent transforms from other classes to non-forest vegetation during this period. Areas of Oxbow lake and river channel were almost unchanged. However, there were still land-cover shifts happened between these classes as river channel activities. Oxbow lake contributed 17.22% of its area to river while river returned 10.14% of its area back to oxbow lakes. Sand decreased 26% in area coverage. 18.05% of sand area in 1999 shifted to forest, 17.14% to wet soil, 16.10% to river channel, and 14.25% to non-forest vegetation. Dry soil continually decreased by 19.5 km^2. The loss was majorly due to the conversion to non-forest vegetation (13.85%) and wet soil (21.33%). Surface coverage shifted from non-forest vegetation and sand consisted of 10.60% and 3.97% of the total dry soil area in 2006, respectively. Wet soil increased by 41.8 km^2 with the gain from dry soil non-forest vegetation and sand.

Table 33. Change of land-covers between Aug 1999 and Jul 2006 shown as percent of the From Class area.

From Class	To Class													
	Forest		Non-forest Vegetation		Oxbow Lake		River		Sand		Dry Soil		Wet Soil	
	C/N	Trans.	C/N.	Trans.	C/N	Trans.	C/N	Trans.	C/N	Trans.	C/N	Trans.	C/N	Trans.
Forest	94.63	0.25	1.16	0.64	0.01	0.00	1.32	0.00	0.76	0.01	0.11	0.16	0.51	0.43
Non-forest Vegetation	1.11	3.83	84.81	2.99	0.04	0.00	1.69	0.00	1.12	0.03	0.32	0.56	1.30	2.21
Oxbow Lake	0.02	0.40	0.30	0.31	75.36	3.04	13.36	3.86	0.39	0.03	0.07	0.10	1.54	1.22
River	0.40	2.80	0.71	2.07	9.06	1.09	54.99	0.76	20.12	0.09	0.46	0.61	2.51	4.33
Sand	3.69	14.37	5.60	8.65	2.47	0.16	15.96	0.14	26.18	0.67	2.35	2.14	9.11	8.53
Dry Soil	0.64	2.10	7.93	5.91	0.71	0.02	1.49	0.01	3.67	0.22	54.79	1.18	9.50	11.83
Wet Soil	5.14	4.97	1.97	3.15	4.16	0.12	6.38	0.12	3.67	0.08	3.14	1.31	62.64	3.14

Table 34. Change of land-covers between Aug 1999 and Jul 2006 shown as percent of the To Class area.

From Class	To Class													
	Forest		Non-forest Vegetation		Oxbow Lake		River		Sand		Dry Soil		Wet Soil	
	C/N	Trans.	C/N.	Trans.	C/N	Trans.	C/N	Trans.	C/N	Trans.	C/N	Trans.	C/N	Trans.
Forest	92.94	0.24	1.51	0.84	0.19	0.02	11.21	0.02	10.88	0.14	1.59	2.40	4.16	3.55
Non-forest Vegetation	0.89	3.08	90.32	3.19	0.48	0.03	11.69	0.02	13.18	0.34	3.85	6.75	8.68	14.76
Oxbow Lake	0.00	0.02	0.02	0.03	70.89	2.86	6.94	2.00	0.34	0.02	0.07	0.09	0.77	0.61
River	0.04	0.30	0.10	0.29	15.05	1.80	50.44	0.70	31.31	0.14	0.73	0.97	2.22	3.83
Sand	0.33	1.29	0.67	1.03	3.47	0.22	12.39	0.11	34.50	0.88	3.16	2.88	6.82	6.39
Dry Soil	0.06	0.18	0.92	0.69	0.97	0.02	1.13	0.01	4.71	0.28	72.00	1.55	6.94	8.65
Wet Soil	0.31	0.30	0.16	0.25	3.88	0.11	3.28	0.06	3.20	0.07	2.80	1.17	31.06	1.56

Figure 22 is a Boolean change map of the Rio Beni floodplain that identifies where land-cover change happened between 1999 and 2006. During this period, 83.28% of pixels remained the same land-cover type, whereas 9.06% experienced land-cover change and 7.65 % experienced transitional land-cover change. During this time period, area coverage with absolute change was much more than the area with transitional change. This might come from the fact that this pair of images had the longest time interval among the four pairs, and significant landscape change should happen more frequently. Clusters of land-cover change were along the main river channel and many oxbow lakes. The transitional change did not scatter throughout the floodplain compared to previous time period. The only clusters were found within and near some oxbow lakes and channel scars.

Figure 23 consists of a set of maps that that depict the land-cover class in 1999 before it changed (a) and the class to which the pixel changed to 2006 (b). The most dominant change types were from clear change. River, sand, and non-forest vegetation were the most active land-cover types. The shift from river to sand was the largest change type. Again, this proves that within this time period, the meander migrations were very dramatic that led to a large amount of riparian areas experienced land-cover change. For non-forest vegetation, the major changes associated with it were the membership increase within itself and the transitions to forest cover. This indicated the existing non-forest vegetation was on stable land without too much disturbance from other land surface processes so that the plants were able to grow gradually.

Figure 22. Map of land-cover change from 1999 to 2006.

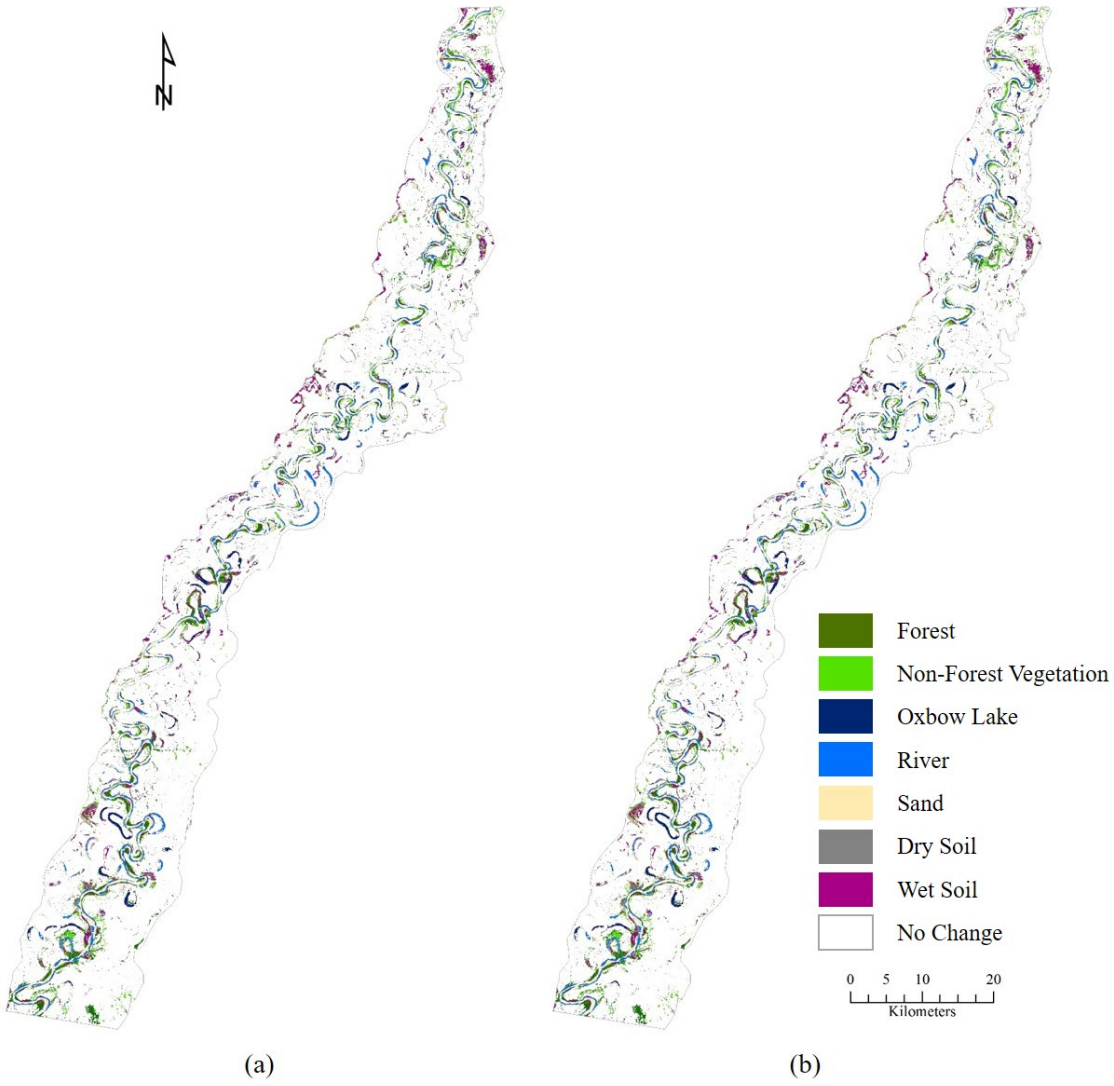

Figure 23. Land-cover changes from 1999 to 2006: (a) land-cover classes in 1999 that experienced change; (b) land-cover classes that previous classes changed to in 2006.

Table 35 shows the percentage of land-cover change types within four spatial buffer zones from 1999 to 2006. The results still showed that landscape change was more dramatic near the main river channel than those areas away from river. Especially in zone 1, the absolute change area occupied 15.62% of the total area. Figure 21 also

demonstrates that this spatial zone experienced a period of very dynamic landscape change.

Table 35. Percentages of land-cover change types within each buffer zone from 1995 to 1999.

Status	Zone 1	Zone 2	Zone 3	Zone 4	Average
No Change (%)	72.96	86.95	89.50	92.80	85.55
Change (%)	15.62	6.56	5.16	3.09	7.61
Transitional Change (%)	11.41	6.49	5.34	4.11	6.84

Regarding situations in the four buffer zones, most types of "from-to" change could be found within each buffer zone. In zone 1, river and sand were the most active land-cover types, as expected. Some river sections converted to sand-bar. But in return, sand transformed back to river channel due to channel migration. A certain amount of vegetation areas were also contributed to the river pixels in 2006. In zone 2, the transitions between river and oxbow lake were significant. Also, two bare soil types and non-forest vegetation experienced some change. In zone 3, a few transition in oxbow lakes could be observed, which indicated this distance might be critical in the hydrologic connectivity of the studied floodplain. In zone 4, only a very small amount of changes could be observed, which most of them were associated with non-forest vegetation.

4.2.2.5 Change from 1987 to 2006

Table 36 and Table 37 show the "from-to" land-cover change from 1987 to 2006, which has the percentages of area classified "from" and "to" each pair of land-cover classes, respectively. 86.78 % area of existing forest in 1987 remained in 2006. A total of 6.61% of forest changed to non-forest vegetation (5.65% from change, 0.96% from transitional change). The rest of forest's lost coverage shifted mostly to river channel (3.15%), sand (2.05%), and wet soil (1.5%). The existing forest in 1987 consisted of about 93%, the forest area in 2006. No land-cover class coverage transformed to forest significantly. Non-forest vegetation had the biggest area increase during this two-decade-period by more than 100 km^2. It was able to retain 87% of its original coverage area while shifting 4.51% to forest and 3.14% to river stream. During this period, increasing non-forest vegetation was primarily derived from forest coverage (12.06% in change, 2.05% in transitional change). The shift from two soil classes also contributed to a total of 14.05% non-forest coverage in 2006. The area of oxbow lakes increased by 12.9 km^2, and the area of main river channel decreased by about 9 km^2. Although the areal change was not huge compared to entire floodplain area, the "from-to" change percentages between river and oxbow lakes were large, indicating many channel cut-offs and reconnections happened during this entire time period. Moreover, due to the channel migration, sand class was also active with a slight increase in total areal coverage but lots of land-cover shifts "from" sand and "to" sand coverage. During this long time frame, the area of dry soil decreased from 83 km^2 to 59.3 km^2. 51.64% of existing dry soil in 1987 remained in 2006, and almost no transitional increase of dry soil could be

found. The most pronounced land-cover shift from dry soil was to non-forest vegetation with 15.77% change and 2.77% transitional change. Dry soil also had 13% and 2.26% of its area changed and transitionally changed to wet soil, respectively. Sand was another major land-cover that dry soil shifted to, which consisted of 4.72% of dry soil's original area. Two vegetation classes, river channel, sand, and wet soil all shifted some small amounts of area to dry soil coverage in 2006. Forest lost about 100 km^2 from 1987 to 2006. The area of wet soil remained almost the same, but more than half of the wet soil coverage in 1987 experienced land-cover change while a similar amount of area from other classes also transformed to wet soil. The mutual change among wet soil, forest, non-forest vegetation, river, and sand could be observed easily. For example, 30.56% of wet soil coverage in 1987 shifted to non-forest vegetation in 2006, and 14.01% shifted to forest cover. In turn, 14.89% of total wet soil coverage in 2006 was shifted from non-forest vegetation, 8.98% from dry soil, 6.73% from main river channel, and 3.47% from sand.

Table 36. Change of land-covers between Aug 1987 and Jul 2006 shown as percent of the From Class area.

From Class	To Class													
	Forest		Non-forest Vegetation		Oxbow Lake		River		Sand		Dry Soil		Wet Soil	
	C/N	Trans.	C/N.	Trans.	C/N	Trans.	C/N	Trans.	C/N	Trans.	C/N	Trans.	C/N	Trans.
Forest	86.63	0.15	5.65	0.96	0.10	0.01	2.58	0.01	1.52	0.01	0.31	0.07	1.77	0.22
Non-forest Vegetation	2.23	2.28	80.81	6.95	0.11	0.02	3.13	0.01	2.02	0.04	0.62	0.29	0.98	0.52
Oxbow Lake	1.10	0.21	2.23	0.20	74.50	1.34	12.07	2.24	1.10	0.01	0.30	0.04	4.44	0.24
River	12.15	0.10	13.35	0.07	16.98	0.79	36.66	0.13	10.56	0.01	1.06	0.02	8.02	0.11
Sand	18.71	0.46	30.37	0.65	2.48	0.05	11.99	0.03	20.99	0.28	3.31	0.27	10.26	0.17
Dry Soil	2.42	1.77	15.77	2.77	1.53	0.10	3.16	0.10	4.62	0.12	51.32	0.32	13.76	2.26
Wet Soil	10.65	3.37	18.29	12.27	0.34	0.05	2.83	0.05	2.16	0.02	1.68	0.52	46.15	1.62

Table 37. Change of land-covers between Aug 1987 and Jul 2006 shown as percent of the To Class area.

From Class	To Class													
	Forest		Non-forest Vegetation		Oxbow Lake		River		Sand		Dry Soil		Wet Soil	
	C/N	Trans.	C/N.	Trans.	C/N	Trans.	C/N	Trans.	C/N	Trans.	C/N	Trans.	C/N	Trans.
Forest	92.84	0.16	12.06	2.05	1.98	0.19	26.95	0.07	29.62	0.27	5.94	1.39	13.23	1.66
Non-forest Vegetation	0.83	0.85	60.34	5.19	0.76	0.12	11.45	0.05	13.74	0.25	4.12	1.93	2.56	1.37
Oxbow Lake	0.04	0.01	0.18	0.02	53.04	0.96	4.74	0.88	0.81	0.00	0.22	0.03	1.25	0.07
River	1.44	0.01	3.16	0.02	35.61	1.65	42.45	0.15	22.76	0.02	2.25	0.04	6.64	0.09
Sand	0.89	0.02	2.88	0.06	2.09	0.04	5.57	0.01	18.16	0.24	2.81	0.23	3.41	0.06
Dry Soil	0.19	0.14	2.52	0.44	2.17	0.14	2.48	0.08	6.73	0.17	73.45	0.46	7.71	1.27
Wet Soil	1.94	0.61	6.63	4.45	1.09	0.15	5.02	0.09	7.15	0.07	5.46	1.67	58.63	2.06

Figure 24 is a Boolean change map of the Rio Beni floodplain that identifies where land-cover change happened between 1987 and 2006. Within the floodplain boundary, 74.4% of pixels remained the same land-cover type, whereas 20% experienced land-cover change and 5.6 % experienced transitional land-cover change. Due to a much longer time span (almost 20 years here) compared to the four sub-time frames, it was expected that the clear change would be more abundant compared to transitional change. The entire river channel, including the active one and many abandoned channels, showed pronounced landscape change which indicated the dynamics of this meandering river. Most pixels with transitional change were found near the boundary of the study area, and not many clusters were observed.

Figure 25 is a set of maps that that depict the land-cover class in 1987 before it changed (a) and the class to which the pixel changed to 2006 (b). Obviously, the most dominant change types were from clear change. River, sand, oxbow lake and vegetation were the most active land-cover types. River, sand, and oxbow lakes were largely involved with the landscape change in the riparian area. Non-forest vegetation was also active, especially gaining coverage from other classes, at the peripheral area. Some clusters of non-forest vegetation change could be easily observed.

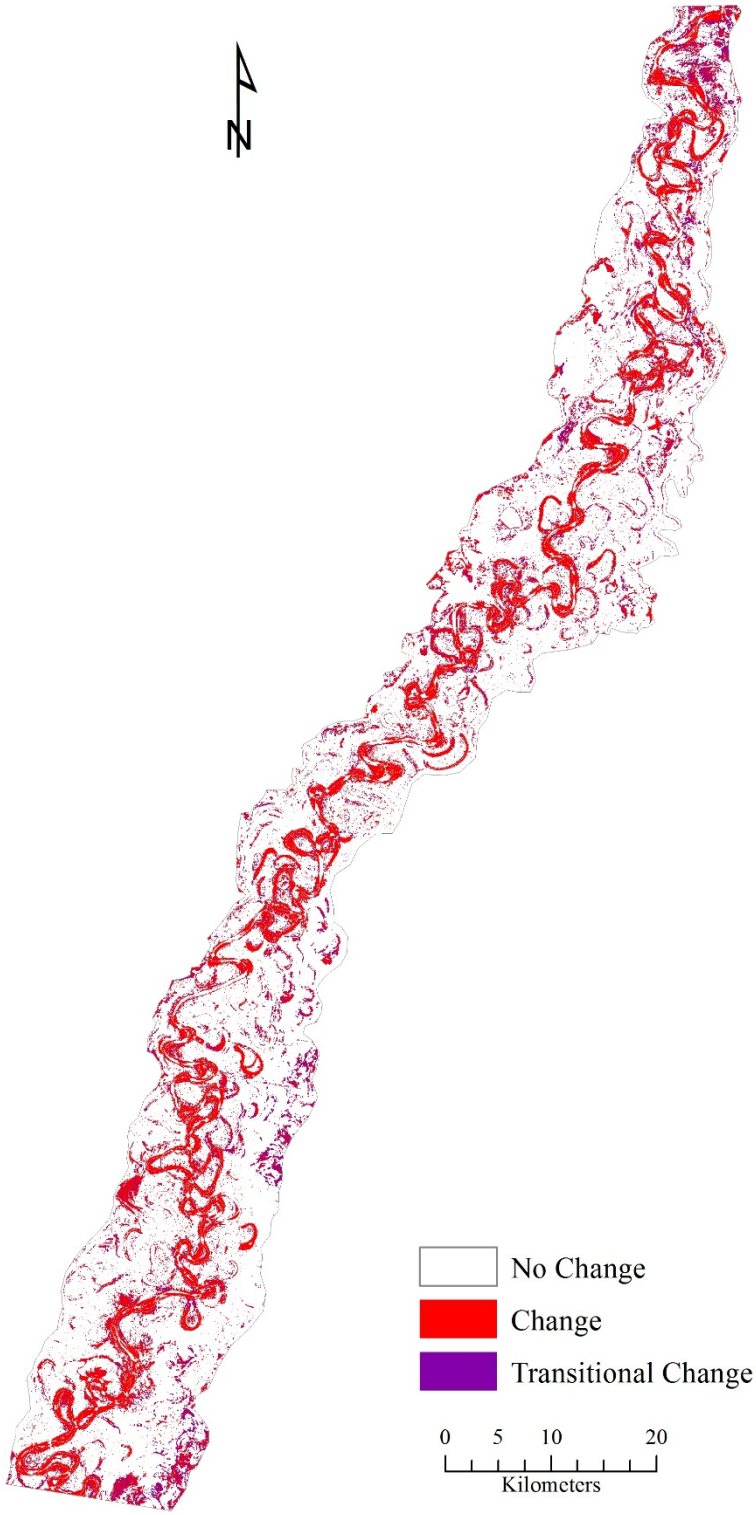

Figure 24. Map of land-cover change from 1987 to 2006.

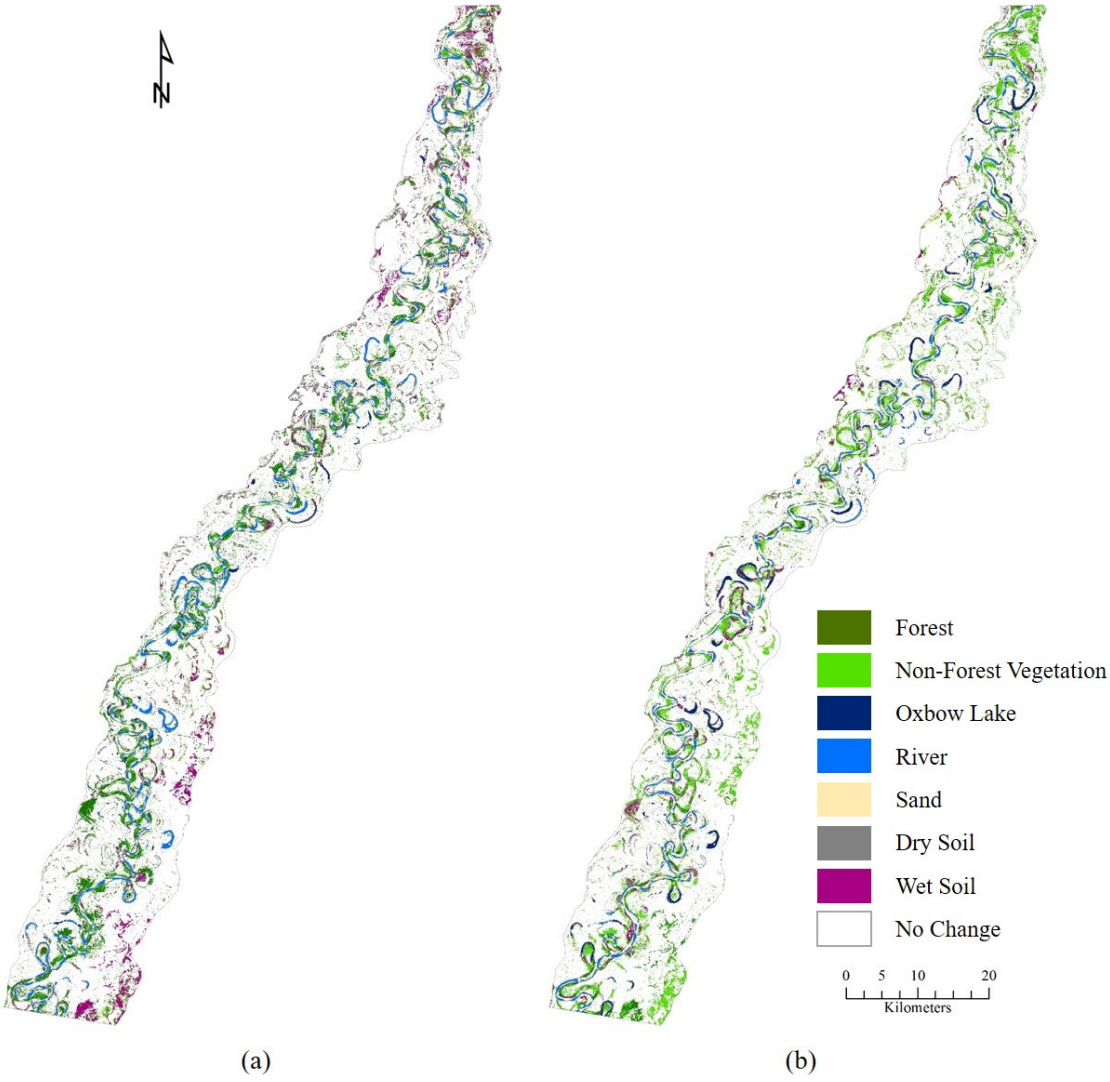

Figure 25. Land-cover changes from 1987 to 2006: (a) land-cover classes in 1987 that experienced change; (b) land-cover classes that previous classes changed to in 2006.

Table 38 shows the percentage of land-cover change types within four spatial buffer zones from 1999 to 2006. The results still showed that landscape change was more drastic near the main river channel than those areas away from river. Especially in zone 1, the change area occupied 30.36% of the total area, and clear change was the

dominant change type as it occupied 25.71%. There was a significant drop of change area from zone 1 to zone 2, then the drop continued but became gradually from zone 2 to zone 4. Such observation indicated that the change was largely concentrated in zone 1.

Table 38. Percentages of land-cover change types within each buffer zone from 1987 to 2006.

Status	Zone 1	Zone 2	Zone 3	Zone 4	Average
No Change (%)	69.64	79.30	83.59	86.25	79.69
Change (%)	25.71	11.94	10.61	8.32	14.15
Transitional Change (%)	4.65	8.76	5.80	5.43	6.16

Regarding situations in the four buffer zones, most types of "from-to" change could be found within each buffer zone. In zone 1, river and sand were the most actively-changing land-cover types, as expected. Non-forest vegetation was also actively changing in zone 1, converting from oxbow lakes, and bare soil. In zone 2, the transitions between river and oxbow lake were pronounced. Forest shifted drastically to other classes in zone 2. In zone 3, forest still actively shifted to other classes. The interaction between non-forest vegetation and soil classes were also prominent. In zone 4, 86.25% of the total area did not experience land-cover, only a very small amount of changes could be observed and mostly were land-cover converted to non-forest vegetation.

4.3 Land-Cover Spatial Structure and Configuration

Thirteen landscape metrics were calculated to provide information regarding spatial configuration, connectivity, and distribution/interspersion of patches associated with the classes of interest. These landscape metrics were calculated at the class level using FRAGSTATS version 4.2 (McGarigal et al. 2012). The results will be shown in subsections below, by each land-cover class. The river class is not be discussed here since the main channel simply constitutes one feature, which minimizes the utility of computing various landscape metrics for that feature type.

4.3.1 Forest

Figure 26 demonstrates the thirteen landscape metrics for forest patches in four spatial buffer zones during the 1987 to 2006 time period. Number of forest patches decreases gradually away from the river banks until a slight increase in zone 4 compared with zone 3. The average patch size increases while moving towards the peripheral floodplain. The coefficient variances of patch area are relatively consistent in zones 1-3, but experience a marked increase in zone 4. These reflect the clusters of forest patches in zone 4 were larger, but some small patches were also scattered throughout this buffer zone. Shapes of forest patches were simple on the floodplain, as both shape-related indices were low. The Related Circumscribing Circle Index ranges from 0.6 to 0.7, which indicates that the forest patches show some degree of elongation in shape. Forest patches were highly connected as the Patch Cohesion Index was very close to its theoretical maximum value (100). In addition, the forest class presented low

Interspersion and Juxtaposition Index values, meaning that forest patches were not proportionately distributed.

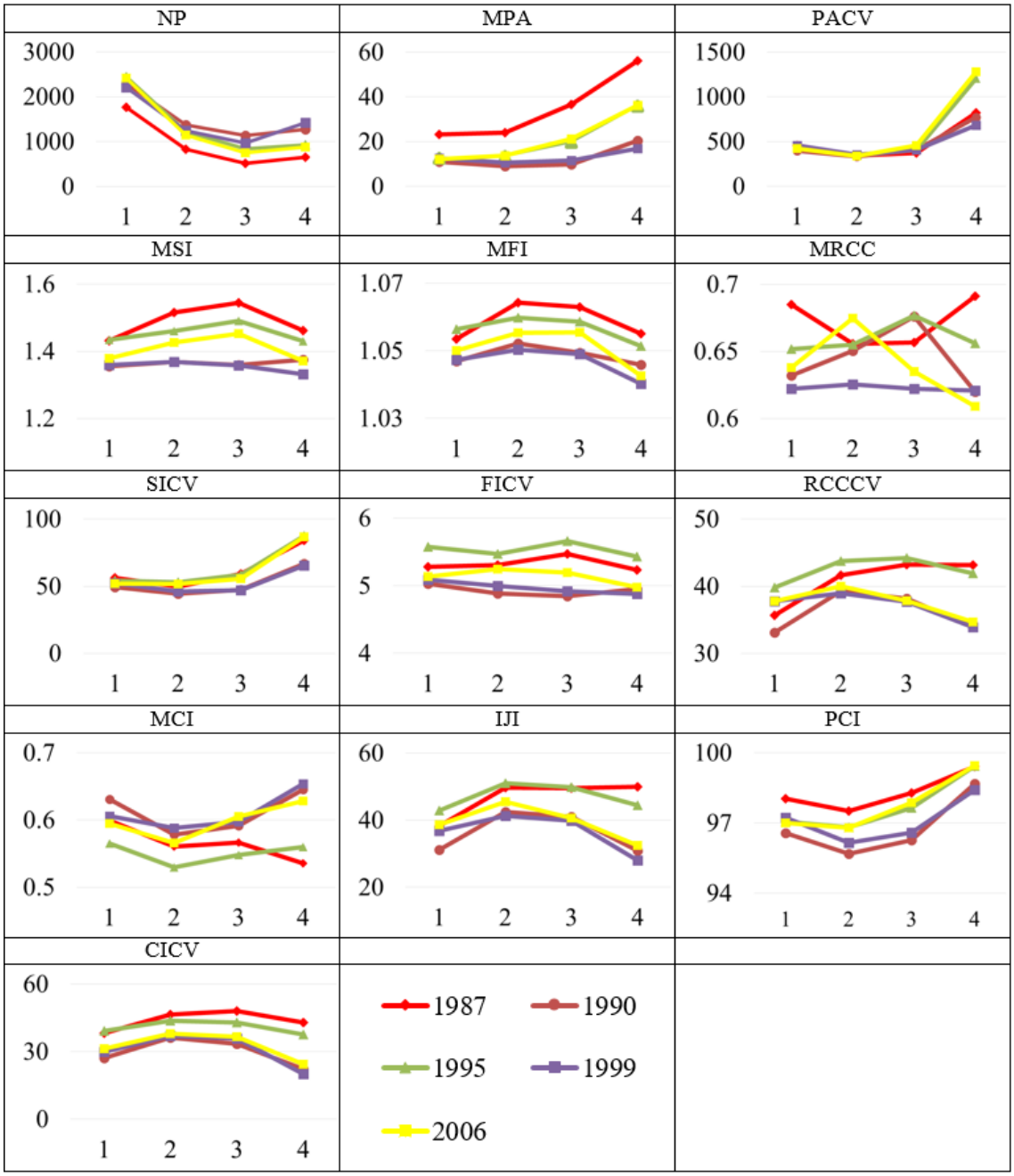

Figure 26. Landscape metrics for forest patches in four spatial buffer zones from 1987 to 2006.

4.3.2 Non-Forest Vegetation

Figure 27 demonstrates the thirteen landscape metrics for non-forest vegetation patches in four spatial buffer zones during the 1987 to 2006 time period. Overall, the number of non-forest vegetation patches decrease gradually from zone 1 to zone 3. But there was a slight increase in zone 4 of patch numbers compared to zone 3. The mean patch area sizes were high in zone 1 and 4 while zone 2 and 3 were lower. This is surprising as we expected the lowest mean patch size would be found in zone 1 as zone 1 usually experienced dramatic landform activities and land-cover tend to be more scattered and fragmentized. The coefficient variances of patch area were also higher in zone 1 and zone 4. Shape index and Fractal Dimension Index indicate that the complexity of non-forest vegetation continually declined from zone 1 to zone 4. The Related Circumscribing Circle Index ranges from 0.6 to 0.7 with significant fluctuations in different years. This indicates that the shapes of non-forest vegetation patches were narrow and elongated, which should be a representation of belt-shape vegetation that colonized the paleochannels. The Contiguity Index was below 0.5 for most of the time, meaning the patches were not very contiguous. Similarly to forest class, the non-forest vegetation class showed low Interspersion and Juxtaposition Index values, meaning that they were not proportionately distributed in the study area. Overall, patch connectivity was high, but zone 1 and zone 4 showed higher values than zone 2 and zone 3. In short, for non-forest vegetation, the configurations in zone 1 and zone 4 look similar while zone 2 and zone 3 look similar.

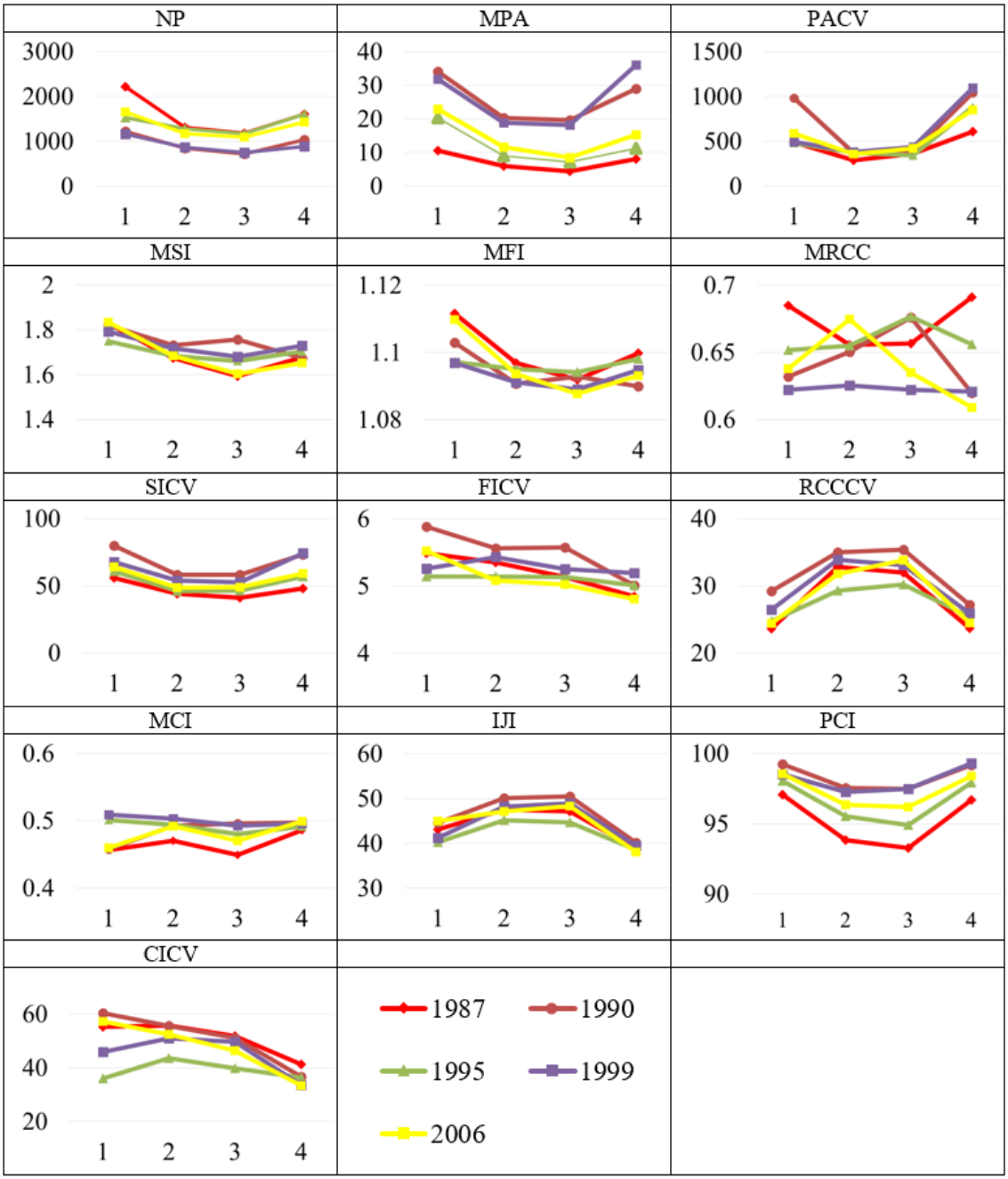

Figure 27. Landscape metrics for non-forest vegetation patches in four spatial buffer zones from 1987 to 2006.

4.3.3 Oxbow Lake

Figure 28 demonstrates the thirteen landscape metrics for oxbow lake patches in four spatial buffer zones during the 1987 to 2006 time period. A Large number of oxbow lake objects were found in zone 1, and the number gradually decreased when moving away from main river channel. This is intuitive as oxbow lakes (abandoned channels) should be found near the river channel. Overall, the Shape Index showed an increasing trend. Low shape index in the first buffer zone indicates shapes of oxbow lakes were simple and regular near the river. But it became more complex and irregular away from the main river channel. The Related Circumscribing Circle Indices range from 0.6 to 0.7, which suggest the shape of oxbow lake patches were more close to elongated shape throughout the study area. Contiguity Index ranges from 0.4 to 0.6 where the lowest value was found in zone 1. The high Contiguity Index in zone 2 - 4 indicates large contiguous patches were more like to be found in these buffer zones. Patch cohesion was high (over 90), which means patches were highly connected.

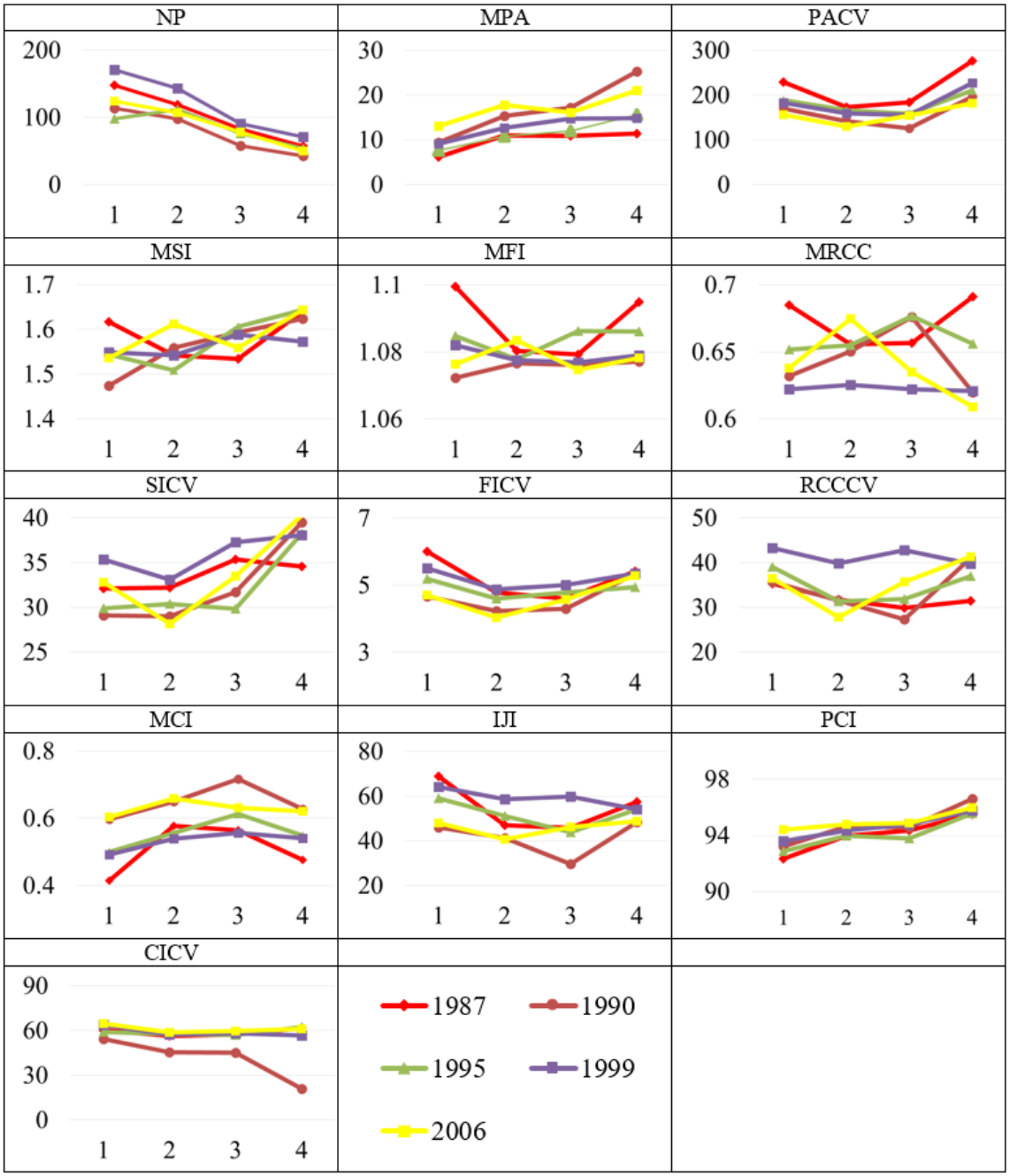

Figure 28. Landscape metrics for oxbow lake patches in four spatial buffer zones from 1987 to 2006.

4.3.4 Sand

Figure 29 demonstrates the thirteen landscape metrics for sand patches in four spatial buffer zones during the 1987 to 2006 period. A large amount of sand patches were found in zone 1, whereas in zone 2 – 4 the sand patches were rare. The largest mean patch area was also found in zone 1, and the value was much higher than those in zone 2- 4. This indicates that sand patches mostly appeared close to the main river channel in a form of sand clusters. In other regions of the floodplain, sand was more likely to be some small patches scattered randomly. For several shape indices, the value in different spatial buffer zones was similar. This is quite surprising as the spatial distribution and configurations were very different in zone 1 than in other three zones. But overall, the indices indicate that the patches in zone 1were slightly complex in shape. The Related Circumscribing Circle Indices were above 0.6, meaning the general object shape was elongated. Contiguity Indices are around 0.5, indicating moderate contiguous object shapes. The sand class presented low Interspersion and Juxtaposition Index values, meaning that they were not proportionately distributed in the study area. Overall, patch connectivity was very high for this land-cover.

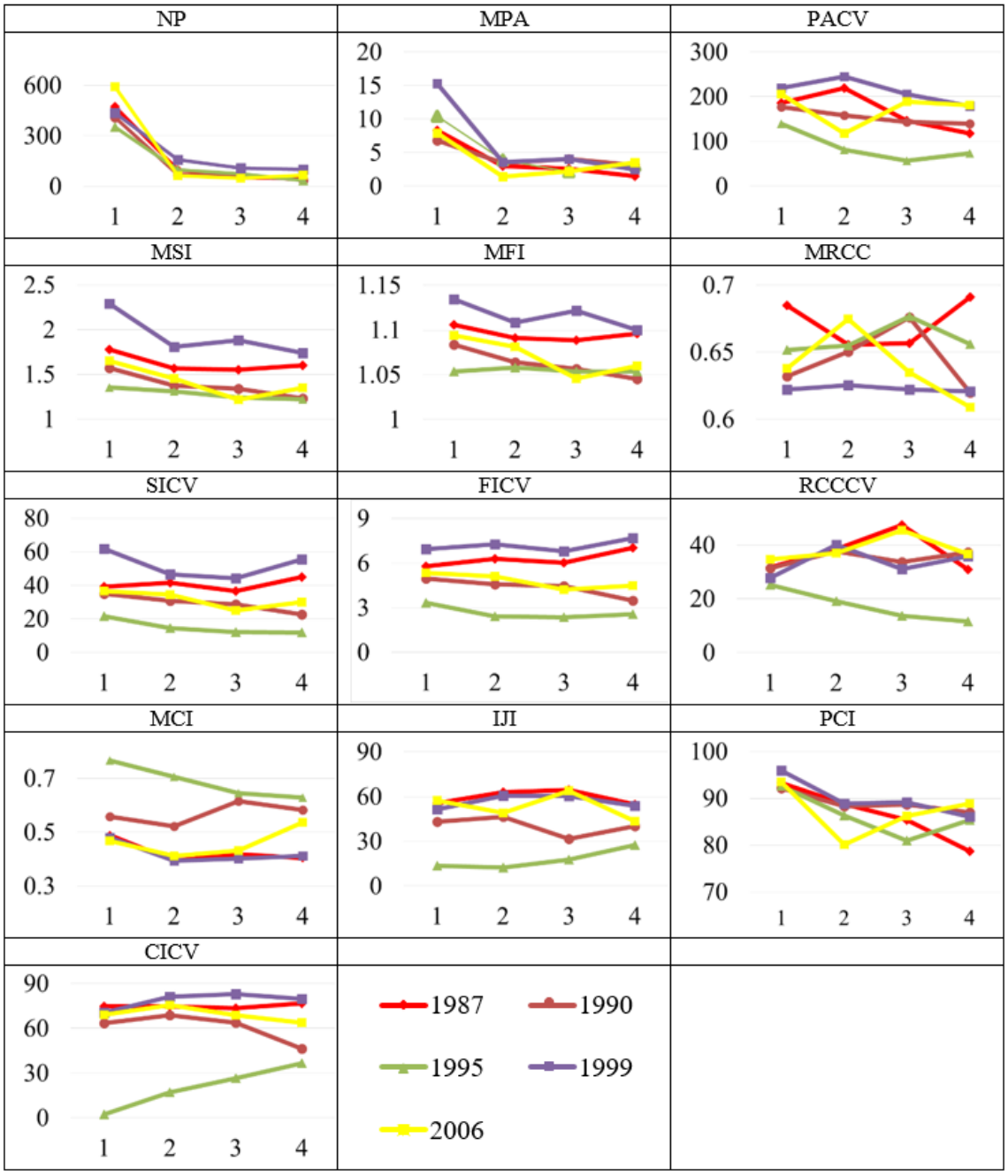

Figure 29. Landscape metrics for sand patches in four spatial buffer zones from 1987 to 2006.

4.3.5 Dry Soil

Figure 30 demonstrates the thirteen landscape metrics for dry soil patches in four spatial buffer zones during the 1987 to 2006 time period. Overall, all landscape metrics have similar patterns in the time series. Number of dry soil patches were largest in zone 1 and it declined as distance to main river channel increased. However, the average patch size indicated an opposite trend where the highest value was in zone 4. This indicates that dry soil patches were more abundant but fragmentized near the river, whereas they were more concentrated and formed larger patches in areas away from the main river channel. The declining Fractal Dimension Index also supported this theory. Other three types of indices showed stable trends with some fluctuations. Landscape metrics associated with connectivity – the Patch Cohesion Index – provide evidence of higher patch connectivity of dry soil class was found in zone 2-4 compared to the value in zone 1.

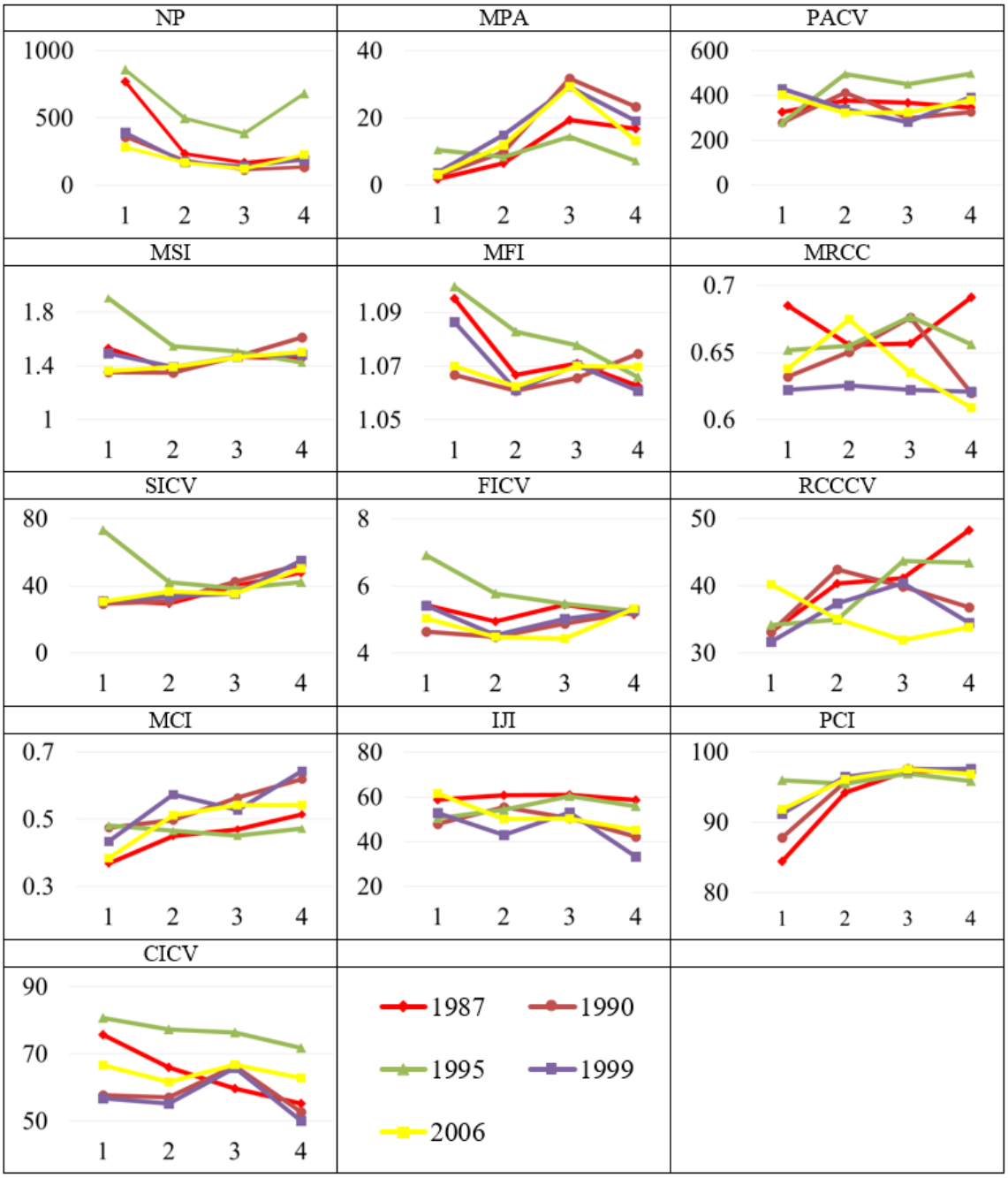

Figure 30. Landscape metrics for dry soil patches in four spatial buffer zones from 1987 to 2006.

4.3.6 Wet Soil

Figure 31 demonstrates the thirteen landscape metrics for wet soil patches in four spatial buffer zones during the 1987 to 2006 time period. Number of wet soil patches was highest in zone 1, and it declined in zones 2 and 3, with a slight increase in zone 4. The average patch size indicated an opposite trend where the lowest value was in zone 1 and the highest value was in zone 4. This indicates a similar situation of dry soil that wet soil patches were fragmentized near the main river channel, whereas they were likely to be clustered into large patches in areas away from the main river channel. Several landscape metrics associated with patch shape were stable in the four buffer zones. A low Fractal Dimension Index (close to 1) indicates that the wet soil patches presented simple structures. The Related Circumscribing Circle Indices were around 0.65 in all zones, meaning the patch shapes were inclined to be regular and elongated. The wet soil class presented a declining trend with the Interspersion and Juxtaposition Index values, meaning that they were getting less proportionately distributed from zone 1 to zone 4. The patch connectivity increased from zone 1 to zone 4 as indicated by the Patch Cohesion Index.

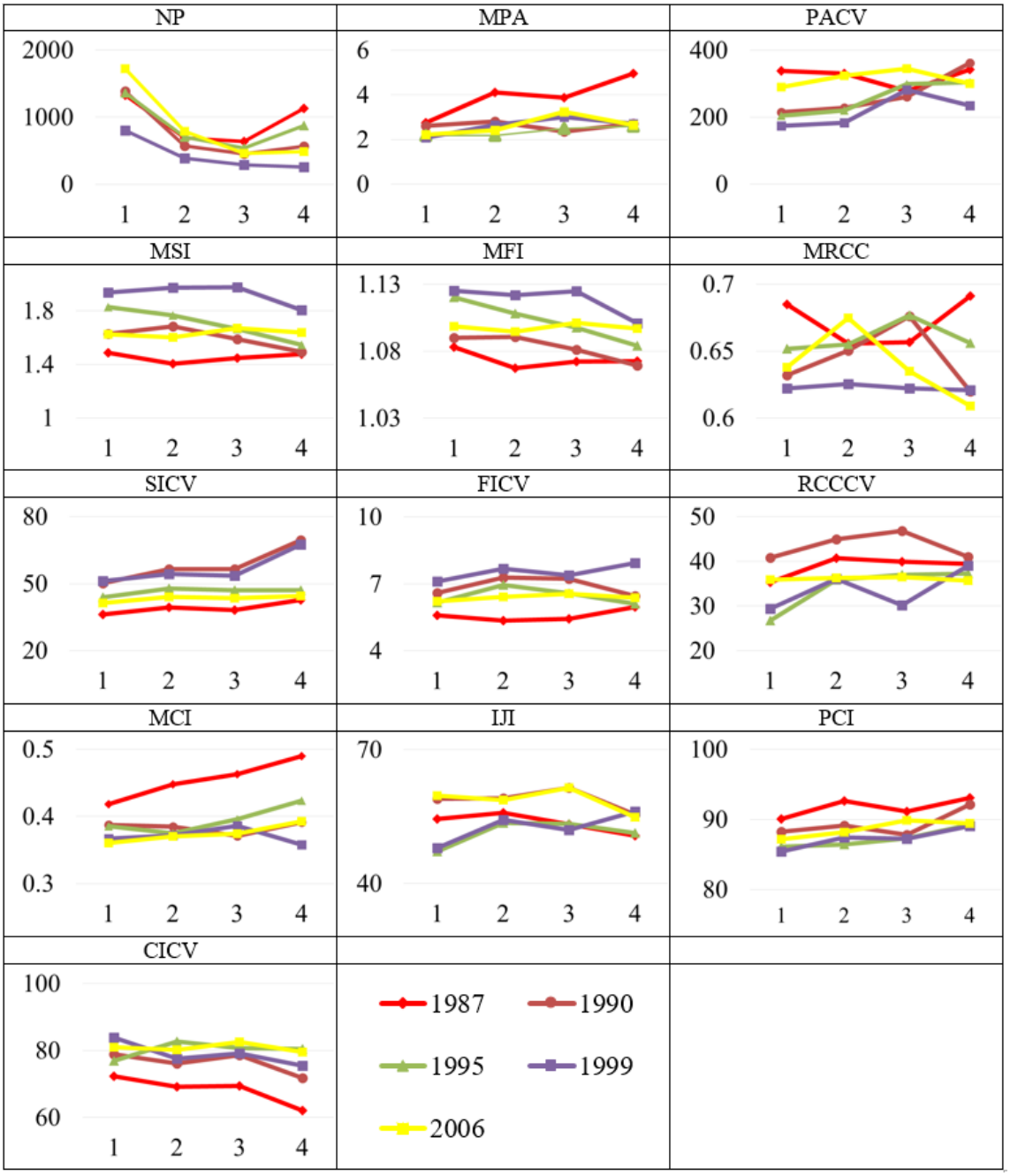

Figure 31. Landscape metrics for wet soil patches in four spatial buffer zones from 1987 to 2006.

5. DISCUSSION

5.1 Image Classification of Dynamic Meandering River Floodplain

To gain an understanding of the land-cover change and landscape evolution within a large area over a multi-decadal time period, a series of accurate land-cover maps is necessary because they provide the critical basis for further analyses. Algorithmic/computer-based image classification of aerial photographs or satellite images has become commonplace in producing accurate land-cover maps. Numerous image classification algorithms have been invented and developed over the past decades. Thus, it is important to select appropriate classification methods based on the study area, the data type, and additional requirements for a specific project. In this research, image classifications of the Rio Beni floodplain were conducted by using three classification algorithms: ISODATA, Bayes classifier, and fuzzy classifier. These three classifiers were selected as representatives based on their characteristics—i.e., whether they are supervised or unsupervised classification algorithms, and whether they are hard or soft classifiers. Specifically, ISODATA is an unsupervised hard/crisp classifier, whereas Bayes classifier and fuzzy classifier are supervised soft classifiers. This selection was made to address a research questions about how the soft classifiers perform compared with a traditional hard classifier, and the utility of additonal information that can be acquired via soft classification for fluvial/floodplain land-cover analysis.

Regarding evaluating image classification performance, accuracy assessment constitutes the standard approach. In this research, an accuracy assessment was

conducted on the three classification results for each image, where 100 accuracy-assessment samples were generated for each land-cover class using a stratified random sample strategy, with manual/visual comparison to reference data. Overall, all three classification algorithms performed approximately equally as well: ISODATA had 90.97% average overall accuracy with Kappa coefficient of 0.8917, Bayes classifier had 90.45% average overall accuracy with Kappa coefficient of 0.8853, and fuzzy classifier had 90.17% average overall accuracy with Kappa coefficient of 0.8800. The statistics for the three tested classification algorithms indicate the differences among these classifications results are small.

Although the classification accuracies are similar among the three tested classification methods, some differences in the final land-cover maps were still found via manual/visual assessment. One noticeable difference is that the land-cover maps from ISODATA were affected by "salt-and-pepper" effect more severely than those land-cover maps generated from Bayes classifier and fuzzy classifier. The "salt-and-pepper" effect in remote sensing refers to the presence of heterogeneous land-cover pixels sparsely distributed within a homogenous land-cover area. In such relatively homogenous areas, isolated pixels can often be misclassified pixels. Thus, from this perspective, the two soft classifiers may produce better land-cover maps for the Rio Beni floodplain than ISODATA did. Another marked difference is with the performance of classifying different land-cover types. Water class had the highest classification accuracy due to its distinct spectral signatures relative to the other land-covers considered in this research. However, ISODATA was able to provide higher user's accuracies. Sand is

another class with high classification accuracy, though the results from Bayes classifier had lower producer's accuracy compared with the other two algorithms. Two bare soil classes had relatively good classification accuracies around 90% from all three tested classification algorithms. Most of the misclassifications with respect to these two bare soil classes arose from the confusion between the soil classes themselves. Such confusion is likely primarily a function of the gradation in spectral reflectance values of bare soil with changing soil moisture and the associated variability in reflectance (Sadeghi, Jones, and Philpot 2015). Also, confusion between bare soil and non-forest vegetation was observable. The gradual colonization of bare-soil areas by vegetation on the floodplain may be the reason for this confusion, as this process tends to translate to less-pure image pixels by a single land-cover class, yielding mixed pixels and classification errors. Forest and non-forest were also confused with one another; thus, the producer's accuracies and user's accuracies of forest and non-forest were lower relative to some other classes (~85%). This was especially the case for non-forest vegetation, as this class was also confused with the bare soil classes; its classification accuracies were the lowest among all land-cover types. Again, such confusion arose from multiple factors, such as similar spectral reflectance and land-cover mixtures within individual pixels. This has been a shortcoming in pixel-based analyses (Blaschke 2010).

Besides classification accuracies, another critical aspect of the results is with differences in information content provided by the classification algorithms investigated. The three tested classification algorithms can provide traditional hard/crisp land-cover

maps. However, the two soft classification algorithms provide additional information relative to the hard/crisp method—i.e., posterior probability layers or fuzzy membership layers for each land-cover class, which hard/crisp classifiers, such as ISODATA, do not provide (Figures 8 and 10). These layers constitute important sources of soft (probabilistic and fuzzy) information regarding land-cover types/ landscape characteristics. Such information is very useful in studying and analyzing the evolution of landscapes with heterogeneous land-cover configurations and dynamic variation in land-cover change. In this research, importantly, fuzzy membership information was used as input data to construct a novel landscape change-detection approach. This new algorithm enabled more subtle analysis of spatial variation and magnitude of change in a land-cover class context. Instances where class membership values changed from time 1 to time 2 without changing the primarily-assigned/dominant class were detected, which could reflect dynamic within-class processes, such as vegetation growth or decrease in canopy cover, or within-pixel changes in land-cover abundances. Also, changes between different land-cover classes were demonstrated in detail, with separation of major change or transitional change. The proposed change-detection algorithm, therefore, provides additional information which fills the gap between discrete classification/change-detection and the continuously-variable land-change processes that occur in reality.

In summary, results indicate similar hard classification accuracies among the classifiers tested, but the two soft classification algorithms provide probability or fuzzy membership information, which can be used subsequent analysis of land

change/landscape evolution. For study areas where land-covers are heterogeneous and landscape change processes are dynamic, a soft classification approach may be considered to be a superior classification strategy relative to a hard classification approach.

5.2 Influence of the Three Fuzzy Indices in Determination of the Transitional 2nd Threshold

Change-detection is necessary to provide maps and other information regarding land-cover change and landscape evolution. Numerous change-detection algorithms have been developed and applied to identify landscape change. Both discrete and fuzzy change-detection algorithms and approaches exist, but they both suffer from some disadvantages. For discrete change-detection approach, which remain popular for its simplicity and clarity in interpretation and analysis of data, does not take into account the continuous boundary and transition of real landscape change. This causes marked loss of information. Conversely, the fuzzy change-detection approach, which has been developed to provide a more continuous representation of land-cover and landscape change, can be sometimes difficult to use and interpret due to the typically large output data volume. In this research, a novel change status, namely "transitional change," is proposed in order to combine the advantages of both discrete and fuzzy approaches. Specifically, this transitional change type represents a less pure, fuzzier change status than a common one-direction pure land-cover change from one land-cover class to another. The "transitional change" class designation contains fuzzy information to some

degree, which can be important to characterize complex environments, such as active meandering river floodplains. Also, as the output is still discrete, it keeps the data interpretation convenient and efficient.

The determination of transitional change is part of the proposed MCVA algorithm. After the separation between changed and unchanged pixels by the dynamic 1st threshold and refinement of FMRF, those changed pixels would compare to the pure training samples to determine whether they exhibited change or transitional change status. Three indices regarding the fuzziness of the nature of change were applied to evaluate the status of change. These three indices were dominant change ratio, pixel uncertainty index, and Shannon's entropy. The average value was used as threshold to further separate changed pixels between transitional change and change. The decision of averaging three indices was made based on the consideration that they cover different aspects of change fuzziness, and an average value would constitute a simple method to combine the aspects that each covers. In order to evaluate this averaging approach, the individual influence of each index would be explored and compared to the averaging approach in this subsection.

5.2.1 Transitional Threshold Based on Dominant Change Ratio Only

Dominant change ratio refers to the ratio of change magnitude from the dominant "from-to" change type to the total change magnitude. If there is complete one-direction land-cover change, the change magnitude should mostly come from the dominant "from-to" change type. This index was created as a direct representation of the fuzziness of change. Figure 32 shows the change maps for all five time periods which transitional change was only determined by the threshold based on the dominant change ratio. This allows an individual assessment of the utility of using dominant change ratio to separate the two change status. Also, Tables 39 (a) - (e) give the ratio between change and transitional change within each time period, which shows the comparison between the averaging three indices threshold and dominant change ratio threshold. Note that as this determination of 2nd threshold did not affect the unchanged pixels, which means the unchanged pixels were the same between the two different thresholding approaches. Compared to the threshold by averaging the three selected indices, the threshold solely based on the dominant change ratio generated results that contained a higher proportion of change pixels than transitional pixels in all time periods. Especially, in the period between 1999 and 2006, the result from the dominant change ratio threshold had 93.07% change pixels defined as pure change, when some of those changes in the peripheral area should more likely to be considered as transitional change. The results from the averaging indices threshold show higher stability in the ratio between change and transitional change during different time periods.

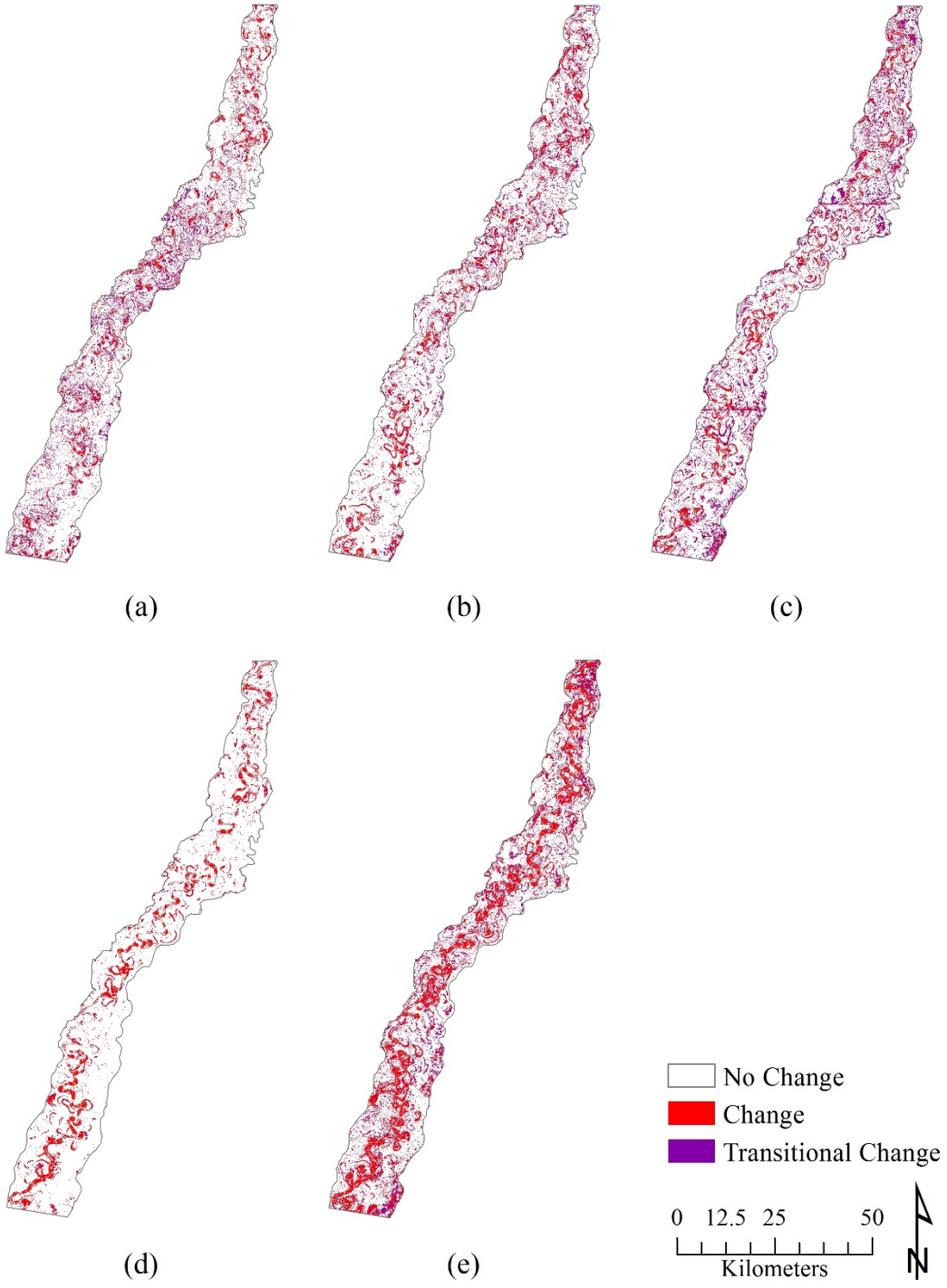

Figure 32. Map of land-cover change status based on dominant change ratio threshold: (a) 1987-1990; (b) 1990-1995; (c) 1995-1999; (d) 1999-2006; and (e) 1987-2006.

Table 39. Comparison of difference between change and transitional change status, whose threshold was based on average of three indices or dominant change ratio: (a) 1987-1990; (b) 1990-1995; (c) 1995-1999; (d) 1999-2006; and (e) 1987-2006.

(a) 1987-1990	Change (%)	Transitional Change (%)
Average of Three Indices	60.23	39.77
Dominant Change Ratio	62.41	37.59

(b) 1990-1995	Change (%)	Transitional Change (%)
Average of Three Indices	67.20	32.80
Dominant Change Ratio	79.47	20.53

(c) 1995-1999	Change (%)	Transitional Change (%)
Average of Three Indices	54.97	45.03
Dominant Change Ratio	67.18	32.82

(d) 1999-2006	Change (%)	Transitional Change (%)
Average of Three Indices	54.23	45.77
Dominant Change Ratio	93.07	6.93

(e) 1987-2006	Change (%)	Transitional Change (%)
Average of Three Indices	74.29	25.71
Dominant Change Ratio	84.48	15.52

5.2.2 Transitional Threshold Based on Pixel Uncertainty Index Only

Pixel uncertainty index is an index is an indicator of how certain a pixel can be classified as a particular land-cover type, as a pixel with higher membership value in one land-cover class has lower pixel uncertainty index. This index was applied to help estimate the fuzziness of change as a clear land-cover change should entail a low pixel uncertainty index after the change. Figure 33 shows the change maps for all five time periods which transitional change was only determined by the threshold based on the pixel uncertainty index. This allows an individual assessment of the utility of using pixel uncertainty index to separate the two change status. Also, Table 40 (a) - (e) lists the ratio between change and transitional change within each time period, which shows the comparison between the averaging three indices threshold and pixel uncertainty threshold. Compared to the threshold by averaging the three selected indices, the threshold solely based on the pixel uncertainty index generated results that contained a higher proportion of transitional change pixels than change pixels in most time periods. This result was not very reasonable, as the area experienced transitional change like riparian transition zones did not cover large amount of total area in the study area. The pixel uncertainty index was incorporated into the three selected indices as a supporting role. It may help correct some situations when the dominant change ratio alone was not able to cover. Situations include when dominant change ratio was low (pixel would be considered as transitional change), but if the pixel uncertainty index was high after the change which means the after land-cover class was very pure, that pixel should actually

be considered as pure change pixel. However, its ability as the only parameter to distinguish transitional change is questionable and lacks of theoretical foundation.

Table 40. Comparison of difference between change and transitional change status, whose threshold was based on average of three indices or pixel uncertainty index: (a) 1987-1990; (b) 1990-1995; (c) 1995-1999; (d) 1999-2006; and (e) 1987-2006.

(a) 1987-1990	Change (%)	Transitional Change (%)
Average of Three Indices	60.23	39.77
Pixel Uncertainty Index	24.04	75.96

(b) 1990-1995	Change (%)	Transitional Change (%)
Average of Three Indices	67.20	32.80
Pixel Uncertainty Index	43.15	56.85

(c) 1995-1999	Change (%)	Transitional Change (%)
Average of Three Indices	54.97	45.03
Pixel Uncertainty Index	38.78	61.22

(d) 1999-2006	Change (%)	Transitional Change (%)
Average of Three Indices	54.23	45.77
Pixel Uncertainty Index	64.09	35.91

(e) 1987-2006	Change (%)	Transitional Change (%)
Average of Three Indices	74.29	25.71
Pixel Uncertainty Index	54.01	45.99

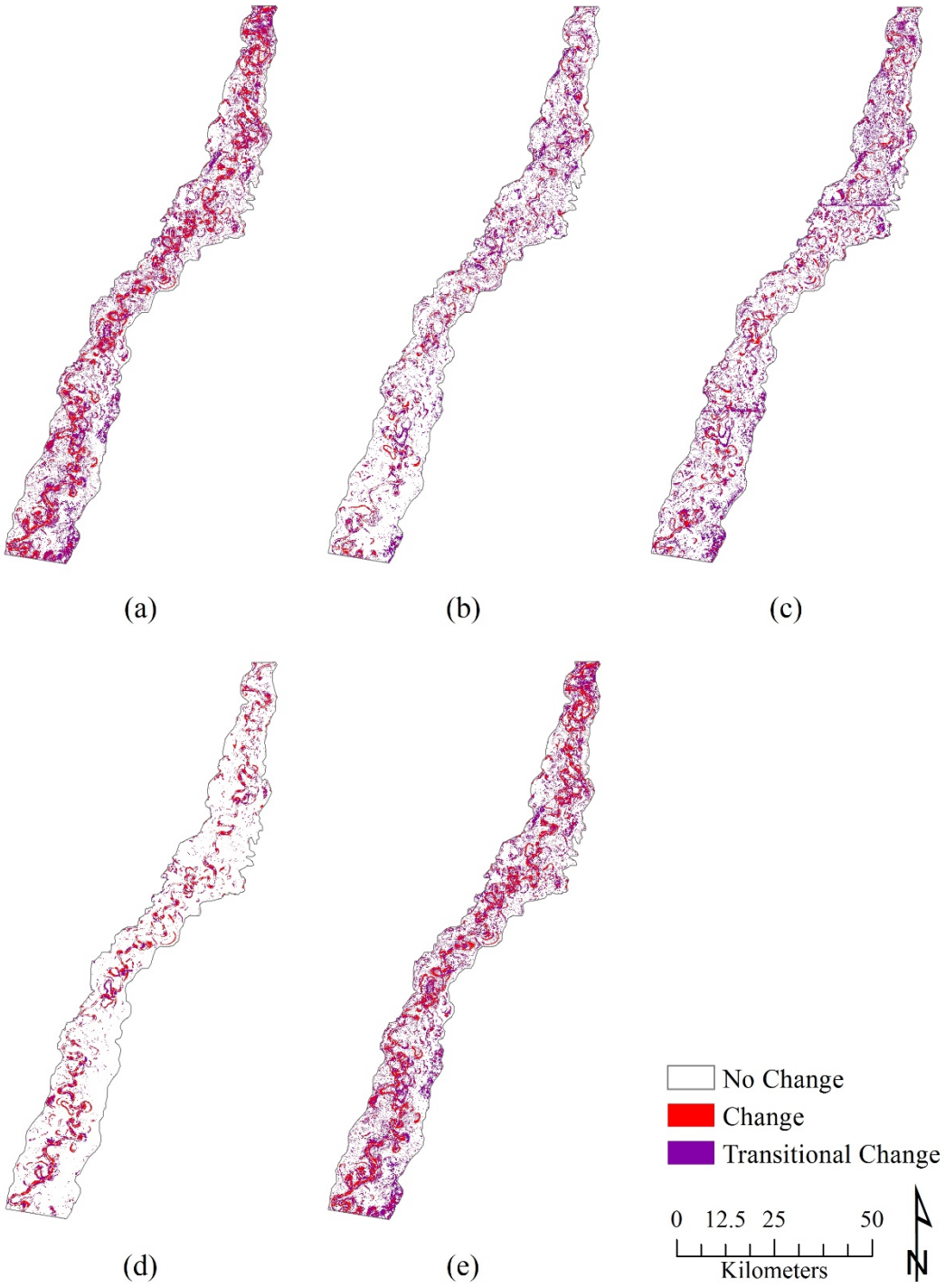

Figure 33. Map of land-cover change status based on pixel uncertainty index threshold: (a) 1987-1990; (b) 1990-1995; (c) 1995-1999; (d) 1999-2006; and (e) 1987-2006.

5.2.3 Transitional Threshold Based on Shannon's Entropy Only

Shannon's entropy is an indicator of membership diversity of a pixel, as lower entropy means a higher concentration of membership in one land-cover class. Similar to pixel uncertainty, this index was applied to the estimation of the fuzziness of change as change status should show lower entropy than transitional change status. Figure 34 shows the change maps for all five time periods which transitional change was only determined by the threshold based on the Shannon's entropy. This allows an individual assessment of the utility of using Shannon's entropy to separate the two change status. Also, Table 41 (a) - (e) lists the ratio between change and transitional change within each time period, which shows the comparison between the averaging three indices threshold and pixel uncertainty threshold. From the figure and table, it is clear that transitional change was more abundant than change pixels in most time periods. Even in the area should show dramatic change in reality, such as area where river channel migration happened, too many pixels were defined as transitional change. These obvious errors have shown that Shannon's entropy should not be considered as the only parameter in determining the transitional 2nd threshold. Similar to pixel uncertainty index, the Shannon's entropy performed a supporting role to help the dominant change ratio better distinguish change and transitional change.

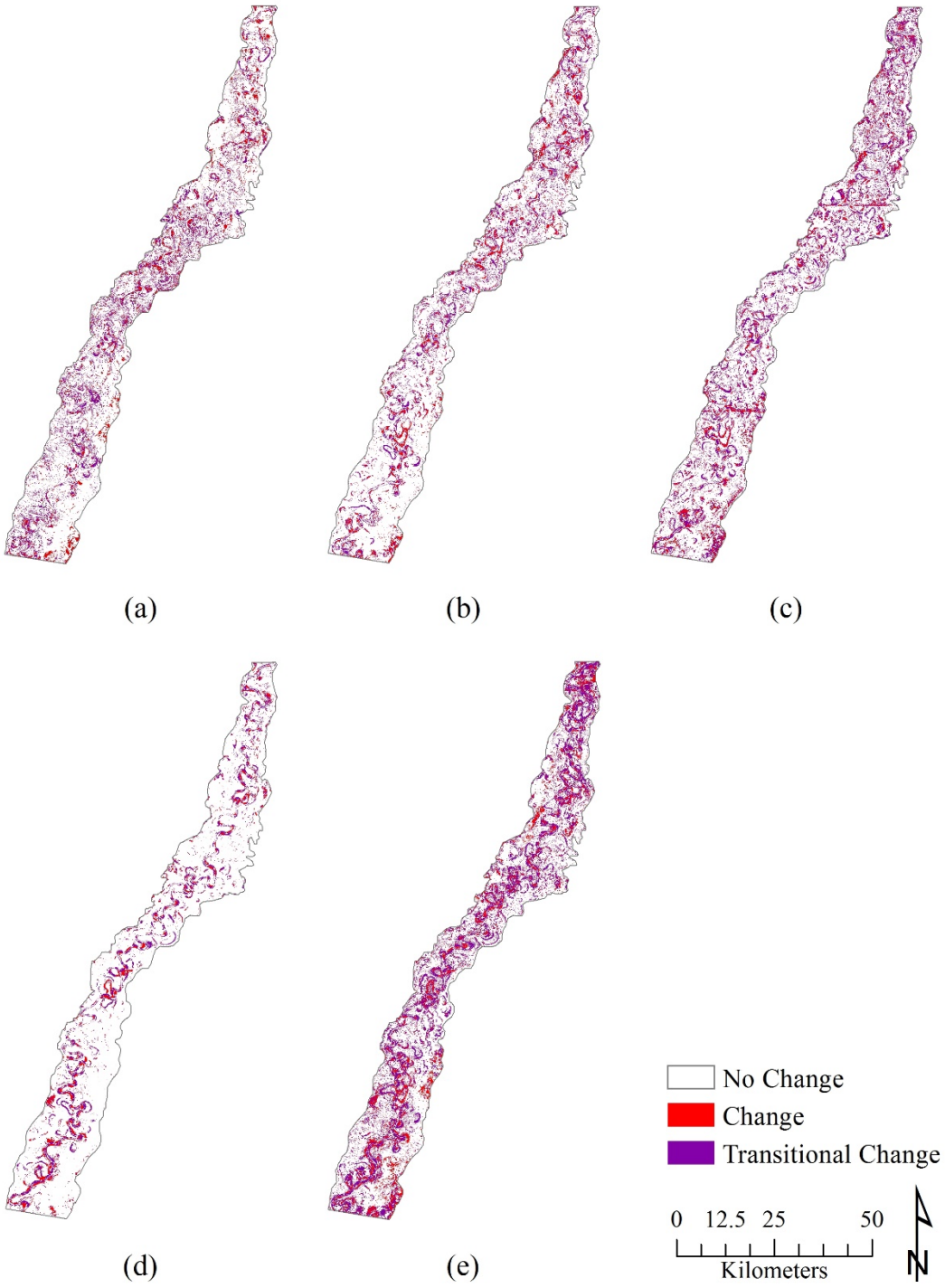

Figure 34. Map of land-cover change status based on Shannon's entropy threshold: (a) 1987-1990; (b) 1990-1995; (c) 1995-1999; (d) 1999-2006; and (e) 1987-2006.

Table 41. Comparison of difference between change and transitional change status, whose threshold was based on average of three indices or Shannon's entropy: (a) 1987-1990; (b) 1990-1995; (c) 1995-1999; (d) 1999-2006; and (e) 1987-2006.

(a) 1987-1990	Change (%)	Transitional Change (%)
Average of Three Indices	60.23	39.77
Shannon's Entropy	50.44	49.56

(b) 1990-1995	Change (%)	Transitional Change (%)
Average of Three Indices	67.20	32.80
Shannon's Entropy	55.58	44.42

(c) 1995-1999	Change (%)	Transitional Change (%)
Average of Three Indices	54.97	45.03
Shannon's Entropy	48.69	51.31

(d) 1999-2006	Change (%)	Transitional Change (%)
Average of Three Indices	54.23	45.77
Shannon's Entropy	45.55	54.45

(e) 1987-2006	Change (%)	Transitional Change (%)
Average of Three Indices	74.29	25.71
Shannon's Entropy	44.22	55.78

In summary, the individual use of any of these three indices to determine the threshold has some problems. For the Shannon's entropy as threshold, errors could be easily observed. It is highly not recommended to apply individually to determine the transitional threshold. For the pixel uncertainty index, although obvious errors were not so abundant, it is also not very reliable to be the only parameter in threshold determination due to its similar characteristics with the Shannon's entropy. For the dominant change ratio, it has the most reasonable theoretical background to become a single parameter in determination of the transitional threshold. The dominant change

ratio directly reflects the degree of change comes from the dominant one-direction change type, which leads to a direct estimation of whether a change is transitional or not. However, it may ignore some situations as discussed above and cause errors. The averaging value of three indices was proposed in this research for a comprehensive consideration for land-cover change fuzziness in different situations. Although this simple approach may not be optimal, it aims to utilize the three indices together to cover as many situations as possible. The current reference data was not able to thoroughly assess whether the threshold by averaging three indices was better the thresholds by individual index, the higher stability and fewer marked errors observed may show the advantages of combining these indices. With a more rigorous dataset that contains fuzzy reference data, future work should consider different methods to combine these indices, such as a voting strategy. Also, additional indices may be further explored to advance the determination of this novel transitional change status.

5.3 Interpretation of the Observed Meandering River Floodplain Dynamics

In this research, five Landsat 5 TM satellite images were used as time-series data to quantify land-cover change over multiple decades in the Rio Beni floodplain landscape. Fuzzy image classifications and change-detections by the proposed MCVA algorithm were conducted to quantitatively characterize such change. Additionally, a set of landscape metrics were computed in order to summarize the structural change of different land-covers over the study period. In this subsection, a synthesized characterization of landscape change, which combines the information from the results in previous sections, is presented in order to interpret the spatiotemporal change.

Between 1987 and 1990, 77.25% of pixels remained as the same land-cover type, whereas 13.7% experienced clear land-cover change, and 9.05% experienced transitional land-cover change. Regarding spatial buffer zones, buffer zone 1, which was the zone closest to the main river channel in 1987, possessed 54.63% of the total clearly-changed area and 49.24% of the total transitional change area, whereas the other three zones almost evenly possessed the rest of the change area. As buffer zone 1 only occupied ~41% of the total floodplain but entailed a larger percentage of the change area which was ~ 53%, buffer zone 1 thus experienced more dramatic change compared with the other three zones. This finding is reasonable since landscape-change effects associated with Rio Beni meander-migration dynamics should be more evident in areas proximal to the river. In terms of specific land-cover classes, variations in change was observed. During this period, two vegetation classes experienced opposite situations: the forest class lost a marked areal extent, whereas non-forest vegetation gained many areas.

Regarding the forest class, it appeared to be more spatially clustered in 1987 than it was in 1990, as the number of forest patches was lower, but average patch area was higher in 1987. Regarding the patch shape, forest patches were more complex from 1987 to 1990 according to Shape Index and Fractal Dimension Index. The decrease in area and the increase in shape complexity may indicate river-channel migration markedly/dramatically affecting forest areas, leading to the loss of some forest coverage. This interpretation may be supported by the fact that large areas of forest in 1987 shifted to wet soil in 1990; the increasing existence of wet soil could be consequences of river-channel migration through time, or of a flood event. On the other hand, non-forest vegetation markedly gained areal coverage during this time period. One large source of this increased area was from the forest class, which seems to imply the emergence of colonizing vegetation following forest destruction via riverine/fluvial and geomorphic processes. The number of patches of non-forest vegetation decreased substantially while the mean patch area increased. Along with the increasing patch cohesion index, this indicates that the newly-grown non-forest vegetation was able to connect existing patches. Although the total area for oxbow lakes and the main river channel did not change substantially, the change maps do show a marked coverage changes between these two types of water bodies, which reflects river-channel migrations, the formation of cut-offs, and river-channel re-connections to oxbow lakes. The average shapes of oxbow lakes were more elongated in 1987 compared with those in 1990, according to the Related Circumscribing Circle Index. In addition, a large percentage of oxbow lakes in the peripheral area of the floodplain, away from the main river channel, changed to

wet soil, which appears to indicate a drying/emptying of the oxbow lakes, possibly implying that a significant hydrological event occurred during this time period that could affect the peripheral area in this manner.

Between 1990 and 1995, 79.4% of pixels remained as the same land-cover type, whereas 13.85% experienced clear land-cover change, and 6.76% of pixels experienced transitional land-cover change. Regarding spatial buffer zones, buffer zone 1, which is the zone closest to the main river channel in 1990, possessed 56.35% of the total clear change area and 51.92% of the total transitional change area, which indicates that buffer zone 1 experienced more dramatic change compared to other three zones. From buffer zone 2 to zone 4, the percentages of unchanged pixels increased from 81.73% to 85.74%, and the percentages of clear change decreased from 11.87% to 9.2%. Regarding specific land-cover classes, variations in change was observed. Dry soil experienced areal an increase, whereas wet soil experienced a small areal decrease. For dry soil, the number of patches increased substantially from 1990 to 1995, especially in zone 1. Also, the shape of dry soil patches in zone 1 was more complex in 1995 compared to those in 1990. 7.3% of non-forest vegetation shifted to forest coverage, leading to a decrease of average patch area from 1990 to 1995. Over 95% of forest in 1990 remained in 1995, and the additional forest area shifted from non-forest vegetation, indicating continuous growth of vegetation. This could lead to the implication of low level of disturbances, including human and natural processes. River-channel migration and other hydrological processes were active in buffer zone 1 during this time period, as land-cover changes among oxbow lakes, river, and sand-bars were very common,

yielding large degrees of change in areal extents for these classes. Overall landscape complexity decreased, as indicated by several shape and aggregation landscape metrics. Although the time extent was longer than the previous time period, floodplain landscape from 1990 to 1995 did not change as much as it did from 1987 to 1990.

Between 1995 and 1999, 73.46% of pixels remained as same land-cover type, whereas 14.59% experienced clear land-cover change, and 11.95% experienced transitional land-cover change. In terms of spatial buffer zones, although buffer zone 1 was still the one with the lowest percentage of unchanged pixels (71.04%), the differences between it and the other three zones were smaller compared with those of other time intervals. From buffer zone 2 to zone 4, the percentages of unchanged pixels, changed pixels, and transitionally-changed pixels were similar, which were approximately 75%, 11%, and 12%, respectively. Buffer zone 4 had the second-highest change ratio, which was surprising, as zone 4 should be least affected by the river-channel migration processes from the Rio Beni. Regarding specific land-cover classes, variations in change was observed. Changes from the main river channel were primarily to oxbow lakes in transitional change, and to sand with clear-change status. As a result, the number of oxbow lake patches and average patch size both increased. Also, the average shape of oxbow lakes in 1999 showed the most elongated form compared to other dates in this time series. Two vegetation classes were still actively changing, as the "from-to" change types that they were associated with occupied a large area of the floodplain. Non-forest vegetation continued to grow, as more than 19% of original non-forest vegetation had transitionally changed within its class, and over 10% shifted to

forest coverage. The non-forest vegetation showed an increase of patch area and connectivity in 1999. With the elongated trend of patches, it is very likely that non-forest vegetation was continuing to colonize the abandoned channel scars. Forest patches show low average area compared with other time intervals. And the decrease of cohesion index indicates the decrease of area affected its connectivity.

Between 1999 and 2006, 83.28% of pixels remained as the same land-cover type, whereas 9.06% experienced clear land-cover change, and 7.65% experienced transitional land-cover change. The percentage of unchanged area was the highest among all four time periods, despite the fact that this time period entailed the longest time extent. Buffer zone 1 had 28% of the area experiencing change (both clear and transitional change), whereas the other three zones only had an average of 6% of the area changing. From these statistics and Figure 22 in the previous section, it is clear that land-cover change was concentrated within the riparian zone proximal to the main river channel, and the degree of concentration of change was the highest among all time periods. Also, the high percentage of clear land-cover change compared to the transitional change in zone 1 reflected the land-cover change processes. Regarding specific land-cover classes, variations in change was observed. As most land-cover changes occurred in buffer zone 1, the main river channel, oxbow lakes, and sand were the most actively-changing land-cover classes during this period. River-channel movement and sediment deposition created many new sand-bars, as the average sand patch area decreased, along with increases in complexity and the fractal index. Zone 2 was where most shifts between oxbow lakes and the main river channel occurred. Two vegetation classes did not

experience much change in terms of total coverage area, although the shift between non-forest vegetation and the main river channel could be readily-detected in (riparian) zone 1. The overall landscape in zones 3 and 4 was similar, as both land-cover areal extents and landscape metrics of most classes remained almost the same. Vegetation colonization on abandoned channel scars was the most observable change in the peripheral area of the floodplain during this time period.

For the entire two decades of observed time series (from 1987 to 2006), 74.4% of pixels remained as the same land-cover type, 20% experienced clear land-cover change, and 5.6% of pixels experienced transitional land-cover change. The percentage of unchanged area was the lowest compared to the four discrete, smaller time intervals, whereas the ratio between change and transitional change was the highest over the entire time period. As the landscape from 1987 to 2006 cumulated the changes during those four smaller time intervals, it was expected that the clear land-cover change would be more abundant compared with transitional change. Regarding the spatial pattern of the land-cover change, buffer zone 1, i.e., the riparian area proximal to the main river channel, experienced the most dramatic change during this entire period. This follows from the results from the four smaller time intervals. And the degree of change decreased rapidly from zone 1 to zone 2, and then continued to decline slowly from zone 2 to zone 4. As results for all five periods showed similar trends, it is indicated that the landscape change associated with river-channel migration mostly occurred within a 1-km spatial buffer along the main river channel. Regarding specific land-cover change, the most pronounced phenomenon was the loss of forest coverage, and the growth of

non-forest vegetation. The transformations among the main river channel, oxbow lakes, and sand constituted another major source of landscape change. The overall landscape in the peripheral areas (i.e., zone 3 and zone 4) was relatively stable from 1987 to 2006. Larger land-cover patches were more abundant in these areas, as less disturbance promoted the continuous growth of vegetation. Therefore, the fractal dimension was lower and the floristic connectivity increased, which has implications for biodiversity (Fahrig 2003).

5.4 Utility of Landscape Metrics for Characterizing Floodplain Landscape Structure

Thirteen (13) landscape metrics in three broad categories (i.e., area, shape, and aggregation), were calculated using FRAGSTATS version 4.2 for each land-cover class. The purpose of including landscape metrics-based analysis to this research was to utilize these metrics, along with the numerical information from the land-cover areal and type change, to characterize the spatial patterns, structures, and configurations of a dynamic meandering floodplain. Combined with the buffer zone analysis, the spatial structures of land-cover classes were assessed. Dry soil patches were more abundant, but fragmented, near the river, whereas they were more clustered and formed larger patches in areas away from the main river channel. Forest patches decreased gradually with distance from the river banks, but the average patch size continued to increase; forest patches were highly connected throughout the entire floodplain. Non-forest vegetation patches possessed similar patch sizes as forest patches, but they had higher fractal dimension

index and were more complex in shape. In particular, the shape of non-forest vegetation patches was narrow and elongated, which may be a result of the belt-shaped vegetation that colonized the abandoned channel scars and dried-up oxbow lakes. A large number of oxbow-lake patches were found in the riparian zone proximal to the main river channel, with high connectivity. Large complex sand patches were found in buffer zone 1, whereas in zones 2 – 4, the sand patches were rare, which indicated that sand patches mostly appeared close to main river channel in the form of sand clusters/sand-bars. Wet soil demonstrated a situation similar to that of dry soil in that patches were fragmented near the main river channel, but they were likely to be aggregated/clustered into large patches in areas away from the main river channel. In short, the landscape metrics revealed the spatial structure and characteristics of land-covers a function of the distance from the main channel of Rio Beni.

However, regarding the multi-temporal comparison of landscape metrics over the study time period, the resulting indices and patterns were very similar at different times, even when the statistics indicated large changes in areal extents of land-covers and in land-cover types. Although such similar patterns may reveal some insights about the floodplain landscape dynamics during this two-decade-period did not greatly change the overall landscape structure, further study is needed to better understand the nature of such land-change. It is quite likely that the observable patterns were similar across different time periods because the spatial resolution of the Landsat images analyzed in this research was too coarse to effectively detect some of the changes in landscape structure. Many of the landscape metrics in the literature are based on the average value

of a specific class or the overall landscape, which already entails a smoothing effect on certain metric values. Furthermore, if a coarse spatial-resolution image is used as input, this compounds the difficulty of capturing the complexity and dynamics of the landscape spatial patterns and configurations (Lausch and Herzog 2002). Therefore, future research should include analysis of higher spatial-resolution images in order to determine whether the patterns associated with floodplain landscape metrics change as a function of remote-sensor image spatial resolution and whether the utility of landscape metrics in this environment is enhanced.

6. CONCLUSIONS

Large meandering river floodplains, especially those in tropical forest area, are critical components of the Earth system to maintain global ecological integrity. Therefore, it is important to advance the understanding of the spatiotemporal patterns of the dynamic floodplain landscape change. Such knowledge would be beneficial to sustainable management and protection of these ecosystems. The research presented in this thesis aims to further study the existing remote-sensing-based mapping and characterization methods of meandering river floodplain. Based on the two decades of Landsat 5 TM image data of the Rio Beni floodplain, this research addressed the following questions and objectives: (1) which classification approach, hard or soft classification, may best map a floodplain landscape; (2) development of a novel change-detection method that promotes the use of fuzzy membership information in order to achieve better detection accuracy and provide informative data; and (3) characterization of long-term floodplain evolution by a multi-temporal analyses.

The soft pixel-based classification was found to be more superior in mapping floodplain environments. In this research, one commonly-used hard classification method (i.e., ISODATA) and two soft classification methods (i.e., Bayes classification and fuzzy classification) were applied to the study area to compare their differences. All three methods were able to achieve about 90% classification accuracy via a hard output. However, the maps generated by ISODATA suffered a more severe “salt-and-pepper” effect compared to the two soft-classified results. Moreover, besides a traditional form of

hard output, the two soft classifiers were able to produce a set of soft layers - Bayesian posterior probability layers or fuzzy membership layers. These layers provide continuous values for the land-cover assignment of a given pixel, which is a more reasonable way to model the actual scenario where land-cover boundaries are seldom discrete. Due to a better classification performance and additional information provided, the soft classification methods should be considered primarily for research on mapping a floodplain environment.

To further understand a dynamic meandering floodplain landscape evolution, high-quality change maps are critical components for a multi-temporal analysis. This research assessed the overlaying issue in traditional thresholding method for determination of changed and unchanged pixels. Then a new dynamic thresholding stage was developed to address the overlaying issue by incorporating change uncertainty information and "from-to" change direction information. Also, a fuzzy Markov Random Field model was applied to overcome the over-smoothing effect of the standard approach. Results from accuracy assessment indicated the proposed modified CVA algorithm achieved a statistically significant improvement compared to three other commonly used methods. Besides, a new transitional change status was also put forward in this research. The transitional change is a sub-status of change, indicating the land-cover change is fuzzier than a pure one-to-one land-cover change. The additional information provided by the "transitional change" class entailed great value in creating a precise, accurate, and more subtle change-detection analyses for complex floodplain/fluvial landscapes.

Multi-temporal analyses were able to demonstrate the landscape change on the Rio Beni floodplain from 1987 to 2006. For the comparison between images in 1987 and 2006, 74.4% of pixels remained the same land-cover, 20% experienced clear land-cover change and 5.6% experienced transitional land-cover change. The riparian area (i.e., zone 1 in this research) experienced more dramatic change than other parts of the floodplain during this period. River channel, oxbow lakes, forest, non-forest vegetation were the most active land-covers. Landscape metrics showed some utilities during the analysis, especially in assessing the characteristics of land-cover patch area. However, higher spatial resolution imagery may be necessary to fully explore the information generated by these indices.

The research in this thesis contributes to the debates on the superiority of applying soft classification and change-detection methods on mapping and characterizing a dynamic meandering river floodplain environment. Also, the presented novel thresholding algorithm provides a solution to the overlapping issue in the traditional change-detection approach, and therefore improves the overall change-detection accuracy. In addition, this research provides useful knowledge regarding long-term landscape characteristics of the Rio Beni floodplain. This knowledge will inform the management and environmental protection of the Rio Beni floodplain and other similar ecosystems in South America.

REFERENCES

Aalto, R., L. Maurice-Bourgoin, T. Dunne, D. R. Montgomery, C. A. Nittrouer, and J. L. Guyot. 2003. Episodic sediment accumulation on Amazonian flood plains influenced by El Nino/Southern Oscillation. *Nature* 425 (6957):493-497.

Aalto, R., and C. A. Nittrouer. 2012. 210Pb geochronology of flood events in large tropical river systems. *Philosophical Transactions of the Royal Society A: Mathematical, Physical and Engineering Sciences* 370 (1966):2040-2074.

Amoros, C., and G. Bornette. 2002. Connectivity and biocomplexity in waterbodies of riverine floodplains. *Freshwater Biology* 47 (4):761-776.

Apan, A. A., S. R. Raine, and M. S. Paterson. 2002. Mapping and analysis of changes in the riparian landscape structure of the Lockyer Valley catchment, Queensland, Australia. *Landscape and Urban Planning* 59 (1):43-57.

Arai, K. 1992. A supervised Thematic Mapper classification with a purification of training samples. *International Journal of Remote Sensing* 13 (11):2039-2049.

Baisantry, M., D. S. Negi, and O. P. Manocha. 2012. Change vector analysis using enhanced PCA and inverse triangular function-based thresholding. *Defense Science Journal* 62 (4):236-242.

Bardossy, A., and L. Samaniego. 2002. Fuzzy rule-based classification of remotely sensed imagery. *IEEE Transactions on Geoscience and Remote Sensing* 40 (2):362-374.

Bastin, L. 1997. Comparison of fuzzy c-means classification, linear mixture modelling and MLC probabilities as tools for unmixing coarse pixels. *International Journal of Remote Sensing* 18 (17):3629-3648.

Bazi, Y., F. Melgani, and H. D. Al-Sharari. 2010. Unsupervised change detection in multispectral remotely sensed imagery with level set methods. *IEEE Transactions on Geoscience and Remote Sensing* 48 (8):3178-3187.

Benz, U. C., P. Hofmann, G. Willhauck, I. Lingenfelder, and M. Heynen. 2004. Multi-resolution, object-oriented fuzzy analysis of remote sensing data for GIS-ready information. *ISPRS Journal of Photogrammetry and Remote Sensing* 58 (3-4):239-258.

Besag, J. 1986. On the statistical-analysis of dirty pictures. *Journal of the Royal Statistical Society Series B-Methodological* 48 (3):259-302.

Bezdek, J. C. 1981. *Pattern recognition with fuzzy objective function algorithms*. Norwell, MA: Kluwer Academic Publishers.

Blaschke, T. 2010. Object based image analysis for remote sensing. *ISPRS Journal of Photogrammetry and Remote Sensing* 65 (1):2-16.

Bone, C., S. Dragicevic, and A. Roberts. 2005. Integrating high resolution remote sensing, GIS and fuzzy set theory for identifying susceptibility areas of forest insect infestations. *International Journal of Remote Sensing* 26 (21):4809-4828.

Bovolo, F., and L. Bruzzone. 2007. A theoretical framework for unsupervised change detection based on change vector analysis in the polar domain. *IEEE Transactions on Geoscience and Remote Sensing* 45 (1):218-236.

———. 2011. An adaptive thresholding approach to multiple-change detection in multispectral images. Paper read at 2011 IEEE International Geoscience and Remote Sensing Symposium (IGARSS), at Vancouver, BC.

Bovolo, F., L. Bruzzone, and M. Marconcini. 2008. A novel approach to unsupervised change detection based on a semisupervised SVM and a similarity measure. *IEEE Transactions on Geoscience and Remote Sensing* 46 (7):2070-2082.

Bruzzone, L., and D. F. Prieto. 2000. Automatic analysis of the difference image for unsupervised change detection. *IEEE Transactions on Geoscience and Remote Sensing* 38 (3):1171-1182.

Burrough, P. A. 1989. Fuzzy mathematical methods for soil survey and land evaluation. *Journal of Soil Science* 40 (3):477-492.

Büttner, G., T. Hajós, and M. Korándi. 1989. Improvements to the effectiveness of supervised training procedures. *International Journal of Remote Sensing* 10 (6):1005-1013.

Camporeale, C., P. Perona, A. Porporato, and L. Ridolfi. 2005. On the long-term behavior of meandering rivers. *Water Resources Research* 41 (12): W12403.

Cazes, T. B., R. Q. Feitosa, and G. L. A. Mota. 2004. Automatic selection of training samples for multitemporal image classification. In *Lecture Notes in Computer Science (including subseries Lecture Notes in Artificial Intelligence and Lecture Notes in Bioinformatics)*, 389-396.

Chen, J., X. Chen, X. Cui, and J. Chen. 2011. Change vector analysis in posterior probability space: A new method for land cover change detection. *IEEE Geoscience and Remote Sensing Letters* 8 (2):317-321.

Chen, J., P. Gong, C. He, R. Pu, and P. Shi. 2003. Land-use/land-cover change detection using improved change-vector analysis. *Photogrammetric Engineering & Remote Sensing* 69 (4):369-379.

Colditz, R. R., M. Schmidt, and S. Dech. 2008. A methodology for advanced change detection with fuzzy image classification. Paper read at 5th International Conference on Electrical Engineering, Computing Science and Automatic Control, CCE 2008, at Mexico City.

Congalton, R. G. 1991. A review of assessing the accuracy of classifications of remotely sensed data. *Remote Sensing of Environment* 37 (1):35-46.

Congalton, R. G., and K. Green. 2009. *Assessing the accuracy of remotely sensed data: principles and practices*. Boca Raton, FL:CRC Press/Taylor & Francis.

Dronova, I., P. Gong, and L. Wang. 2011. Object-based analysis and change detection of major wetland cover types and their classification uncertainty during the low water period at Poyang Lake, China. *Remote Sensing of Environment* 115 (12):3220-3236.

Eastman, J. R. 2009. IDRISI Taiga guide to GIS and image processing. *Clark Labs Clark University, Worcester, MA*.

Fahrig, L. 2003. Effects of habitat fragmentation on biodiversity. In *Annual Review of Ecology, Evolution, and Systematics*, 487-515.

Fangju, W. 1990. Improving remote sensing image analysis through fuzzy information representation. *Photogrammetric Engineering & Remote Sensing* 56 (8):1163-1168.

Fernandes, M. R., F. C. Aguiar, and M. T. Ferreira. 2011. Assessing riparian vegetation structure and the influence of land use using landscape metrics and geostatistical tools. *Landscape and Urban Planning* 99 (2):166-177.

Ferreira, M. T., F. C. Aguiar, and C. Nogueira. 2005. Changes in riparian woods over space and time: Influence of environment and land use. *Forest Ecology and Management* 212 (1–3):145-159.

Filippi, A. M., and J. R. Jensen. 2006. Fuzzy learning vector quantization for hyperspectral coastal vegetation classification. *Remote Sensing of Environment* 100 (4):512-530.

Fisher, P., C. Arnot, R. Wadsworth, and J. Wellens. 2006. Detecting change in vague interpretations of landscapes. *Ecological Informatics* 1 (2):163-178.

Food and Agriculture Organization of the United Nations. 2010. Global forest resources assessment 2010: Terms and definitions. Available at http://www.fao.org/docrep/014/am665e/am665e00.pdf (last accessed 9 June 2016).

Foody, G. 2010. Assessing the accuracy of remotely sensed data: principles and practices. *The Photogrammetric Record* 25 (130):204-205.

Foody, G. M. 2005. Local characterization of thematic classification accuracy through spatially constrained confusion matrices. *International Journal of Remote Sensing* 26 (6):1217-1228.

Foody, G. M., and M. K. Arora. 1996. Incorporating mixed pixels in the training, allocation and testing stages of supervised classifications. *Pattern Recognition Letters* 17 (13):1389-1398.

Foody, G. M., and D. S. Boyd. 1999. Detection of partial land cover change associated with the migration of inter-class transitional zones. *International Journal of Remote Sensing* 20 (14):2723-2740.

Foody, G. M., and A. Mathur. 2006. The use of small training sets containing mixed pixels for accurate hard image classification: Training on mixed spectral responses for classification by a SVM. *Remote Sensing of Environment* 103 (2):179-189.

Forman, R. T. T., and M. Godron. 1981. Patches and structural components for a landscape ecology. *BioScience* 31 (10):733-740.

Freeman, R. E., E. H. Stanley, and M. G. Turner. 2003. Analysis and conservation implications of landscape change in the Wisconsin River floodplain, USA. *Ecological Applications* 13 (2):416-431.

Gautier, E., D. Brunstein, P. Vauchel, J.-M. Jouanneau, M. Roulet, C. Garcia, J. L. Guyot, and M. Castro. 2010. Channel and floodplain sediment dynamics in a reach of the tropical meandering Rio Beni (Bolivian Amazonia). *Earth Surface Processes and Landforms* 35 (15):1838-1853.

Gautier, E., D. Brunstein, P. Vauchel, M. Roulet, O. Fuertes, J. L. Guyot, J. Darozzes, and L. Bourrel. 2007. Temporal relations between meander deformation, water discharge and sediment fluxes in the floodplain of the Rio Beni (Bolivian Amazonia). *Earth Surface Processes and Landforms* 32 (2):230-248.

Ghosh, A., N. S. Mishra, and S. Ghosh. 2011. Fuzzy clustering algorithms for unsupervised change detection in remote sensing images. *Information Sciences* 181 (4):699-715.

Guevara, S., and J. Laborde. 2008. The landscape approach: Designing new reserves for protection of biological and cultural diversity in Latin America. *Environmental Ethics* 30 (3):251-262.

Gurnell, A. M. 1997. Channel change on the River Dee meanders, 1946-1992, from the analysis of air photographs. *Regulated Rivers: Research and Management* 13 (1):13-26.

Gurnell, A. M., M. Bickerton, P. Angola, D. Bell, I. Morrissey, G. E. Petts, and J. Sadler. 1998. Morphological and ecological change on a meander bend: the role of hydrological processes and the application of GIS. *Hydrological Processes* 12 (6):981-993.

Gustafson, J. E. 1998. Quantifying landscape spatial pattern: What is the state of the art? *Ecosystems* 1 (2):143-156.

Hamilton, S. K., J. Kellndorfer, B. Lehner, and M. Tobler. 2007. Remote sensing of floodplain geomorphology as a surrogate for biodiversity in a tropical river system (Madre de Dios, Peru). *Geomorphology* 89 (1-2):23-38.

Hamylton, S. M., and T. Spencer. 2011. Geomorphological modelling of tropical marine landscapes: Optical remote sensing, patches and spatial statistics. *Continental Shelf Research* 31 (2 SUPPL.):S151-S161.

Herzog, F., A. Lausch, E. Müller, H. H. Thulke, U. Steinhardt, and S. Lehmann. 2001. Landscape metrics for assessment of landscape destruction and rehabilitation. *Environmental Management* 27 (1):91-107.

Hollenhorst, T. P., G. E. Host, and L. B. Johnson. 2006. Scaling issues in mapping riparian zones with remote sensing data: Quantifying errors and sources of uncertainty. In *Scaling and Uncertainty Analysis in Ecology*, eds. J. Wu, K. B. Jones, H. Li and O. Loucks, 275-295: Springer Netherlands.

Hudson, P. F., F. T. Heitmuller, and M. B. Leitch. 2012. Hydrologic connectivity of oxbow lakes along the lower Guadalupe River, Texas: The influence of geomorphic and climatic controls on the " flood pulse concept". *Journal of Hydrology* 414-415:174-183.

Hughes, F. M. R. 1997. Floodplain biogeomorphology. *Progress in Physical Geography* 21 (4):501-529.

Hussain, M., D. Chen, A. Cheng, H. Wei, and D. Stanley. 2013. Change detection from remotely sensed images: From pixel-based to object-based approaches. *ISPRS Journal of Photogrammetry and Remote Sensing* 80:91-106.

Ibrahim, M. A., M. K. Arora, and S. K. Ghosh. 2005. Estimating and accommodating uncertainty through the soft classification of remote sensing data. *International Journal of Remote Sensing* 26 (14):2995-3007.

Jensen, J. R. 2005. *Introductory digital image processing : a remote sensing perspective, 3rd ed*. Upper Saddle River, N.J. : Prentice Hall.

Jung, H. C., J. Hamski, M. Durand, D. Alsdorf, F. Hossain, H. Lee, A. K. M. Azad Hossain, K. Hasan, A. S. Khan, and A. K. M. Zeaul Hoque. 2010. Characterization of complex fluvial systems using remote sensing of spatial and temporal water level variations in the Amazon, Congo, and Brahmaputra rivers. *Earth Surface Processes and Landforms* 35 (3):294-304.

Kaufman, Y. J., A. E. Wald, L. A. Remer, B.-C. Gao, R.-R. Li, and L. Flynn. 1997. MODIS 2.1-μm channel - correlation with visible reflectance for use in remote sensing of aerosol. *IEEE Transactions on Geoscience and Remote Sensing* 35 (5):1286-1298.

Kavzoglu, T. 2009. Increasing the accuracy of neural network classification using refined training data. *Environmental Modelling & Software* 24 (7):850-858.

Kent, J. T., and K. V. Mardia. 1988. Spatial classification using fuzzy membership models. *IEEE Transactions on Pattern Analysis and Machine Intelligence* 10 (5):659-671.

Lausch, A., and F. Herzog. 2002. Applicability of landscape metrics for the monitoring of landscape change: Issues of scale, resolution and interpretability. *Ecological Indicators* 2 (1-2):3-15.

Legleiter, C. J., and M. F. Goodchild. 2005. Alternative representations of in-stream habitat: Classification using remote sensing, hydraulic modeling, and fuzzy logic. *International Journal of Geographical Information Science* 19 (1):29-50.

Li, P., and H. Xu. 2010. Land-cover change detection using one-class support vector machine. *Photogrammetric engineering and remote sensing* 76 (3):255-263.

Liu, D., K. Song, J. R. G. Townshend, and P. Gong. 2008. Using local transition probability models in Markov random fields for forest change detection. *Remote Sensing of Environment* 112 (5):2222-2231.

Looy, K., P. Meire, and J.-G. Wasson. 2008. Including riparian vegetation in the definition of morphologic reference conditions for large rivers: A case study for Europe's western plains. *Environmental Management* 41 (5):625-639.

Lu, D., P. Mausel, E. Brondízio, and E. Moran. 2004. Change detection techniques. *International Journal of Remote Sensing* 25 (12):2365-2401.

Lu, D., and Q. Weng. 2007. A survey of image classification methods and techniques for improving classification performance. *International Journal of Remote Sensing* 28 (5):823-870.

Marpu, P. R., A. Wijaya, and R. Gloaguen. 2008. Soft classification and assessment of kalman filter neural network for complex landcover of tropical rainforests. Paper read at International Geoscience and Remote Sensing Symposium (IGARSS), at Boston, MA.

McGarigal, K. 2014. Landscape pattern metrics. In *Wiley StatsRef: Statistics Reference Online*: John Wiley & Sons, Ltd.

McGarigal, K., S. Cushman, and E. Ene. 2012. FRAGSTATS v4: Spatial pattern analysis program for categorical and continuous maps. Computer software program produced by the authors at the University of Massachusetts, Amherst. Available at http://www.umass.edu/landeco/research/fragstats/fragstats.html (last accessed 9 June 2016).

McGarigal, K., S. A. Cushman, K. McGarigal, and S. A. Cushman. 2005. The gradient concept of landscape structure. In *Issues and Perspectives in Landscape Ecology*, eds. J. A. Wiens and M. R. Moss, 112-119. Cambridge: Cambridge University Press.

Mertes, L. A. K., D. L. Daniel, J. M. Melack, B. Nelson, L. A. Martinelli, and B. R. Forsberg. 1995. Spatial patterns of hydrology, geomorphology, and vegetation on the floodplain of the Amazon river in Brazil from a remote sensing perspective. *Geomorphology* 13 (1-4):215-232.

Michalková, M. 2009. Diachronic analysis of floodplain lakes of the sacramento river. *Geograficky Casopis* 61 (4):257-268.

Mishra, N. S., S. Ghosh, and A. Ghosh. 2012a. Combination of fuzzy clustering algorithms for change detection in remote sensing images. Paper read at 2012 3rd International Conference on Emerging Applications of Information Technology (EAIT), at Kolkata.

———. 2012b. Fuzzy clustering algorithms incorporating local information for change detection in remotely sensed images. *Applied Soft Computing Journal* 12 (8):2683-2692.

Mountrakis, G., J. Im, and C. Ogole. 2011. Support vector machines in remote sensing: A review. *ISPRS Journal of Photogrammetry and Remote Sensing* 66 (3):247-259.

Okujeni, A., S. van der Linden, L. Tits, B. Somers, and P. Hostert. 2013. Support vector regression and synthetically mixed training data for quantifying urban land cover. *Remote Sensing of Environment* 137:184-197.

Pavri, F., and J. Aber. 2004. Characterizing wetland landscapes: A spatiotemporal analysis of remotely sensed data at Cheyenne Bottoms, Kansas. *Physical Geography* 25 (1):86-104.

Pepe, M., L. Boschetti, P. A. Brivio, and A. Rampini. 2010. Comparing the performance of fuzzy and crisp classifiers on remotely sensed images: A case of snow classification. *International Journal of Remote Sensing* 31 (23):6189-6203.

Pereira, V. F. G., R. G. Congalton, and D. J. Zarin. 2002. Spatial and temporal analysis of a tidal floodplain landscape - Amapá, Brazil - using geographic information systems and remote sensing. *Photogrammetric engineering and remote sensing* 68 (5):463-472.

Perkins, T., S. Adler-Golden, M. Matthew, A. Berk, G. Anderson, J. Gardner, and G. Felde. 2005. Retrieval of atmospheric properties from hyper- and multi-spectral imagery with the FLAASH atmospheric correction algorithm. In: Schäfer, K., et al. (Eds.), Remote Sensing of Clouds and the Atmosphere X (Proc. SPIE, vol. 5979). SPIE, Bruges, Belgium: 59790E-59791–59790E-59711.

Pontius Jr, R. G., and M. Millones. 2011. Death to Kappa: Birth of quantity disagreement and allocation disagreement for accuracy assessment. *International Journal of Remote Sensing* 32 (15):4407-4429.

Poole, G. C., C. A. Frissell, and S. C. Ralph. 1997. In-stream habitat unit classification: Inadequacies for monitoring and some consequences for management. *Journal of the American Water Resources Association* 33 (4):879-896.

Radke, R. J., S. Andra, O. Al-Kofahi, and B. Roysam. 2005. Image change detection algorithms: A systematic survey. *IEEE Transactions on Image Processing* 14 (3):294-307.

Raina, R., and M. Thomas. 2012. Fuzzy vs. probabilistic techniques to address uncertainty for radial distribution load flow simulation. *Energy and Power Engineering* 4 (2):99-105.

Ramankutty, N., and J. A. Foley. 1999. Estimating historical changes in global land cover: Croplands from 1700 to 1992. *Global Biogeochemical Cycles* 13 (4):997-1027.

Roper, B. B., J. L. Kershner, E. Archer, R. Henderson, and N. Bouwes. 2002. An evaluation of physical stream habitat attributes used to monitor streams. *Journal of the American Water Resources Association* 38 (6):1637-1646.

Sadeghi, M., S. B. Jones, and W. D. Philpot. 2015. A linear physically-based model for remote sensing of soil moisture using short wave infrared bands. *Remote Sensing of Environment* 164:66-76.

Schmitt, R., S. Bizzi, and A. Castelletti. 2014. Characterizing fluvial systems at basin scale by fuzzy signatures of hydromorphological drivers in data scarce environments. *Geomorphology* 214:69-83.

Schramm Jr, H. L., M. S. Cox, T. E. Tietjen, and A. W. Ezell. 2009. Nutrient dynamics in the lower Mississippi river floodplain: Comparing present and historic hydrologic conditions. *Wetlands* 29 (2):476-487.

Schuft, M. J., T. J. Moser, P. J. Wigington Jr, D. L. Stevens Jr, L. S. McAllister, S. S. Chapman, and T. L. Ernst. 1999. Development of landscape metrics for characterizing riparian-stream networks. *Photogrammetric engineering and remote sensing* 65 (10):1157-1167.

Shanmugam, P., Y. H. Ahn, and S. Sanjeevi. 2006. A comparison of the classification of wetland characteristics by linear spectral mixture modelling and traditional hard classifiers on multispectral remotely sensed imagery in southern India. *Ecological Modelling* 194 (4):379-394.

Shannon, C. E. 1948. A mathematical theory of communication. *Bell System Technical Journal* 27 (3):379-423.

Shoshany, M., and E. Kelman. 2006. Assessing mutuality of change in soil and vegetation patch pattern characteristics by means of Cellular Automata simulation. *Geomorphology* 77 (1-2):35-46.

Singh, A. 1989. Review Articlel: Digital change detection techniques using remotely-sensed data. *International Journal of Remote Sensing* 10 (6):989-1003.

Singh, S., and R. Talwar. 2015. Performance analysis of different threshold determination techniques for change vector analysis. *Journal of the Geological Society of India* 86 (1):52-58.

Song, C., C. E. Woodcock, K. C. Seto, M. P. Lenney, and S. A. Macomber. 2001. Classification and change detection using Landsat TM data: When and how to correct atmospheric effects? *Remote Sensing of Environment* 75 (2):230-244.

Song, X., and C. Bo. 2011. Change detection using change vector analysis from Landsat TM images in Wuhan. Paper read at Procedia Environmental Sciences.

Suess, S., S. Van Der Linden, A. Okujeni, P. J. Leitão, M. Schwieder, and P. Hostert. 2015. Using class probabilities to map gradual transitions in shrub vegetation from simulated EnMAP data. Remote Sensing 7 (8):10668-10688.

Tewkesbury, A. P., A. J. Comber, N. J. Tate, A. Lamb, and P. F. Fisher. 2015. A critical synthesis of remotely sensed optical image change detection techniques. *Remote Sensing of Environment* 160 (0):1-14.

Thomas, R. F., R. T. Kingsford, Y. Lu, and S. J. Hunter. 2011. Landsat mapping of annual inundation (1979-2006) of the Macquarie Marshes in semi-arid Australia. *International Journal of Remote Sensing* 32 (16):4545-4569.

Tormos, T., P. Kosuth, S. Durrieu, S. Dupuy, B. Villeneuve, and J. G. Wasson. 2012. Object-based image analysis for operational fine-scale regional mapping of land cover within river corridors from multispectral imagery and thematic data. *International Journal of Remote Sensing* 33 (14):4603-4633.

Townsend, P., and S. Walsh. 2001. Remote sensing of forested wetlands: application of multitemporal and multispectral satellite imagery to determine plant community composition and structure in southeastern USA. *Plant Ecology* 157 (2):129-149.

Tso, B., and R. C. Olsen. 2005. A contextual classification scheme based on MRF model with improved parameter estimation and multiscale fuzzy line process. *Remote Sensing of Environment* 97 (1):127-136.

Turner, M. G. 1989. Landscape ecology: the effect of pattern on process. *Annual review of ecology and systematics. Vol. 20*:171-197.

Turner, M. G. 1990. Spatial and temporal analysis of landscape patterns. *Landscape Ecology* 4 (1):21-30.

Turner, R. E., N. N. Rabalais, D. Justic', and Q. Dortch. 2003. Global patterns of dissolved N, P and Si in large rivers. *Biogeochemistry* 64 (3):297-317.

Van Der Linden, S., A. Janz, B. Waske, M. Eiden, and P. Hostert. 2007. Classifying segmented hyperspectral data from a heterogeneous urban environment using support vector machines. *Journal of Applied Remote Sensing* 1 (1): 013543-013543-17.

Velloso, M. L. F., and F. J. d. Souza. 2002. Change-detection using contextual information and fuzzy entropy principle. In *Proceedings of the 8th Ibero-American Conference on AI: Advances in Artificial Intelligence*, 285-293: Springer-Verlag.

Wang, F. 1989. Fuzzy expert system for remote sensing image analysis. *Digest - International Geoscience and Remote Sensing Symposium (IGARSS)* 2:848-851.

Wang, X., and H. Wang. 2004. Markov random field modeled range image segmentation. *Pattern Recognition Letters* 25 (3):367-375.

Warner, T. 2005. Hyperspherical direction cosine change vector analysis. *International Journal of Remote Sensing* 26 (6):1201-1215.

WeatherSpark. 2016. Average weather for Rurrenabaque, Bolivia. Available at https://weatherspark.com/averages/33611/Rurrenabaque-Beni-Bolivia (last accessed 9 June 2016).

Xian, G., C. Homer, and J. Fry. 2009. Updating the 2001 National Land Cover Database land cover classification to 2006 by using Landsat imagery change detection methods. *Remote Sensing of Environment* 113 (6):1133-1147.

Ye, S., D. Chen, and J. Yu. 2016. A targeted change-detection procedure by combining change vector analysis and post-classification approach. *ISPRS Journal of Photogrammetry and Remote Sensing* 114:115-124.

Zadeh, L. A. 1965. Fuzzy sets. *Information and Control* 8 (3):338-353.

Zhang, J., and N. Stuart. 2001. Fuzzy methods for categorical mapping with image-based land cover data. *International Journal of Geographical Information Science* 15 (2):175-195.

Zhu, Z., C. E. Woodcock, and P. Olofsson. 2012. Continuous monitoring of forest disturbance using all available Landsat imagery. *Remote Sensing of Environment* 122:75-91.